ERDC/CRREL TR-17-4

US Army Corps of Engineers®
Engineer Research and Development Center

ERDC
INNOVATIVE SOLUTIONS for a safer, better world

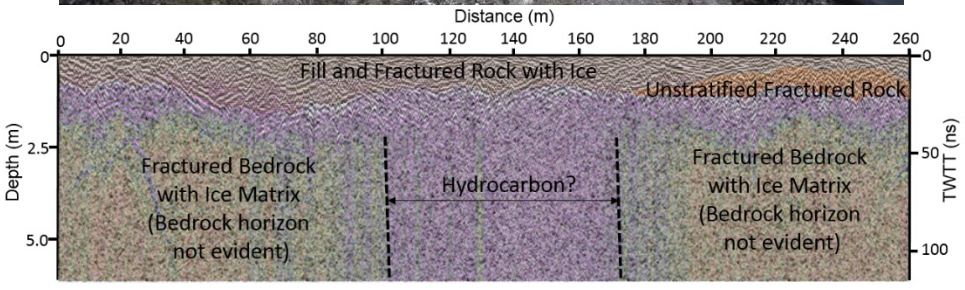
Engineering for Polar Operations, Logistics, and Research (EPOLAR)

Subsurface Assessment at McMurdo Station, Antarctica

Rosa T. Affleck, Seth Campbell, Samantha Sinclair, and Bruce Tischbein

February 2017





Approved for public release; distribution is unlimited.

Cold Regions Research and Engineering Laboratory

The U.S. Army Engineer Research and Development Center (ERDC) solves the nation's toughest engineering and environmental challenges. ERDC develops innovative solutions in civil and military engineering, geospatial sciences, water resources, and environmental sciences for the Army, the Department of Defense, civilian agencies, and our nation's public good. Find out more at www.erdc.usace.army.mil.

To search for other technical reports published by ERDC, visit the ERDC online library at http://acwc.sdp.sirsi.net/client/default.

ERDC/CRREL TR-17-4
February 2017

Subsurface Assessment at McMurdo Station, Antarctica

Rosa Affleck, Seth Campbell and Samantha Sinclair

U.S. Army Engineer Research and Development Center (ERDC)
Cold Regions Research and Engineering Laboratory (CRREL)
72 Lyme Road
Hanover, NH 03755-1290

Bruce Tischbein

Lockheed Martin, Antarctic Support Contract
7400 S. Tucson Way
Centennial, CO 08112

Final Report

Approved for public release; distribution is unlimited.

Prepared for National Science Foundation, Office of Polar Programs
Antarctic Infrastructure and Logistics
Arlington, VA 22230

Under Engineering for Polar Operations, Logistics, and Research (EPOLAR)
EP-ANT-15-19, “Geotechnical Assessment for McMurdo Station Landscape and Infrastructure Improvements”

Abstract

Installations built on massive ice, permafrost, or seasonal frozen ground require careful design to avoid melting issues. Therefore, efforts to rebuild McMurdo Station, Antarctica, to improve operational efficiency and to consolidate energy resources require knowledge of geology and geotechnical information, particularly soil indices within the near-surface layer subjected to temporal fluctuations and the ice-cemented layer.

Therefore, this study collected both 200 and 400 MHz ground-penetrating radar (GPR) data in McMurdo during January, October, and November of 2015 to detect the active layer, permafrost or massive ice, fill thickness, solid bedrock depth, and buried utilities or construction and waste debris. Five soil pits were excavated to collect soil, ice, and rock samples for gradation, density, and moisture content tests. Information extracted from the soil pits also aided in ground-truthing the GPR profiles. Subsurface investigations revealed distinct features, including ice-bonded fractured basaltic boulders, rocks, and gravelly sand; massive ice; and constructed (friable) fill layer. This paper describes the soil temperature and moisture during austral summers. The presented results are important for designs of new engineered structures at McMurdo Station.

DISCLAIMER: The contents of this report are not to be used for advertising, publication, or promotional purposes. Citation of trade names does not constitute an official endorsement or approval of the use of such commercial products. All product names and trademarks cited are the property of their respective owners. The findings of this report are not to be construed as an official Department of the Army position unless so designated by other authorized documents.

DESTROY THIS REPORT WHEN NO LONGER NEEDED. DO NOT RETURN IT TO THE ORIGINATOR.

Contents

Abstract ii

Figures and Tables v

Preface ix

Acronyms and Abbreviations x

Unit Conversion Factors xii

Executive Summary xiii

1 Introduction 1

1.1 Background 1
1.2 Objective 3
1.3 Approach 4

2 Site Background 5

3 Methods 9

3.1 Ground-penetrating radar (GPR) 9
3.1.1 GPR post-processing 10
3.1.2 GPR interpretation and assumptions 10
3.2 Excavation of pits 12
3.2.1 Visual assessment 13
3.2.2 Ice density 15
3.2.3 Rock density 15
3.2.4 Soil gradation, moisture, density, and ice content 15
3.3 Soil-moisture and soil-temperature instrumentation 19

4 Results 20

4.1 Pit profiles 20
4.1.1 Site 1 23
4.1.2 Site 2 23
4.1.3 Site 3 24
4.1.4 Site 4 25
4.1.5 Site 5 26
4.2 Soil gradation 28
4.3 Moisture content by weight 31
4.4 Density and volumetric ratios of frozen materials 31
4.5 Density of rocks 32
4.6 Ice characteristics 33
4.7 GPR interpretation of bedrock and fill 34
4.8 GPR and pits comparison 36
4.8.1 Site 1 36

4.8.2 Site 2 ..... *37*
4.8.3 Site 3 ..... *39*
4.8.4 Site 4 ..... *39*
4.8.5 Site 5 and hydrocarbons in soil *41*
4.8.6 Boreholes *42*
4.9 Soil-temperature profiles 43
4.10 Temporal soil moisture 50

5 Discussion 52
5.1 Active layer, permafrost and ice 52
5.2 Ground-temperature comparison 52
5.3 Surface snowmelt and frost susceptibility 53
5.4 Buried hydrocarbons and contaminant implications 55
5.5 Buried utilities 56
5.6 General impacts on engineered structures 56
5.7 Study limitations 58
5.7.1 GPR limitations *58*
5.7.2 Additional GPR and ground-truthing *59*
5.7.3 Shallow pits *60*

6 Summary and Conclusion 61

References 64

Appendix A: Ground-Penetrating-Radar Raw Data 69

Appendix B: Picture and Notes for Individual Pits 80

Appendix C: Grain Size 95

Report Documentation Page (SF 298) 99

Figures and Tables

Figures

1 Map of Hut Point Peninsula on Ross Island, Antarctica, showing McMurdo Station (McM) relative to other major geographic features. (The background is from DigitalGlobe, Inc., satellite image WorldView-3 taken from the 6 December 2015 panchromatic band.) 2

2 Soil temperature with depth collected from 1994 to 1996 by Tumeo and Cummings (1996) 8

3 Map of all GPR profiles collected at McMurdo Station in 2015 (*pink lines*). *Green circles* depict areas where soil pits were dug and *blue crosses* show the location of boreholes documented in Fenwick and Winkler (2016) 10

4 Map illustrating the locations of the soil pits and rock samples collected at McMurdo Station in this study. M&T #1 and M&T #2 stand for moisture and temperature sensors locations 13

5 Ice-rich soil at Site 1 20

6 Buried massive ice at Site 2 21

7 and buried massive ice at Site 4 21

8 Man-made fill with buried contaminations at Site 3 22

9 Reddish fill on the top and gray fractured rock with ice lenses at Site 5 22

10 Cross section of Site 1 showing profile descriptions, soil indices, and ice properties 23

11 Cross section of Site 2 showing profile descriptions, soil indices, and ice properties 24

12 Cross section of Site 3 showing profile descriptions, soil indices, and ice properties 25

13 Cross section of Site 4 showing profile descriptions, soil indices, and ice properties 26

14 Cross section of Site 5 showing profile descriptions, soil indices, and ice properties 27

15 Mean relative density of various type of rocks collected at locations shown in Fig. 3. Error bars signify the (positive and negative) standard deviations from the mean 33

16 Map of GPR profiles showing interpreted thickness of stratified fill. *Green circles* indicate the five soil pits dug in the area, *blue crosses* show boreholes dug near GPR profiles, and each *yellow box* shows the close-up map with the GPR profiles and pits comparison in Figs. 18, 20–25 35

17 Map of GPR profiles showing interpreted depth to bedrock. *Green circles* indicate five soil pits dug in the area, and *blue crosses* show boreholes dug near GPR profiles 35

18 200 MHz unprocessed GPR transect along Site 1 (*middle*) and translated profile (*bottom*) showing interpretation of fill and fractured rock over ice-rich fractured bedrock (*bottom*). Zoomed in map showing Site 1 (*top*) of box 1 from Fig. 16 37

19 200 MHz processed GPR profile (*top*) between T-Site and Observation Hill oriented parallel to and north of Main Street. Profile is located east of Site 1

where a ground truth pit was excavated. The interpretation (*bottom*) shows snow and ice over a stratified ice-rich matrix, and bedrock at greater depths 37

20 A 200 MHz GPR profile collected across Site 2 (*middle*), which was excavated from a raised fill platform along the transect location in yellow box 2 in Fig. 16 (*top*), with GPR profiles marking from *B* to *B'*. The profile reveals dipping stratified fill, with primarily horizons likely representing ice lenses within fill deposits (*bottom*). Fill is truncated at depth by a higher $\acute{\varepsilon}$ relative to the fill. We interpret this horizon to represent a transition to solid bedrock 38

21 A 200 MHz profile (*middle*) collected across and perpendicular to Main Street, also crossing a pit extracted from Site 3 (*top*) for ground-truth. Our interpretation (*bottom*) shows bedrock exposed at the surface on Main Street and the bedrock horizon dipping under stratified fill to the north and south. Also note multiple underground utilities and a culvert line to the north and South of Main Street 39

22 A 200 MHz GPR profile (*middle*) and interpretation (*bottom*) of the location of Site 4 and the extent of massive ice along the transect location (*top*). Note the clear and speckle-free massive ice relative to the surrounding geology 40

23 A 200 MHz GPR profile (*middle*) with interpretation (*bottom*) along the transect on the map (*top*) in area shown in Fig. 16, showing the fill and fractured rock 41

24 A 200 MHz GPR profile (*top*) with interpretation (*bottom*) showing approximate extent of hydrocarbon pollution within the fill and fractured rock, which significantly increases attenuation and noise in the radar signal along the transect in box 5 in Fig. 16 42

25 A 200 MHz GPR profile (*middle*) with interpretation (*bottom*) showing the GPR transect location (*top*) of stratified fill and fractured ice-rich rock situated over bedrock 43

26 Air and soil temperature collected in the ground every 15 minutes at (*a*) the M&T #1 site and (*b*) the M&T #2 site from 17 to 19 December 2009 45

27 Air and soil temperature collected in the ground every 15 minutes at (*a*) the M&T #1 site and (*b*) the M&T #2 site from 17 to 19 December 2010 45

28 Maximum and minimum daily air and mean daily soil temperatures at the M&T #1 site for austral summers 2009–10, 2010–11, and 2015–16 46

29 Maximum and minimum daily air and mean daily soil temperatures at the M&T #2 site for austral summers 2009–10 and 2010–11 47

30 Vertical profiles of mean daily soil temperatures for selected dates at M&T #1 during austral summers 2009–10, 2010–11, and 2015–16 49

31 Vertical profiles of mean daily soil temperatures for selected dates at the M&T #2 site during austral summers 2009–10 and 2010–11 49

32 Vertical profiles of mean daily soil moisture from PR2 sensors at the M&T #1 site for selected dates during austral summers 2009–10, 2010–11, and 2015–16 51

33 Vertical profiles of mean daily soil moisture at the M&T #2 site for selected dates during austral summers 2009–10 and 2010–11 51

34 Ground-temperature data collected at the T-site for design and construction of a foundation for a wind turbine (after Oswell et al. 2010) 53

35 Examples of surface snowmelt eroding the thawed permeable soil and its effects on freezing. The *left* photo shows gullies that formed in the summer of 2008–09 on a gentle sloping pad. The *right* photo shows aufeis formation underneath a building in the summer of 2009–10 54

A-1 400 MHz unprocessed GPR profile showing the transect location in the map 69

A-2 Another 400 MHz unprocessed GPR profile for transect west and north of Crary and ending north of Building 166 70
A-3 200 MHz unprocessed GPR profile for transect on the road north of Building 4 towards Main Street and looping around Dorm 210 70
A-4 200 MHz unprocessed GPR profile showing the transect location in the map 71
A-5 200 MHz unprocessed GPR profile for transect southwest and north of building 155 71
A-6 200 MHz unprocessed GPR profile showing the transect location in the map 72
A-7 200 MHz unprocessed GPR profile for transect between Buildings 155 and 147 towards building 136 72
A-8 200 MHz unprocessed GPR profile for a transect starting from building 136 and going across the road toward the pads 73
A-9 200 MHz unprocessed GPR profile for a transect on the pads north of Main Street 73
A-10 200 MHz unprocessed GPR profile for transect north of tank farms toward Scott Base 74
A-11 200 MHz unprocessed GPR profile for a transect north of tank farms towards Crary 74
A-12 200 MHz unprocessed GPR profile for a transect along open space east of Crary 75
A-13 200 MHz unprocessed GPR profile showing the transect behind Building 136 and across Building 182 75
A-14 200 MHz unprocessed GPR profile showing the transect location around Crary Lab 76
A-15 200 MHz unprocessed GPR profile showing the transect along the road toward the sea ice transition 76
A-16 200 MHz unprocessed GPR profile showing the transect location on the sea ice transition 77
A-17 200 MHz unprocessed GPR profile showing the transect between Buildings 136 and 191, across the Main Street to the pad 77
A-18 200 MHz unprocessed GPR profile showing the transect location in the pad area 78
A-19 200 MHz unprocessed GPR profile for transect towards Arrival Heights 78
A-20 200 MHz unprocessed GPR profile for transect along Main Street all the way down to Hut Point 79
A-21 200 MHz unprocessed GPR profile for transect along the slope above the pier 79
B-1 The active or thawed layer 80
B-2 The bottom of the active showing ice lenses at 1.5 ft 81
B-3 Hammering and breaking the ice-cemented hard rock 81
B-4 Close-up profile of the ice-cemented rock and sands in the pit at Site 1 81
B-5 Overall profile at Site 1 82
B-6 Excavated fractured boulder, rocks, and sands for Site 1 82
B-7 Materials near the surface 83
B-8 The profile at the fill and ice interface 84
B-9 Digging into the consolidated snow and ice by using the ripper tooth to break the layer 84

B-10 Site 2 profile and close-up photos at various depths showing compacted sediments and foreign debris in ice....85
B-11 Excavated ice from the pit at Site 2....85
B-12 Overall profile for Site 2....86
B-13 Relatively easy digging for the first few scoops....87
B-14 The active or thawed layer....87
B-15 Using the hammer attachment to break the frozen materials....88
B-16 The soil profile from the surface down to 4 ft bgl (*left*) and debris found below 5 ft depth (*right*)....88
B-17 The overall soil pit profile at Site 3....89
B-18 The fill layer on top....90
B-19 Ice layers at Site 4. *Bottom right* shows hard rock (gray basaltic material) layer at the bottom of pit....90
B-20 Site 4 profile and excavation down to 10 ft....91
B-21 Site 5 thawed layer....92
B-22 Digging and using a ripper attachment (*left*) and hammer below five ft (*right*) to loosen the frozen layer at Site 5....92
B-23 Profiles at various depths at Site 5 showing ice lenses....93
B-24 Entire profile of the pit at Site 5 showing red fill materials, gray fractured rocks, and ice lenses....94
C-1 Grain-size distribution for samples collected in Site 1....95
C-2 Grain-size distribution for samples collected in Site 2....96
C-3 Grain-size distribution for samples collected in Site 3....96
C-4 Grain-size distribution for samples collected in Site 4....97
C-5 Grain-size distribution for samples collected in Site 5 down to 1.83 m....97
C-6 Grain-size distribution for samples collected in Site 5 down to 2.74 m....98

Tables

1 Ross Sea region soil characteristics (Balks et al. 2013)....6
2 Frozen soil and subsurface strata classification used in the study (ASTM 2016; Andersland and Ladanyi 1994)....14
3 Particle size distribution (%) at Sites 1–3 for the gravelly sand earth fractions of the soils collected at various depths and the corresponding USCS identification....29
4 Particle size distribution (%) at Sites 4–5 of gravelly sand earth fractions of the soils collected at various depths and the corresponding USCS identification....30
5 Statistical summary of rock-sample density from various locations at McMurdo Station....33

Preface

This study was conducted for the National Science Foundation (NSF), Office of Polar Programs (OPP), under Engineering for Polar Operations, Logistics, and Research (EPOLAR) EP-ANT-15-19, "Geotechnical Assessment for McMurdo Station Landscape and Infrastructure Improvements." The technical monitor was Margaret Knuth (program manager), NSF-OPP, U.S. Antarctic Program; and she also provided logistical guidance and technical supervision.

The work was performed by the Force Projection and Sustainment Branch (CEERD-RRH), the Engineering Resources Branch (CEERD-RZE), and the Terrestrial and Cryospheric Sciences Branch (CEERD-RRG), U.S. Army Engineer Research and Development Center, Cold Regions Research and Engineering Laboratory (ERDC-CRREL). At the time of publication, Dr. Sarah Kopczynski was Chief, CEERD-RRH; Jared Oren was Chief, CEERD-RZE; J. D. Horne was Chief, CEERD-RRG; and Janet Hardy was the program manager for EPOLAR Antarctica. The Deputy Director of ERDC-CRREL was Dr. Lance Hansen, and the Director was Dr. Robert Davis.

The success of several summers of fieldwork at McMurdo Station would not have been possible without assistance from the environmental and operations staff of Antarctic Support Contract, including Ryan Wallace, Robert DeValentino, William Ames (former staff), Dale Rivers, and Tyonek McAdams, Megan Whitmore, Thomas Verville, and Corey Biddle (Survey Department). The authors are grateful for the assistance provided by shipping, receiving, supply, and logistics support at McMurdo Station during the fieldwork. The authors also thank the following CRREL staff for their contributions: Brian Tracy and Jennifer MacPherson for imagery support, Renee Melendy for superb office administrative and logistical support, and Joni Quimby for shipping and receiving the equipment and supplies used during the fieldwork. Emily Moynihan provided our editing support. Technical reviews were provided by Kevin Bjella (CRREL), James Buska (retired CRREL), and Janet Hardy (CRREL).

Existing geospatial data used for this report were provided by the Antarctic Geospatial Information Center (AGIC), http://www.agic.umn.edu.

The Commander of ERDC is COL Bryan S. Green, and the Director of ERDC is Dr. Jeffery P. Holland.

Acronyms and Abbreviations

AGIC	Antarctic Geospatial Information Center
bgl	Below Ground Level
CRREL	Cold Regions Research and Engineering Laboratory
EPOLAR	Engineering for Polar Operations, Logistics and Research
ERDC	U.S. Army Engineer Research and Development Center
FIR	Finite Impulse Response
GP	Poorly Graded Gravel
GP-GM	Poorly Graded Gravel with Silt and Sands
GPR	Ground-Penetrating Radar
GPS	Global Positioning System
GSSI	Geophysical Survey Systems Incorporated
GW	Well-Graded Gravel
GW-GM	Well-Graded Gravel with Silt and Sands
IGY	International Geophysical Year
M&T	Moisture and Temperature
MEC	Mechanical Equipment Center
NSF	National Science Foundation
OPP	Office of Polar Programs
ppm	Parts per Million
RTK	Real-Time Kinematic
SP	Poorly Graded Sands
SP-SM	Poorly Graded Sand with Silt

SW	Well-Graded Sands
SW-SM	Well-Graded Sand with Silt
TWTT	Two-Way Travel Time
USAP	U.S. Antarctic Program
USCS	Unified Soil Classification System
USDA	U.S. Department of Agriculture

Unit Conversion Factors

Multiply	By	To Obtain
degrees Fahrenheit	(F-32)/1.8	degrees Celsius
feet	0.3048	meters
inches	0.0254	meters
miles (U.S. statute)	1,609.347	meters

Executive Summary

The current planned redevelopment at McMurdo Station involves modernizing large engineered structures with more efficient facilities and infrastructure. This modernization encompasses a significant and drastic change to the topography and extensive site preparation to construct foundations for large buildings and to improve existing infrastructure. Although there have been several extensive studies on soils in continental Antarctica, there has been little focus on the geotechnical information at McMurdo Station related to soil indices within the near-surface layer subjected to diurnal and seasonal temperature fluctuations, the layer subjected to thawing or freezing (active layer), and subsurface characterization of the ice-cemented materials or permanently frozen layer.

This study used ground-penetrating radar (GPR) and conducted site excavation at five locations to examine the near-subsurface stratigraphy, engineering classification, and density of materials and to quantify the ice content at McMurdo Station. This study also identified buried utilities, conduits, debris, and other anthropogenic structures that were encountered along the GPR path and in the soil pits. Lastly, this report briefly highlights implications of material properties and ground conditions found at McMurdo Station with emphasis on design considerations of engineered structures for future development.

Soil pits were excavated at five locations to provide visual observation and characterization of soil properties and ice features. Sites 1 and 3 were dug down to 1.5 and 1.7 m below the ground level (bgl), respectively, with a 4.6 m by 1.8 m surface-trench size. Site 2 was excavated down to 3.25 m bgl, and Sites 4 and 5 were dug down to 3.05 m bgl, with approximately a 12 m by 4 m surface trench size for Sites 2, 4, and 5. With firm, frozen material, two sides of the excavated trenches provided relatively vertical profiles, allowing visual observation and quantitative subsurface conditions; and representative samples of the materials were extracted at various depths. The profile at Site 1 consisted of a mechanically constructed layer from the surface down to between 0.3 and 0.45 m, and below 0.45 m bgl was an ice-cemented coarse-stratified layer consisting of fractured basaltic boulders, rocks, gravelly sand, and segregated ice. Site 2 is on a pad built from a man-made deposit of snow or ice with approximately 0.6 m of reddish fine sand material on top of it. Site 3 is on a pad of friable soil littered

with wood and plastic debris with distinct and strong off-gas of hydrocarbons. Site 4 is on a sloping site with clear ice layers below the fill; the massive ice was evidence of ephemeral surface flow that seasonally pooled and froze. At Site 5, ice lenses were visible at approximately 0.46 m; and at approximately 1.37 m, an ice-cemented layer was composed of interconnected boulders, rock, gravelly sand, and irregular segregated ice features. The gravelly sand with silts found collected in the soil pits is characterized as permeable and homogeneous coarse-grained materials. Measurements of gravimetric moisture showed that water contents were very low (<12%) in the upper horizons of the active layer and increased significantly towards and immediately below the permafrost table (with values between 64% and 150% at Sites 1 and 5); these indicated significant amounts of excess ice interlayered with soil in the horizon. The total volumetric ice content within the ice-rich layer ranged from 21% to 83% at both Sites 1 and 5.

GPR data were collected in January, November, and December of 2015, on and off roads and trails covering both disturbed and undisturbed surfaces, by using a SIR-4000 GPR control unit coupled with a model 5106 200 MHz antenna and a model 50400 400 MHz antenna. The GPR was synced with a Trimble 5700 and Zephyr geodetic antenna to record the locations. The GPR profiles were post-processed, including the time-zero correction, integration of GPS data into the files, horizontal filtering to remove ringing and the direct wave within the data, and stacking to improve signal-to-noise ratios and visualization of horizontal reflectors. The boundaries for the horizons were picked between stratified and unstratified material; bedrock; and finite targets of interest, including areas of massive ice and buried utilities. GPR depths were calibrated or verified by using available ground-truth data, which included pits excavated and described in this study and borehole logs from November to December 2015 (Fenwick and Winkle 2016). Approximately 40% of collected GPR transects were post-processed and translated for this study along where the ground-truth data were located (see the Methods section for more information on assumptions for GPR profile interpretation). These ground-truth points were generally within 1–2 m of GPR profiles, providing reasonable accuracy of structure and stratigraphic thicknesses, assuming changes in these structures did not occur within 1–2 m laterally. Interpretation of the 200 MHz GPR transect collected across Site 1 revealed two subparallel and continuous horizons of fill and fractured rock over ice-rich fractured bedrock. The 200 MHz GPR profile collected across Site 2 was interpreted with an ex-

tended ice-rich matrix along dipping stratified horizons of fractured bedrock and likely including ice lenses in the matrix. The 200 MHz profile collected across Site 3 identified several underground utilities and crossed exposed bedrock perpendicular to the road, and the bedrock layer deepened under stratified fill to the north and south. The same 200 MHz GPR transect collected across Main Street and Site 3 continued southward downslope toward Site 4; the GPR profile in this section identified a pocket of massive ice and the fractured bedrock below 1 to 2.5 m with the 100 m transect. Site 5 is near the beginning of the 200 MHz GPR profile and the transect identified the fill and fractured rock with ice along with high-frequency speckle noise and signal attenuation potentially from high concentrations of buried hydrocarbons.

The ground was typically fully frozen in October with temperatures well below −12°C within the 0.6 m soil profile, and seasonal ground warming followed the air-temperature trend from November to late January. The large diurnal variation of surface temperature was influenced by the oscillations of heating and cooling events. During the study period, the maximum active layer in a partially shaded area was 0.26 m and was 0.37 m in an open area. The ground temperature gradually lost heat sometime at the end January as lower air temperatures advanced, causing the ground to refreeze. The temporal changes in soil moisture during the austral summer varied with time mainly within the active layer and at the permafrost table; this seasonal variation confirmed that there was some subsurface movement of water at this layer. However, soil-moisture contents in the permafrost stayed consistent throughout the summer season.

Soil and permafrost properties are strongly influenced by the climate and impact moisture, thermal conditions, and excess ice. These factors have engineering design implications. The discussion section (Section 5) highlights ground temperature, the interaction of soil with water and ice, the importance of eliminating the presence of ice for frost susceptible soils, the implications of thaw unstable ground conditions, and the study limitations. This study presents near-surface geotechnical information that is important for designs of new engineered structures at McMurdo Station.

1 Introduction

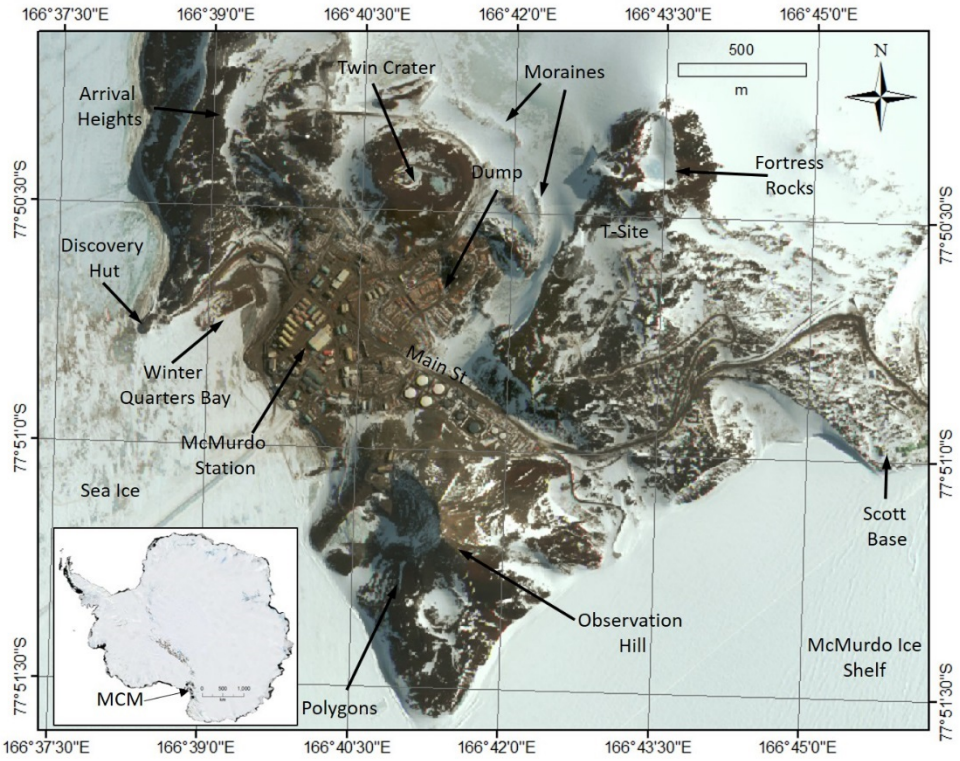
1.1 Background

McMurdo Station, located on Hut Point Peninsula of Ross Island, was first used as a shoreline base in 1902 to explore inland Antarctica. In the mid-1950s, the United States started permanent occupation and established the U.S. Naval Air Facility McMurdo as a permanent logistics base for supporting and constructing a research facility at the geographic South Pole during the 1957–1958 International Geophysical Year (IGY) (Sullivan 1957). In late 1961, the base changed its name to McMurdo Station. McMurdo Station expanded in the late 1960s, and rapid development continued over the following decades (Klein et al. 2008). McMurdo Station (also referred to as "the Station" in this paper) is a research facility and logistics hub of the U.S. Antarctic Program (USAP) with a large operational component that supports research in the region and around the continent (Klein et al. 2008).

McMurdo Station's existing facilities were constructed on an outcrop of barren volcanic rock on a series of constructed flat fill platforms, resulting in terraced-like topography. The Station is bordered by Fortress Rocks, Crater Hill, and Arrival Heights to the north; the Ross Sea to the south; Winter Quarters Bay to the west; and Observation Hill to the east (Figure 1). As a research facility and an operational hub, the terrain at McMurdo Station has been altered to accommodate the increase of science support activities (Klein et al. 2008; Kennicutt et al. 2010). Land scraping, quarrying, and earthworks have been repeatedly part of operations to harvest materials for building sites, road construction, fuel storage, and wharf facilities. Significant landscape disturbances occurred in the late 1950s during the U.S. Navy occupation and continued into the 1970s as construction activities accommodated expansion (Klein et al. 2008). From 1970 until the present, operational activities at the Station continued to create landscape changes and environmental disturbances (Crockett 1998; Klein et al. 2008; Klein et al. 2012; Kennicutt et al. 2010). These activities have destroyed natural geomorphic features and have caused permafrost retreat and associated landscape instability (Campbell and Claridge 2004; Klein et al. 2004). Activities around McMurdo Station (i.e., vehicle traffic) have spread airborne dust over adjacent snow and ice-covered surfaces, causing

changes in albedo and retreating of local snow along with accelerated snowmelt runoff or stream flows, sedimentation, and erosion (Affleck et al. 2012, 2014a, 2014b; Affleck and Carr 2015). Moreover, dust generation is influenced by the unique environment, land disturbance, and dry climatic conditions (Seman and Affleck 2012).

Figure 1. Map of Hut Point Peninsula on Ross Island, Antarctica, showing McMurdo Station (McM) relative to other major geographic features. (The background is from DigitalGlobe, Inc., satellite image WorldView-3 taken from the 6 December 2015 panchromatic band.)



Human activity around the Station also has introduced a wide variety of foreign materials and wastes into the soils in some locations. Accidental spills and chemical contamination from leaking fuel and materials (lubricants, paints, etc.) brought to and used at the Station have caused environmental alterations (Klein et al. 2008; Kennicutt et al. 2010). Other expected contaminants include garbage and debris from construction and shipping materials. As natural soil biological and chemical activity is low because of low ambient temperature and the dry climate, the introduction

of most of the contaminants would essentially be permanent. Furthermore, the contaminants have had a tendency to be transported in the runoff during heavy snowmelt periods (Affleck et al. 2014c).

The current plan at McMurdo Station involves a large development (engineered structures) to modernize the facilities with more efficient infrastructure. This modernization plan encompasses a significant and drastic change to the topography and extensive site preparation to construct foundations for large buildings and to improve existing infrastructure. We recommend that the ground ice content and soil characteristics of the area be assessed quantitatively to determine the ultimate range of possibilities for foundation types and alternatives to design. With legacy releases of hydrocarbons and other contaminants in the subsurface, we also recommend assessment of the extent and constraints on contaminant levels to incorporate into the new infrastructure development at McMurdo Station.

Although there have been several extensive studies on soils in continental Antarctica, there has been little focus on the geotechnical information at McMurdo Station, particularly soil indices within the near-surface layer subjected to diurnal and seasonal temperature fluctuations, the layer subjected to thawing or freezing (active layer), and subsurface characterization of the ice-cemented materials or permanently frozen layer. Evaluation of volumes of ground ice in the upper (near-surface) permafrost is important for engineering and environmental evaluations. This part of the permafrost is the first to be affected by various environmental and operational impacts because the landscape changed from its natural state at the Station. In addition, information is lacking on the extent of the existing disturbance in the subsurface layer from creating a terraced-like topography and the man-made fill to accommodate the infrastructure and buildings at the Station.

1.2 Objective

The objectives of this study are to

1. identify massive ice or ice content in the permafrost;
2. characterize extent and thickness of stratified or unstratified till over bedrock;

3. examine the properties of active and permafrost layers, including the material characteristics, excess ice (water or ice content), the fractured rock features, and the material density, void ratio, and temperature variations;
4. differentiate between anthropogenic and natural material;
5. assess the properties of man-made fill or mechanically constructed sites and compare the structural characteristic to undisturbed permafrost;
6. locate buried utilities, conduits, debris, or other anthropogenic structures that would have implications for long-term infrastructure planning;
7. develop recommendations for broader geotechnical planning based on the near-surface geology and geomorphology determined from geophysics; and
8. discuss the implications of material properties and ground conditions found at McMurdo Station to highlight design considerations of engineered structures for future development.

1.3 Approach

This introductory chapter is followed by site background information based on existing literature on the terrain, geology, general soil description, and previous ground temperature of the area. Then, the following chapter discussed the methods used in this study, including geophysical surveys and site excavations to examine the stratigraphy and soil indices. The subsequent sections include results and discussion related to ground temperature comparisons, the active layer, permafrost, massive ice, the implications of buried hydrocarbons in the area, and engineered structures. These sections are followed by study limitations, a summary, and conclusions.

2 Site Background

The terrain at McMurdo Station is composed of high ridges and sloping hills of barren volcanic rock, frozen ground, and perennial snow and ice fields. Early literature described the terrain around McMurdo Station and the surrounding area as having polygonal and sand-wedge features indicative of a typical permafrost landscape (Péwé 1959, 1991; Bockheim 1997). Péwé (1959) suggested that the formation of "polygons and sand wedges is similar to the origin of foliated ice wedges and polygons in the Arctic. Periodic contraction cracks in the perennially frozen ground around McMurdo Sound, cracks produced by the great change in temperature from summer to winter, are gradually filled with clean sand which filters down from above in the spring and summer." These features are still visible in a few small places, including the escarpment on Arrival Heights and Observation Hill (Klein et al. 2004), but most of the sand-wedge polygons in the area are indiscernible because of significant landscape disturbance and human activity.

Earlier description of the soils in Antarctica classify the region as "cold desert zone" (Tedrow and Ugolini 1966; Tedrow 1977; Ugolini and Bockheim 2007). The soil landscape formation in the coastal Ross Sea region was formed in the Holocene period and was exposed during the Last Glacial Maximum ice retreat (Balks et al. 2013). Organic matter is very minimal with isolated mosses and lichen in a few places. Soils within the Ross Sea region were recently classified as Cryosols (International Union of Soil Sciences 2006) or Gelisols (Soil Survey Staff 2010) with a wide range of soil properties based on the climate and glacially ablated parent (geologic) materials (Campbell and Claridge 2004, 2009). The ablated or barren surface of McMurdo Sound is composed of boulders, rock, and coarse-grained soils from weathered volcanic flows. These materials are single-grained structures with lithochromic grayish colors reflecting the parent materials and some reddish materials due to oxidation of iron minerals. The presence of ice-cemented permafrost within Ross Island is common (Balks et al. 2013). The general summary of key soil properties in the Russ Sea region (Table 1) indicated that the material is predominantly gravelly sands texture with a single-grained structure. Observations of active layers during summer indicated that the ground thaws between 0.15 m in partially shaded area or near buildings and 0.30 m on flat or open areas at

McMurdo Station (Affleck et al. 2012) and on a hillside 100 m from the building at Scott Base (Adlam et al. 2010; Seybold et al. 2010).

Table 1. Ross Sea region soil characteristics (Balks et al. 2013).

Soil property	Description
USDA[1] Classification	Gelisols ranging from Typic Haplorthels to Salic Antyorthels
Texture	Predominantly gravelly sands
Structure	Generally loose, single grained; some weakly developed platy structures occur where soil materials are weakly cemented
Colors	Often reflect parent materials; some a redder color owing to oxidation of iron minerals
Presence of ice-cemented permafrost[2]	Occurs in coastal areas and in areas with younger ablation tills and moisture source (absent if in older soils in inland dry-valley regions where moisture is limited)
Depth of active layer[3]	Varies with altitude, ranging from 0 to approx. 80 cm, predominantly 20–50 cm
pH	Commonly alkaline
Nutrient Availability	Water, rather than nutrients, is the main limitation to microbial and plant growth

[1] **USDA**—United States Department of Agriculture

[2] **Permafrost**—the thermal condition in which the temperatures in earth materials (the ground) remain below 0°C (32°F) for at least two consecutive winters and the intervening summer; moisture in the form of water and ground ice may or may not be present

[3] **Active layer**—the top layer of ground that is subject to annual freezing and thawing

The geologic mapping of Hut Point Peninsula of Ross Island and the ice-free surface of McMurdo Station has been outlined by Cole et al. (1971). The predominant geologic features are characterized as basaltic and pyroclastic flows interbedded with widespread tills. In general, the fractured rocks and boulders are classified as (olivine-augite) basalts (Cole et al. 1971) at Fortress Rock, Arrival Heights, and Crater Hill, including trachytes rocks at Observation Hill (Figure 1). Because Fortress Rock, Arrival Heights, Crater Hill, and Observation Hill are within 1 km of each other, the general description of the surface geology of McMurdo Station is varying amounts of scoria and basalt fragments in ice matrix and fractured basalt bedrock. The fractured basalts can vary from compact (dense gray rock) to vesicular basalts (rocks with tiny holes). Some rocks have a redder color owing to oxidation of iron minerals and are differentiated as felsitic scoria. Compact rocks from much harder crystalline flows are found at deeper depths and at various locations. The fine-grained materials exist

due to the physical and natural (thermally and cryogenically) changes with time.

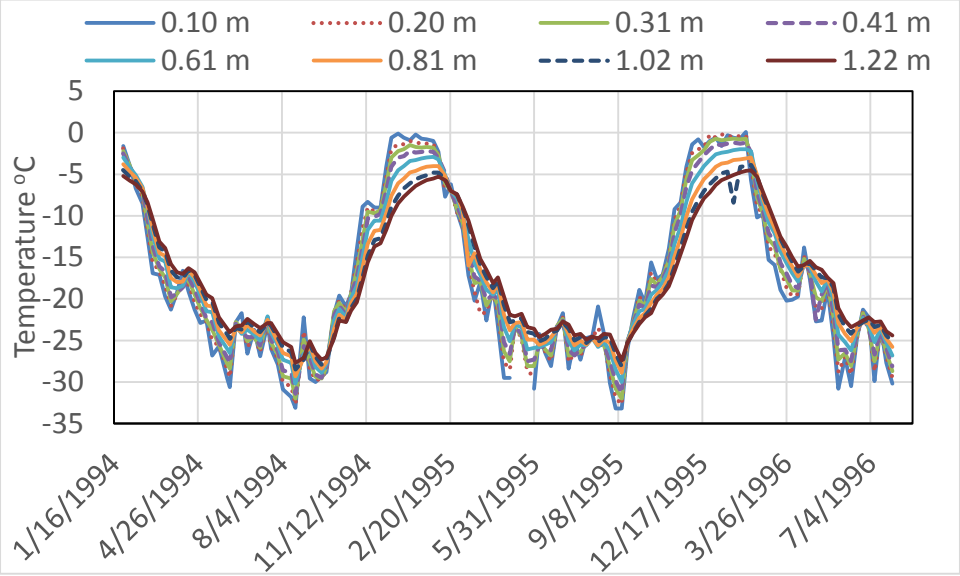
Since the development of McMurdo Station, the natural surface of the area has been altered by constructing fill to create flat areas or platforms, thus creating mixed anthropogenic and cryostructure changes. Fill material is defined as a man-made or mechanically constructed layer using locally sourced materials and is common across McMurdo Station as flat fill platforms or ground. These platforms are used as pads, outdoor storage locations, and access areas. Fill could be in excess of 3 m thick in places. Although significant ice lenses are uncommon within the fill layer, snow and massive ice could potentially be overlaid with fill.

Records of the dry densities, relative toughness values, and crushability factors of reddish and gray materials were published by Knuth and Melendy (2012) and Affleck et al. (2012). (High relative toughness and low crushability values mean that the material is dense and hard.) The dry densities of reddish and gray materials were recorded with approximate values of 1.18 g/cc and 1.79 g/cc, respectively. The estimated relative toughness values and crushability factors for reddish soil were 1.2 and 0.9, respectively; the gray material had a relative toughness value of 2.3 and a crushability factor of 0.75 (Affleck et al. 2012; Knuth and Melendy 2012). A certain amount of rock materials is constantly harvested from nearby hillsides for various purposes, including new projects, infrastructure improvements, fill, maintenance or road repair, pads, and landscaping around or under buildings (Knuth and Melendy 2012). The gray soil is used primarily on roads and pads and for foundation while the reddish materials are used surfacing the pier and in less trafficked areas. The permeability of the gravelly sand samples from McMurdo Station ranged from 0.07 to 0.11 cm per second (Affleck et al. 2012). With these permeability values, the soil is classified as a good drainage material for sandy gravel soil (Holtz and Kovacs 1981). Thus, the active layer is porous and permeable, allowing melt water to flow both through the interstices and laterally along the permafrost table or pond and to refreeze at the permafrost table.

Early records of soil temperatures were measured by Tumeo and Cummings (1996) (Figure 2) to assess the potential effects of contamination migration in the subsurface frozen soil by installing the thermistors at the site where

an accidental fuel spill occurred. The temperature data were collected manually four or five times per month in one location at McMurdo Station from February 1994 to July 1996. Tumeo and Cummings (1996) indicated that the permafrost layer at this location was approximately 0.1 m below the surface and that an ice-rich permafrost existed at 0.23 m below the surface. From his records, the average near-surface temperature (i.e., 0.1 m) for the month of January was recorded to be −1.0°C and was −29°C in September. The average temperatures measured at 1.22 m below the surface were −5.6°C and −26.1°C for January and September, respectively. These soil temperatures provided the seasonal trend of the area; however, diurnal temperature extremes near the surface impact the drier soils in the summer months due to surface albedo of the bare ground.

Figure 2. Soil temperature with depth collected from 1994 to 1996 by Tumeo and Cummings (1996).



Campbell et al. (1994) measured the gravimetric soil-moisture measurements approximately 3 km away from McMurdo Station in the disturbed and undisturbed areas at Scott Base. The soil moisture (by weight) of the active layer ranged from 6.0% to 6.5% and from 1.4% to 8.2% at the surface down to 0.30 m in disturbed and undisturbed areas respectively. Their measurements in the ice-cemented layer (at 0.30–0.60 m) showed significantly higher soil moisture or ice content ranges of 23.8%–150.1% in the undisturbed areas than the moisture content in the disturbed areas of 6.3%–8.4%. They argued that considerable decrease in water or ice in the near-surface permafrost layer was because of land disturbance.

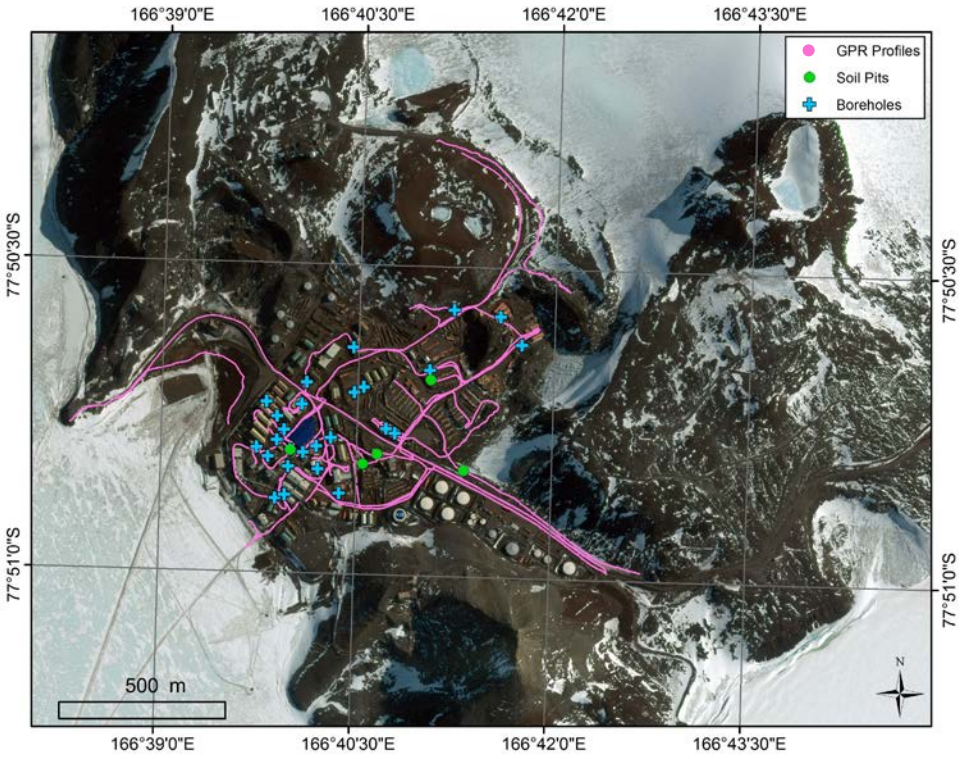
3 Methods

This study used two methods to examine the subsurface conditions at McMurdo Station: geophysical survey using ground-penetrating radar (GPR) and site excavation at five locations to examine the stratigraphy, engineering classification, and density of materials and quantify the ice content.

3.1 Ground-penetrating radar (GPR)

GPR data were collected in January, November, and December of 2015 on and off roads and trails covering both disturbed and undisturbed surfaces (Figure 3, also in Appendix A). We used a SIR-4000 GPR control unit coupled with a model 5106 200 MHz antenna and a model 50400 400 MHz antenna, each unit manufactured by Geophysical Survey Systems Incorporated (GSSI). The GPR was synced with a Trimble 5700 and Zephyr geodetic antenna that recorded GPS (Global Positioning System) locations at a frequency of 1 Hz. GPR scans were recorded at 24 scans s^{-1}, and antennas were towed by hand on plastic sleds at approximately 0.5 m s^{-1}, resulting in traces being recorded every 2 cm in horizontal distance, approximately. GPR profiles were collected using a real-time kinematic (RTK) radio that transmitted at 418 MHz for 200 MHz profiles, resulting in 1–10 cm surface precision of profiles. The 400 MHz profiles were collected without an RTK system because the radio interfered with the 400 MHz antenna data, and we were unable to filter the signal without significantly degrading the data. Therefore, the 400 MHz data accuracy is estimated to have spatial uncertainty between 1 and 3 m. Scans were recorded for 150–250 ns TWTT (two-way travel time) with 1024 samples per scan, resulting in about 4 samples ns^{-1}. Given that the relative permittivity ($\dot{\varepsilon}$) in volcanic rock for McMurdo Station ranges between 6 and 12, which has associated wave velocities of 0.122–0.087 m ns^{-1} for lower to higher values of $\dot{\varepsilon}$, respectively, 50–60 samples m^{-1} were recorded vertically, which is more than sufficient to maintain a smooth waveform given the frequencies used. Range gain and high- and low-pass finite impulse response (FIR) filtering between 100–800 MHz were both applied during data collection.

Figure 3. Map of all GPR profiles collected at McMurdo Station in 2015 (*pink lines*). *Green circles* depict areas where soil pits were dug and *blue crosses* show the location of boreholes documented in Fenwick and Winkler (2016).



3.1.1 GPR post-processing

Profiles were post-processed using GSSI Radan Version 7.0 proprietary software. Post processing included time-zero correction, integration of GPS data into the files, horizontal filtering to remove ringing and the direct wave within the data, and stacking to improve signal-to-noise ratios and visualization of horizontal reflectors. GPS locations were interpolated between each GPS measurement by using Radan. We used the same software to pick boundaries between stratified and unstratified material; bedrock; and finite targets of interest, including areas of massive ice and buried utilities.

3.1.2 GPR interpretation and assumptions

We calibrated GPR depths by using available ground-truth data, which included pits excavated for this study and borehole logs from November to December 2015 (Fenwick and Winkle 2016). Approximately 40% of collected GPR transects were post-processed and translated for this study

along the location of the ground-truth data. These ground-truth points were generally within 1–2 m of GPR profiles, providing reasonable accuracy of structure and stratigraphic thicknesses, assuming changes in these structures did not occur within 1–2 m laterally. We linked stratigraphic thicknesses, apparent dip, orientations, and continuity of major horizons in pits (which were typically 3–10 m long) to similar features displayed within GPR profiles. We used typical $\acute{\varepsilon}$ values for permafrost (5.3), basalt (6–12), fill (6–12), and ice (3) to determine expected geophysical responses at interfaces between geological structures (Elshafie and Heggy 2012, 2013; Rust et al. 1999). Waveform polarity of the first three half cycles results from an interface between two materials that have $\acute{\varepsilon}$ contrasts. When a positive (+ − +) triplet occurs, it suggests that the deeper layer has a higher $\acute{\varepsilon}$; and when a negative (− + −) triplet occurs, it suggests that the deeper layer has a lower $\acute{\varepsilon}$, each relative to the shallower layer. For example, massive ice buried below frozen till would display a negative triplet response because of the transition from higher to lower $\acute{\varepsilon}$. Recognizing that there is some overlap of $\acute{\varepsilon}$ values between different geological materials, we attempted to incorporate other geophysical methods into estimates of $\acute{\varepsilon}$. We used migration and diffraction analyses of GPR profiles to confirm or provide ranges for $\acute{\varepsilon}$ and therefore associated wave velocities and depths of features imaged using GPR. Surface diffractions and migrations consistently estimated values of $\acute{\varepsilon}$ between 8 and 12, which is consistent with erosion-resistant basalts (Elshafie and Heggy 2012, 2013). These assumptions and calculations were used in areas where GPR profiles were collected but ground-truth information was not available.

Following the geophysical and ground-truth assumptions above, we also applied geomorphological and geological knowledge of near-surface structures to our GPR interpretations. For example, we assumed that horizontal and relatively continuous horizons were anthropogenically altered and layered fill or stratified fine-grain materials. In contrast, regions that exhibited unstratified or discontinuous horizons and numerous diffractions or hyperbolas were interpreted as buried undisturbed till or heavily fractured and weathered bedrock. These assumptions were based on the expected physical responses from GPR in till and bedrock environments (e.g., Arcone et al. 2014). Because of the heavily fractured and variable or rough exposed bedrock surfaces surrounding McMurdo, we developed a strategy to interpret bedrock horizons under stratified or unstratified material

through two primarily assumptions. First, we assumed that consistent terminations of stratified till against an unconformity was likely a bedrock contact. Second, the interface between fill and bedrock often consisted of discrete but multiple hyperbolas that created a relatively continuous horizon, suggesting a rough but definitive surface between the overburden matrix relative to material below. Multiple ground-truth points where bedrock outcrops occur at or near the surface in McMurdo support our interpretation that these geophysical signatures likely do represent a fill and bedrock contact. Finally, GPR profiles over surface-exposed bedrock revealed high attenuation rates, suggesting that below a fill–bedrock horizon, signal penetration would significantly diminish. Therefore, in some cases, we used a combination of the horizon triplet response, diffractions, and high attenuation below the horizon as grounds for bedrock interpretations.

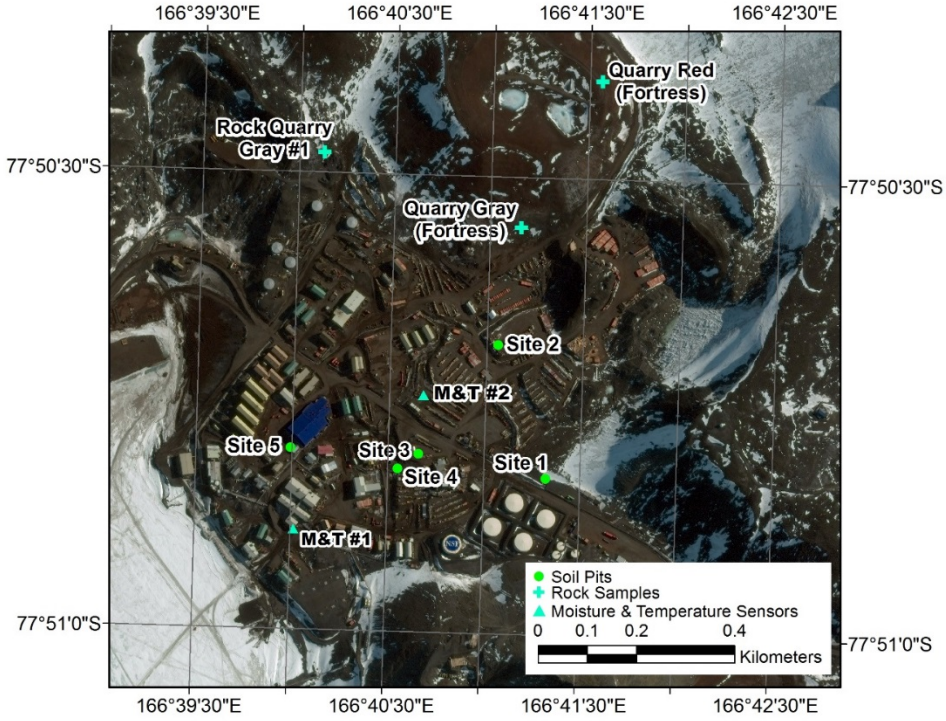
The interpretation method above results in a classification that distinguishes between stratified fill (such as road fill), unstratified material (such as naturally deposited till or heavily fractured bedrock), and structurally sound bedrock. We note that in most cases, bedrock interpretations have a greater uncertainty in terms of depth and actual interpretation relative to stratified and unstratified fill. This is because most ground truth does not extend to bedrock depth, the depth of bedrock is near the maximum depth of penetration for either GPR antenna, and the depth of bedrock integrates errors associated with average wave velocities dependent on a locally variable $\acute{\varepsilon}$ for the material above.

3.2 Excavation of pits

Soil pits were excavated in selected locations to provide visual observation and characterization of subsurface material conditions (Figure 4, also shown in Appendix B). This method was chosen over other methods such as coring because of (1) logistical simplicity (heavy equipment already existed on-site for operation and future construction) and (2) the ability to examine the extent of the lateral stratigraphy. Excavation of pits was allowed only in areas that would not interfere with operations, logistics, and public safety. The pits were dug on 23 and 24 December 2015, and on 11 January 2016 by using a heavy-duty excavator (Caterpillar 336E) with the bucket for digging the materials and ripper and hydraulic hammer attachments for breaking the hard layer. Five excavation pits were dug. Sites 1

and 3 were dug down to 1.5 to 1.7 m below the ground level (bgl), respectively, with a 4.6 m by 1.8 m surface trench size. Site 2 was excavated down to 3.25 m bgl, and Sites 4 and 5 were dug down to 3.05 m bgl, with approximately a 12 m by 4 m surface trench size for Sites 2, 4, and 5. With firm frozen material, two sides of the excavated trench provided relatively vertical profiles, allowing visual observation and quantitative subsurface conditions; and representative samples of the materials were extracted at various depths. The characterization included background information, soil indices, subsurface features, and ice characteristics.

Figure 4. Map illustrating the locations of the soil pits and rock samples collected at McMurdo Station in this study. M&T #1 and M&T #2 stand for moisture and temperature sensors locations.



3.2.1 Visual assessment

We characterized the soil pit profile based on visual characterizations for describing frozen soils (ASTM 2016 [ASTM D4083-89]; Andersland and Ladanyi 1994) (Table 2) and took pictures of each profile as part of the visual survey. Because much of McMurdo Station was built on fill materials to develop flat grounds for buildings, pads, and roads, fill materials varied in depths as noted in this study.

Table 2. Frozen soil and subsurface strata classification used in the study (ASTM 2016; Andersland and Ladanyi 1994).

Subsurface State	Major Group Description (Designation)	Subgroup Description (Designation)
Frozen soil	Segregated ice not visible by eye (N)	Poorly bonded or friable (Nf)
		Well bonded, no excess ice (Nbn)
		Well bonded, excess ice (Nbe)
	Segregated ice visible by eye - ice less than 25 mm thick (V)	Individual ice crystals or inclusions (Vx)
		Ice coatings on particles (Vc)
		Random or irregularly oriented ice formations (Vr)
		Stratified or distinctly oriented ice formations (Vs)
		Uniformly distributed ice formations (Vu)
Substantial Ice strata	Ice greater than 25 mm thick (Ice)	Ice with soil inclusions (Ice + soil type)
		Ice without soil inclusions (Ice)

Ice/Soil Symbols



Definitions:

Candled ice is ice that has rotted or otherwise formed into long columnar crystals and is very loosely bonded together.
Clear ice is transparent and contains only a moderate number of air bubbles.
Cloudy ice is translucent but essentially sound and non-pervious.
Friable denotes a condition where material is easily broken up under light to moderate pressure.
Granular ice is composed of coarse (more or less equidimensional) weakly bonded together ice crystals.
Ice coatings on particles are discernable layers of ice found on or below the larger soil particles in a frozen soil mass.
Ice crystals are very small individual ice particles visible in the face of a soil mass. Crystals may be present alone or in a combination with other ice formations.
Ice inclusions are individual ice masses visible in the face of a soil mass. Inclusions may be present alone or in a combination with other ice formations.
Ice lenses are ground ice features or lenticular ice formations in soil, generally normal to the direction of the heat loss and commonly in repeated layers.
Ice segregation is the growth of ice as distinct lenses, layers, veins, and masses in soils, commonly but not always oriented normal to direction of heat loss.
Massive ice is a large mass of ice, typically nearly pure and relatively homogenous.
Poorly bonded signifies that the soil particles or materials are weakly held together by ice and that the frozen soil has poor resistance to chipping or breaking.
Thaw-stable frozen soils are soils that when thawed would not lose their strength below normal conditions and would not produce detrimental settlement.
Thaw-unstable frozen soils are soils that when thawed would lose their strength below normal and would produce significant and detrimental settlement because of the melting of the excess ice in the soil.
Well bonded signifies that the soil particles are strongly held or cemented together by the ice and that the frozen soil possesses relatively high resistance to chipping or breaking (without the aid of heavy equipment).

3.2.2 Ice density

In pits where massive ice was found, we collected ice samples at various depths and immediately preserved them in −10°C cold rooms in Crary Lab, an in-house laboratory at the Station. Ice samples were trimmed with a saw in the cold room and then were measured with a caliper and weighted to calculate the mass and volume for density estimates. Sediments in the ice were quantified for earth-material inclusions by drying the ice samples and weighting the materials left.

3.2.3 Rock density

Aside from ice, a significant amount of materials at McMurdo consists of fractured boulders and rocks. The density of fractured basalts vary and is attributed in the way they were formed from harder crystalline rocks (gray color) to less dense vesicular rocks (gray and red color) with tiny holes. This study randomly collected representative rock samples ranging from 1550 to 12,200 g in mass from the existing quarries as shown in Figure 4. The relative or bulk densities of the rocks were determined using the standard volume-displacement method (ASTM 2009a [ASTM D7263-09, Method A]) based on the relationship in Eq. (1):

$$\rho_r = M_r / ([M_r - M_{sub}]/\rho_w) \quad (1)$$

where

M_r = the mass of rock,
M_{sub} = the mass of rock in water, and
ρ_w = the density of water at the test temperature.

3.2.4 Soil gradation, moisture, density, and ice content

During the excavation, we obtained representative samples of thawed and frozen (chunk) materials, rock, and ice to determine soil index properties. The samples were taken immediately into a −10°C freezer in Crary Lab and were analyzed for grain size, moisture content, and density. The average mass of the samples was approximately 3330 g. A set of representative samples was analyzed mainly for gravimetric moisture content by weighing the mass of samples before and after materials were oven-dried (ASTM 2010 [ASTM D D2216-10]) and then for grain size (ASTM 2009b [ASTM

D6913-04]) as characterized based on Unified Soil Classification System (USCS) engineering identification. For frozen samples, we conducted density analyses and then oven-dried the sample for moisture content and grain-size analyses.

The total gravimetric moisture content (w_t) of soil is composed of ice (visible ice and invisible pore ice) plus the unfrozen water inclusions between mineral aggregates relative to mass of the dry soil (after the soil is dried in the oven). The calculation for estimating total gravimetric water contents was as follows (Andersland and Ladanyi 1994; Holtz and Kovacs 1981):

$$w_t = (M_t / M_s)100 \quad (2)$$

where

M_t = weight of the ice (visible and invisible) and
M_s = the weight of the dry soil.

Frozen earth materials with gravimetric moisture values greater than 100% are considered soils with significant amounts of ice in the soil matrix. Conversion from gravimetric moisture content to total volumetric water content can be found in Kanevskiy et al. (2013).

In frozen soil, bulk density is associated with mass–volume relationships of the soil as a function of particles, pore space, ice, unfrozen water, and air. Dry density is the in situ density of the frozen materials after it is fully dried. Both bulk and dry densities provide indication of whether the soil is loose or dense. Likewise, total volumetric water content is determined from the mass–volume relationships. The relationships among soil phases can be applied to frozen soils in terms of void ratio, porosity, and degree of saturation (Andersland and Ladanyi 1994).

Density of the sample was taken using the water displacement method—the frozen sample was coated with paraffin in a cold room; the sample was weighed before and after the coating was applied and in submerged water for volume displacement (ASTM 2009a [ASTM D7263-09, Method A]). Once the paraffin was peeled off, the sample was oven dried for moisture content and grain size analyses. Bulk density (ρ_m) of the frozen material

was determined using this relationship (ASTM 2009a [ASTM D7263-09, Method A]):

$$\rho_m = M_t/[([M_c - M_{sub}]/\rho_w) - ([M_c - M_t]/\rho_p)] \quad (3)$$

where

M_t = mass of wet or frozen soil specimen,
M_c = the mass paraffin-coated specimen,
M_{sub} = the mass of wax-coated specimen in water,
ρ_p = the density of the paraffin, and
ρ_w = the density of water at test temperature.

The dry density of the specimen was calculated from the bulk density and moisture content.

In an unfrozen soil state, a 100% saturation indicates a fully saturated soil where voids are filled between aggregates. For frozen soil, the degree of saturation represents what percentage of the total void's volume is filled with ice. The corresponding degree of saturation with ice, S_i, defined as the ratio of ice volume to pore volume in frozen soil, is given by Andersland and Ladanyi (1994):

$$S_i = w_t G_s \rho_w / \rho_i e_t \quad (4)$$

where

w_t = the water or ice content in the soil,
G_s = the specific gravity of soil materials (assuming a value of 2.70), and
ρ_i = the density of ice (0.9168 g/cc at 0°C).

The total void ratio is calculated as

$$e_t = V_v / V_s \quad (5)$$

where

V_v = the total volume of voids and
V_s = the volume of solids.

For gravelly sand materials, the fines (i.e., amount finer than 0.02 mm) and the void ratio value are required to provide an indication of whether the soil is possibly frost susceptible or not. Also, the void ratio value, e_t, provides an estimate of the fraction of ice with respect to the soil (or whether the ice-cemented material has more ice than soil), assuming the volume of voids is totally filled with ice. In many cases, frozen soil would exhibit S_i values greater than 100% because the volume of ice in the soil could exceeded the total pore volume due to large ice inclusions or massive-ice deposits that the ground have under natural conditions (Andersland and Ladanyi 1994).

The total volumetric ice content (V_{ice}) in the ice-rich soil can then be calculated using total porosity, n_t, and degree of saturation, S_i, as follows:

$$V_{ice} = S_i \, n_t \tag{6}$$

where S_i is Eq. (4) and the total porosity, n_t, is

$$n_t = V_v / V_t \tag{7}$$

as the ratio of total volume of voids to the total volume of the materials, expressed in percent.

The total volumetric ice content (V_{ice}) is written by substituting Eqs. (4) and (7) into Eq. (6) as

$$V_{ice} = [(w_t \, G_s \, \rho_w) / (\rho_i \, e_t)] \, (V_v / V_t). \tag{8}$$

Another approach for calculating the total volumetric water or ice content of fully saturated soils is by converting the gravimetric moisture content and assuming the total volumetric water content is equal to the total soil porosity (Kanevskiy et al. 2013; Campbell et al. 1994). Using a G_s value of 2.70, conversion from gravimetric moisture content to total volumetric ice content can be found as (Kanevskiy et al. 2013)

$$V_{ice} = (2.7w_t + V_i)(1 + 2.7w_t) \quad (9)$$

where w_t is the water or ice content in the soil and V_i is the volume of visible ice.

This study used Eq. (8) to calculate the total volumetric water or ice content from density samples and Eq. (9) for estimating the total volumetric water or ice content from gravimetric water content samples.

3.3 Soil-moisture and soil-temperature instrumentation

Soil-temperature and soil-moisture probes were installed at two locations on Station (Affleck et al 2012). One was installed on a partially shadowed, gently sloping area near a building (M&T #1) and the other was on an open flat pad (M&T #2), as shown in Figure 4. Temperature probes (thermocouples) fabricated by the U.S. Army Cold Regions Research and Engineering Laboratory (CRREL) were attached on a wooden dowel to maintain the spacing and were installed in early December 2009 to measure the soil-temperature profiles. Soil-temperature profiles were taken at depths of 0 (at the ground level), 76, 150, 305, 460, and 610 mm bgl. Data collection was conducted with continuous readings (using a datalogger) during austral summer months in 2009–10, 2010–11 and 2015–16, except the sensors were damaged at the M&T #2 site in 2015–16.

Adjacent to the soil-temperature sensors (Figure 4), the tube to insert the soil-moisture probes was installed in early December 2009 to measure a continuous volumetric soil-moisture changes (Affleck et al 2012). PR2 probes, made by Delta-T Devices Ltd., were used for detecting the soil-moisture content by volume (%vol. or m^3/m^3) by transmitting electromagnetic fields radially approximately 100 mm into the soil. The PR2 probe has been used in unfrozen and frozen soils for providing relative changes in soil moisture with time at specific depths. Data collection was conducted during austral summer months only (2009–10, 2010–11, and 2015–16) with daily continuous readings.

4 Results

4.1 Pit profiles

We found distinct features in the soil pits, as shown in the example photographs in Figures 5–9 of the entire pit with segregated ice at Site 1, massive ice at Site 2 and Site 4, man-made fill at Site 3, and ice lenses at Site 5.

Figure 5. Ice-rich soil at Site 1.



Figure 6. Buried massive ice at Site 2.



Figure 7. and buried massive ice at Site 4.



Figure 8. Man-made fill with buried contaminations at Site 3.



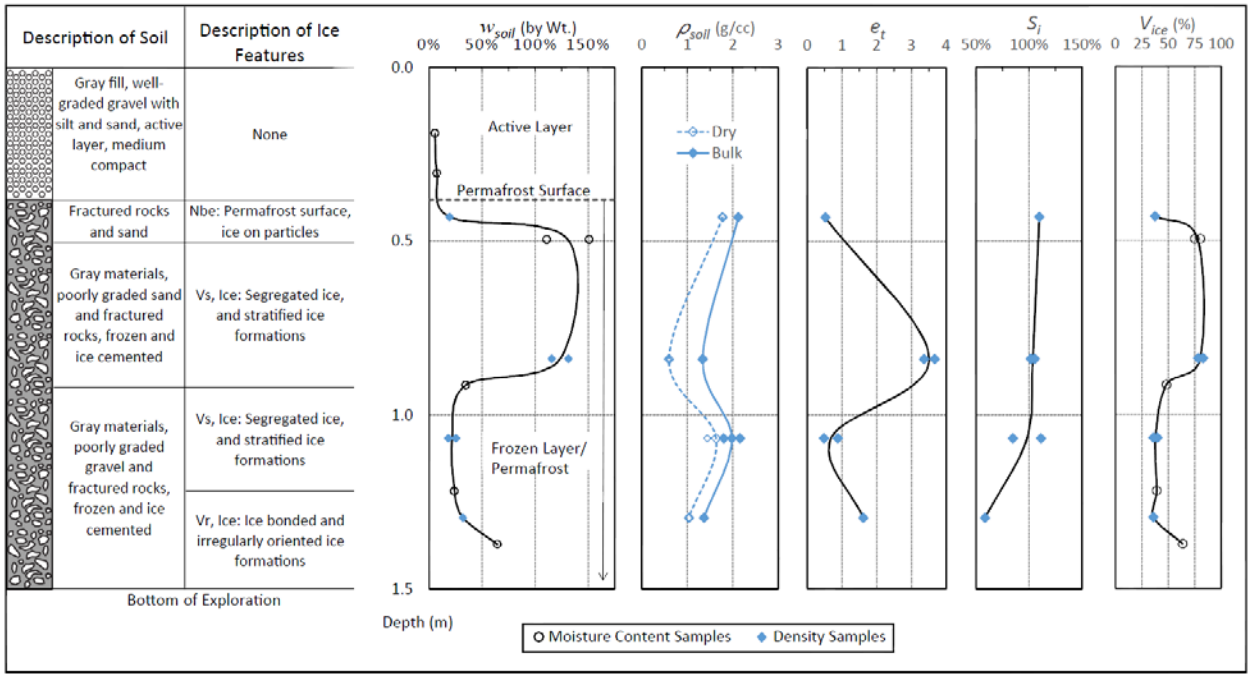
Figure 9. Reddish fill on the top and gray fractured rock with ice lenses at Site 5.



4.1.1 Site 1

At Site 1, the thawed or active layer during the excavation was approximately from the surface down to 0.3 m; and ice lenses (mainly segregated ice) were found just below 0.3 m (Figure 10). The excavator was able to scoop down to 0.46 m; and from 0.46 to 1.5 m, the hammer was used to break the materials. Visual analysis indicated that a mechanically constructed layer stretched from the surface down to between 0.3 and 0.45 m. Below the surface layer was ice-rich glacial till of a coarse-stratified layer, which was composed of a conglomeration of fractured basaltic boulders, rocks, gravelly sand, and ice. Within the excavation opening, there was no apparent spatial or horizontal pattern in the distribution of ice lenses in the soils. The segregated and stratified ice formations were irregularly distributed throughout the profile (Figure 10).

Figure 10. Cross section of Site 1 showing profile descriptions, soil indices, and ice properties.

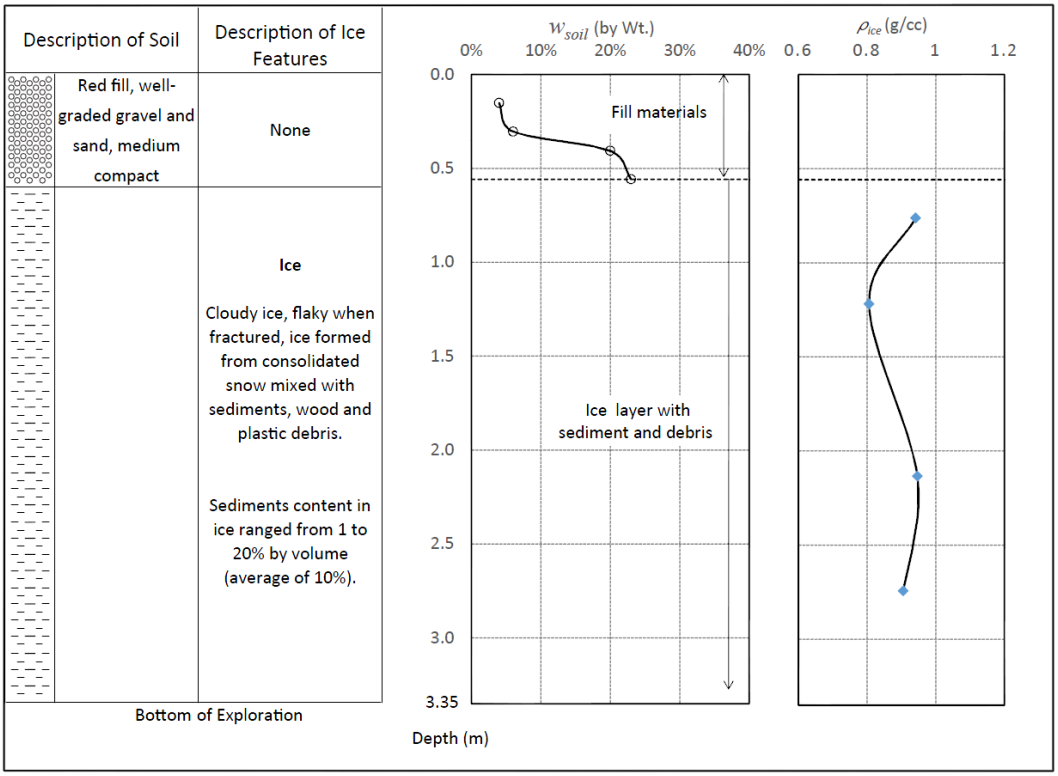


4.1.2 Site 2

The material on the surface at Site 2 was mostly reddish fine sand and was littered with wood chips. From the visual analysis, the top 0.61 m consisted of a man-made fill of reddish fine sand material; and a massive-ice layer was encountered at 0.61 m from a man-made deposit of snow or ice from a consolidated snow deposit (Figure 11). This area was used as a snow

dump to pile snow every year until 1995 (Ames 2015). During that time, the ground was bladed to expose snow in the summer months as part of the process to melt the snow. As the snow layer became stable, fill materials were placed; and the area is now used as a storage pad. The ice layer from 0.61 to 3.35 m was mixed with rocks, sediments, and debris (i.e., wood chips and plastic materials). The ice was flakey with some platy-like chunks when excavated (Figure 11).

Figure 11. Cross section of Site 2 showing profile descriptions, soil indices, and ice properties.

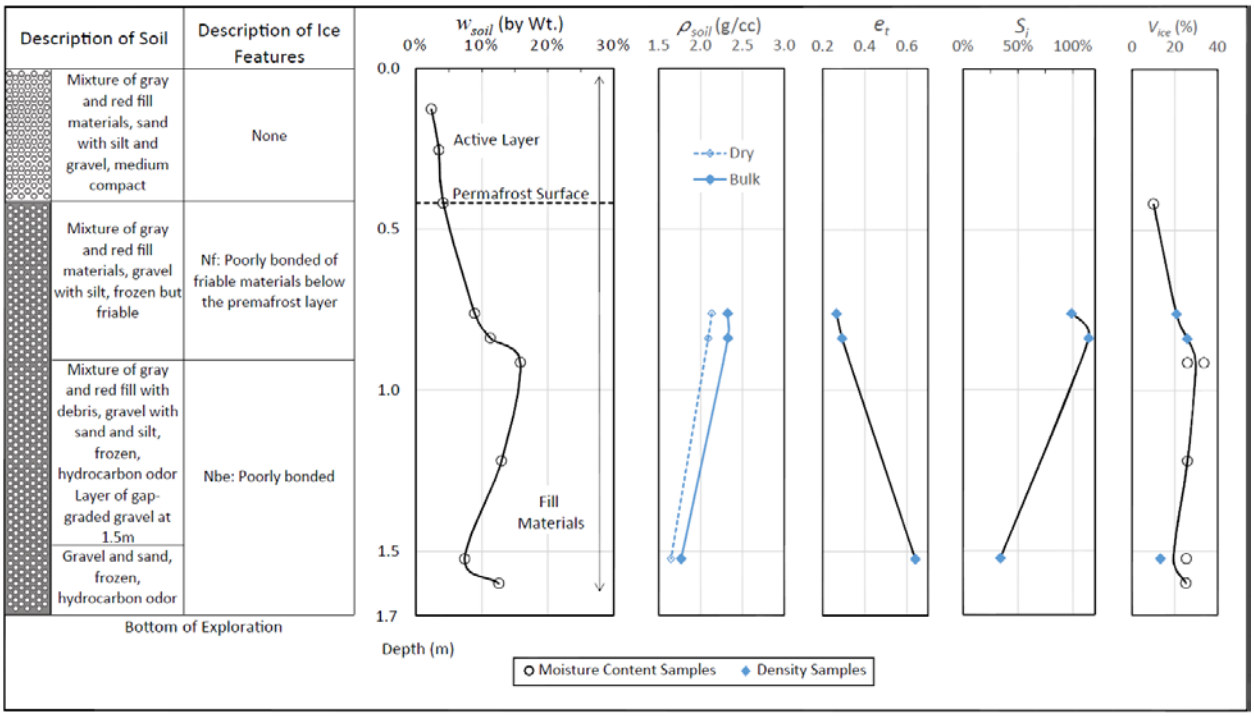


4.1.3 Site 3

Based on the visual survey of Site 3 (Figure 12), the material in the top 0.15 m was composed of a mixture of gray and light brown fine sand with small rocks. The active layer was down to 0.61 m; at the permafrost table, the material was friable with pickax or hand shovel and was very easy to crumble with hand pressure. Hydrocarbon odor in the soil was encountered while digging. Because wood debris was found at various profiles and at the bottom of the pit at a 1.68 m depth, it is probable that polluted soils were used in the fill, hydrocarbons and other pollutants were buried in the

fill, or a spill occurred at the site (Figure 12). Extensive contaminant monitoring and sampling studies across the entire station were conducted by Texas A&M (Kennicutt et al. 2010; Klein et al. 2004, 2012) for several years to examine the spatial extent and variability of contamination in soils; however, soil samples used for their study were limited to the upper 0.02–0.055 m depth. According to Kennicutt et al. (2010) and Klein et al. (2004, 2012), this location was one of the hot spots from fuel spills; and spatial analyses revealed that the soil surface at this location contained total petroleum hydrocarbons in excess of 500 parts per million (ppm). Potential migration of contaminants are likely to penetrate into the permafrost or frozen soils due to soil-moisture migration in the active layer of porous soil. No information exists on how deep the man-made fill is at this location; however, we believe that the fill is variable.

Figure 12. Cross section of Site 3 showing profile descriptions, soil indices, and ice properties.

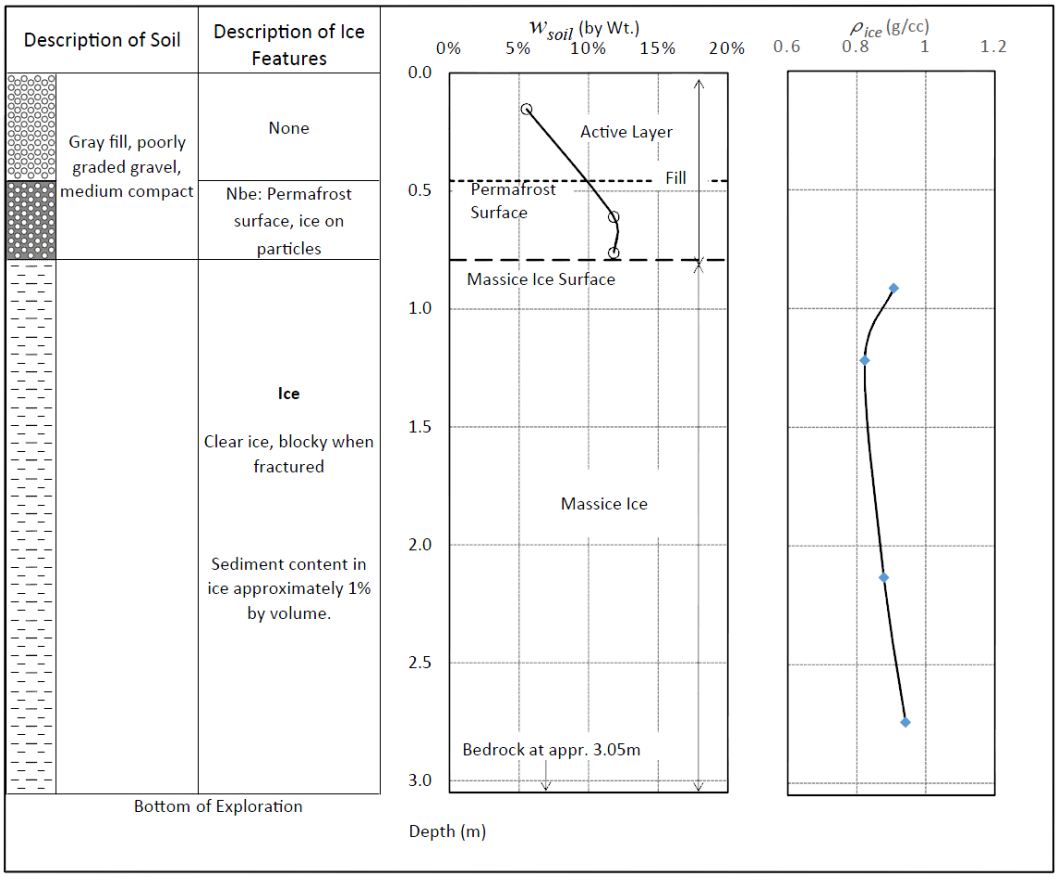


4.1.4 Site 4

Massive ice was found at Site 4 between 0.38 and 0.76 m from the surface soil fill, as shown in Figure 13, and the ice extended to the bottom of the pit, as shown in Figure 5 (Site 4 photo). The massive ice below was likely formed from meltwater or ephemeral surface flow that seasonally pooled and froze in the area; the ice consisted of several layers of seasonal melt

and freezing cycles. The ice layers were clear ice with visible tiny voids from air bubbles and no foreign debris in the ice (Figure 13). In each layer, the ice was sandwiched with fine sediments. During the excavation, the ice broke in irregular big chunks (not small and crumbly). A hard rock (gray basaltic material) layer was found below the massive ice at the bottom of the pit approximately at 3.05 m bgl.

Figure 13. Cross section of Site 4 showing profile descriptions, soil indices, and ice properties.

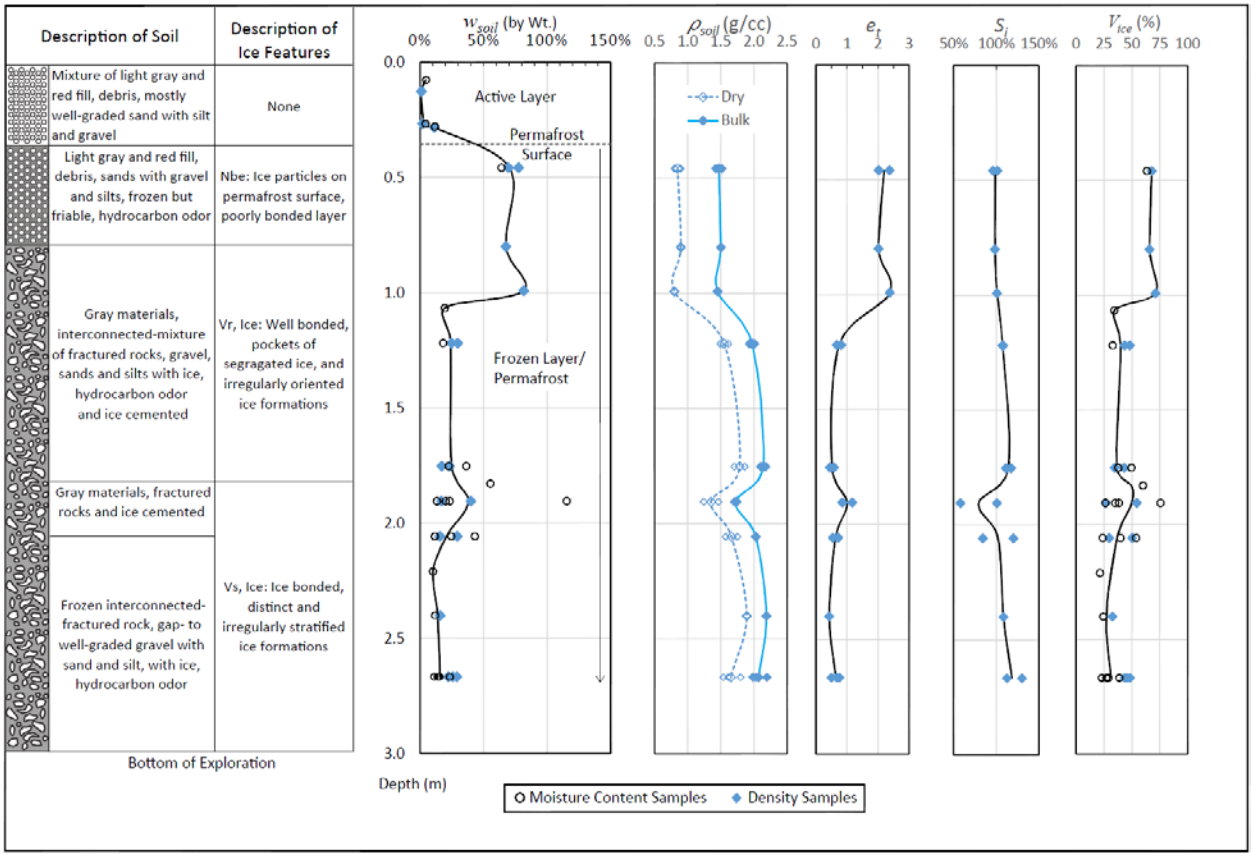


4.1.5 Site 5

At Site 5 (Figure 14), the top 0.23 m was composed of reddish fine fill; and a mixture of red and gray fill materials was encountered down to 0.36 m. The bottom of the active layer was at 0.36 m. Hydrocarbon odor in the soil was encountered while digging the permafrost. Also, according to spatial analyses of Kennicutt et al. (2010) and Klein et al. (2012) of contamination in soils at the surface, this area was mapped with total petroleum hydrocarbons in excess of 500 ppm but below 1000 ppm. Potential migration of

contaminants is likely to penetrate into the permafrost or frozen soils because distinct and strong off-gas of hydrocarbons were observed when samples taken at 2.70 m were stored and oven dried. Ice lenses were visible at approximately 0.46 m, and the ground was hard to excavate with the bucket; a ripper attachment was used to loosen the materials. An ice-cemented layer of stratified glacial till was found at approximately 1.37 m; this layer was composed of interconnected boulders, rock, gravelly sand, and ice materials (Figure 14). This layer was much harder to loosen and excavate with the ripper than the layer above it; a hammer attachment was used to break the layer of ice-rich boulder, rock, and gravel materials. In the trench and along the horizon cut, there was no apparent spatial or horizontal pattern in the distribution of excess ice in the soils. The layers were well bonded with segregated and stratified ice formations that were irregularly distributed throughout the profile.

Figure 14. Cross section of Site 5 showing profile descriptions, soil indices, and ice properties.



4.2 Soil gradation

Particle size and shape are related to pore space and water-holding capacity, which characterize the soil conditions. Soils collected are generally coarse-grained soil, such as gravel and sands fragments. This gradation study analyzed gravelly sand earth fractions(i.e., small rocks or gravel sizes less than 300 mm), which are summarized in Tables 3 and 4 (and the graphical format is shown in Appendix C). As characterized in USCS types, the soil included

- well-graded gravel (GW) and well-graded gravel with silt and sands (GW-GM),
- poorly graded gravel (GP) and poorly graded gravel with silt and sands (GP-GM),
- well-graded sands (SW) and well-graded sand with silt (SW-SM), and
- poorly graded sands (SP) and poorly graded sand with silt (SP-SM).

These coarse-grained materials were typified as angular and subangular grains. The silt contents were relatively low; but the values were somewhat higher at 0.5–1.23 m in the undisturbed locations (i.e., Sites 1 and 5), especially at the base of the active layer into the well-bonded and stratified ice formation horizons. Sites 2, 3, and 4 contained mechanically (man-made) constructed fill that consisted of local reddish and gray materials.

Table 3. Particle size distribution (%) at Sites 1–3 for the gravelly sand earth fractions of the soils collected at various depths and the corresponding USCS identification.

Depth, m	Samples	Cobbles	Gravel		Sand			Silt	Unified Soil Classification System (USCS) Type
			Coarse	Fine	Coarse	Medium	Fine		
		>76 mm	75-19 mm	19-4.75 mm	4.75-2 mm	2-0.425 mm	0.425-0.075 mm	<0.074 mm	
Site 1									
0.15-0.23 (Fill)	MC		24	28	11	17	14	6	GW-GM
0.25-0.35	MC		30	27	10	16	10	7	GW-GM
0.41-0.46	D			7	31	38	20	4	SW
0.46-0.53	MC		2	22	15	28	21	12	SP-SM
0.76-0.91	D		21	15	11	25	18	10	SP-SM
0.76-0.91	D		15	16	12	27	19	11	SP-SM
0.91-1.22	D	22	23	12	7	12	18	6	GP-GM
0.91-1.22	D	85	6	2	2	2	2	1	GP
1.22-1.32	D	24	26	20	10	13	6	1	GP
Site 2 (Man-made or Constructed Fill)									
0.15-0.30	MC		14	29	16	20	14	7	SW-SM
0.41	MC		11	24	16	24	17	8	SW-SM
0.41-0.56	MC		25	20	14	16	7	3	GP
Site 3 (Man-made or Constructed Fill)									
0.10-0.15	MC		8	26	16	25	16	9	SW-SM
0.2-0.30	MC		17	15	15	24	23	6	SP-SM
0.38-0.46	MC		21	20	14	22	18	5	SP-SM
0.61-0.91	D	10	24	24	13	17	7	5	GW-GM
0.76-0.91	D	12	21	24	12	17	8	6	GW-GM
0.91	MC		45	18	8	14	10	5	GW-GM
1.22	MC		26	23	11	20	13	7	GP-GM
1.52	MC		20	18	15	29	17	1	SP
1.52	D	78	1	3	4	8	4	2	GP-GM
1.52-1.68	MC		4	19	16	32	19	10	SW-SM

Samples Description:

MC = from Moisture Content Samples

D = from Density Samples

Unified Soil Classification System (USCS) Description:

GP = Poorly graded gravel with sands

GP-GM = Poorly graded gravel with silt and sands

GW = Well-graded gravel with sand

GW-GM = Well-graded gravel with silt and sand

SM = Sand-silt with gravel

SP = Poorly graded sand with gravel and small amount of silt

SP-SM = Poorly graded sand with silt and gravel

SW = Well-graded sand with gravel

SW-SM = Well-graded sand with silt and gravel

Table 4. Particle size distribution (%) at Sites 4–5 of gravelly sand earth fractions of the soils collected at various depths and the corresponding USCS identification.

Depth, m	Samples	Cobbles	Gravel		Sand			Silt	Unified Soil Classification System (USCS) Type
			Coarse	Fine	Coarse	Medium	Fine		
		>76 mm	75-19 mm	19-4.75 mm	4.75-2 mm	2-0.425 mm	0.425-0.075 mm	<0.074 mm	
Site 4 (Man-made or Constructed Fill)									
0.61-0.76	D	97		1	1		1		GP
Site 5									
0.025-0.10 (Fill)	MC		18	18	13	21	21	9	SP-SM
0.23-0.33 (Fill)	MC		7	17	19	30	20	7	SW-SM
0.25-0.33 (Fill)	MC		8	20	16	28	19	9	SW-SM
0.46	MC		13	18	14	27	21	7	SP-SM
0.46	D	19	4	16	12	23	21	5	SP-SM
0.46	D		12	11	12	28	31	6	SP-SM
0.76-0.84	D		7	14	14	26	28	11	SP-SM
1.0-1.14	MC		6	16	15	29	18	16	SM
1.23	MC		25	12	13	22	15	13	SM
1.23	D		11	18	15	27	21	8	SP-SM
1.68-1.83	D		4	7	15	45	19	10	SW-SM
1.68-1.83	MC	19	34	21	8	10	5	3	GW
1.68-1.83	D	70	6	8	5	7	3	1	GP
1.83-1.98	MC		47	20	8	14	8	3	GW
1.83-1.98	D		43	27	10	13	5	2	GW
1.83-1.98	MC	24	39	16	5	10	4	2	GP
1.98-2.13	MC	18	43	16	6	8	6	3	GW
1.98-2.13	MC		42	26	9	13	6	4	GW
1.52-2.13	MC		21	32	15	19	8	5	GW-GM
1.98-2.13	MC		27	23	18	21	7	4	GW
1.98-2.13	MC	43	25	9	5	10	5	3	GP-GM
Below 2 m	D		22	18	13	30	12	5	SW-SM
Below 2 m	D		18	16	11	26	9	20	SM
2.13-2.29	MC	50	20	11	5	8	3	3	GP-GM
2.29-2.44	MC	32	24	12	8	13	7	4	GP-GM
2.29-2.44	D		82	8	3	4	3	0	GP
2.59-2.74	MC		19	22	18	29	8	4	SP
2.59-2.74	MC		8	15	23	34	16	4	SP

Samples Description:

MC = from Moisture Content Samples

D = from Density Samples

Unified Soil Classification System (USCS) Description:

GP = Poorly graded gravel with sands

GP-GM = Poorly graded gravel with silt and sands

GW = Well-graded gravel with sand

GW-GM = Well-graded gravel with silt and sand

SM = Sand-silt with gravel

SP = Poorly graded sand with gravel and small amount of silt

SP-SM = Poorly graded sand with silt and gravel

SW = Well-graded sand with gravel

SW-SM = Well-graded sand with silt and gravel

4.3 Moisture content by weight

The soil-moisture contents were very low (<12%) in the upper horizons of the active layer and increased significantly towards the permafrost table. There was a significant increase in moisture content immediately below the permafrost table (i.e., Sites 1 and 5, Figure 10 and Figure 14) with evidence that the pore spaces were occupied with both segregated and stratified ice in the soil matrix. The water contents at 0.5–1.0 m deep for Site 1 ranged from 110% to 150% (Figure 10) and between 64% and 82% at Site 5 (Figure 14); these indicated significant amounts of excess ice interlayered with soil in the horizon. The lower portion of the frozen horizon, however, exhibited lower moisture content than in the upper horizons in the permafrost layer. For the man-made fill location (Site 3, Figure 12), the soil-moisture-content values between the active and frozen layers remained somewhat similar; however, soil-moisture content in the permafrost layers was significantly higher at Sites 1 and 5 (undisturbed glacial till) than at Site 3 (a fill location) by a factor of four in some cases.

4.4 Density and volumetric ratios of frozen materials

Density is associated with the mass–volume relationships of the soil particles, pore space, ice, unfrozen water, and air at a frozen state. The values for both bulk (i.e., density of frozen materials) and dry (frozen materials after they are fully dried) densities are indicative of the looseness or denseness of the soil. In general, the soil densities within the permafrost layer varied with depth (Figure 10, Figure 12, and Figure 14). Near the permafrost table for the natural glacial till layer, Site 1 had a relatively dense layer compared to Site 5; but the permafrost layer soil densities increased below 1 m at Site 5. The variability in soil densities reflected in the corresponding void ratio (Figure 10, Figure 12, and Figure 14) profiles. The void ratio values in the lower horizons (i.e., below 1 m) of the permafrost ranged from 0.4 to 1.2 and from 0.5 to 1.6 at Sites 5 and 1, respectively. The values of 0.70 for e_{max} (the loosest void ratio) and 0.13 for e_{min} (the densest void ratio) are typical of well-graded gravel with a sand, silt, and clay mixture (Andersland and Ladanyi 1994). Thus, the soils found in this study could be considered loose, based on typical values for e_{max}. The corresponding degree of saturation with ice, S_i, showed near or greater than 100% in some cases, indicating that the pores were fully filled with large ice inclusions or ice deposits in the soil (Figure 10 and Figure 14). Although the values for total volumetric ice con-

tent (V_{ice}) varied with depth, V_{ice} below the permafrost table in the undisturbed, natural glacial till for Sites 1 and 5 had much higher values than in the lower part of the permafrost. The total volumetric ice content (V_{ice}) for Site 1 within the ice-rich layer ranged from 36% to 83% while the variations at Site 5 were found to be between 21% and 75%. The variations at Site 3 for total volumetric ice content were within 10% and 34%. These values are similar to those measurements by Campbell et al. (1994) in the ice-cemented layers in the undisturbed and disturbed sites at the Scott Base area. The total volumetric ice content on the undisturbed natural glacial till showed much higher than man-made fill (disturbed, Figure 12) because excess ice had been removed when the soil was mechanically compacted during construction of the fill.

4.5 Density of rocks

The characteristics of the rock found across the Station (Figure 4) differed, from dense (gray basalt) rocks formed with much harder crystalline to less dense rocks with vesicular or tiny holes and an oxidized reddish color (Figure 15; Table 5). These rock samples were randomly collected to represent the predominant rock types from existing quarries and soil pits. The densest rocks from all samples collected in this study were from the samples collected in the pit at Site 5, with mean density of 2.65 g/cc. The next densest rocks were the gray rocks collected at the Rock Quarry Gray #1 (location northeast of Hut Point in Figure 4 where gray rocks are currently harvested for local use), with mean density of 2.48 g/cc. The typical density of basalt is 2.77 g/cc (Goodman 1980); thus, some of the rocks found in Site 5 (Table 5) had densities higher than the typical value of basalt. The mean density for the reddish materials from the Quarry Red (Fortress) that are harvested for local use was 1.96 g/cc; this value is significantly higher than the value reported in the early record of 1.18 g/cc by Knuth and Melendy (2012) and Affleck et al. (2012). The discrepancy in values from the previous record could potentially be due to the methodology used or a sampling error.

Figure 15. Mean relative density of various type of rocks collected at locations shown in Fig. 3. Error bars signify the (positive and negative) standard deviations from the mean.

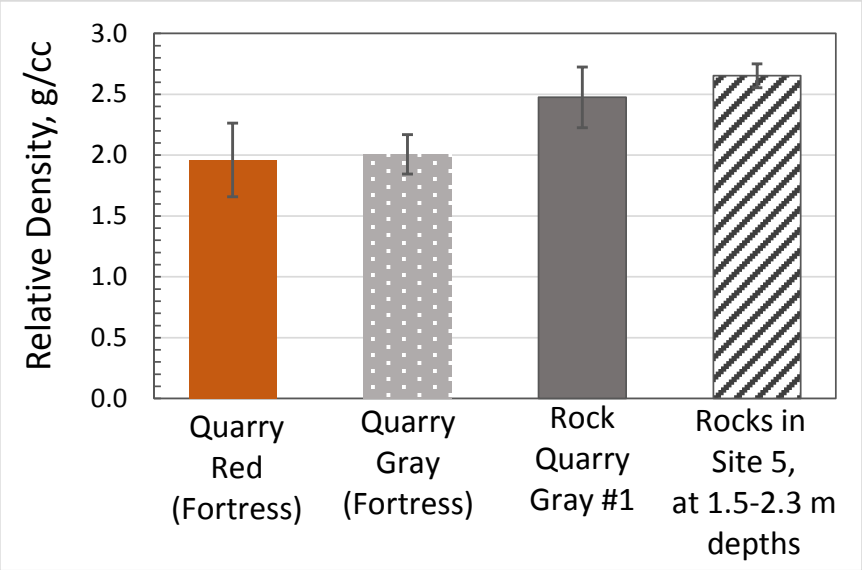


Table 5. Statistical summary of rock-sample density from various locations at McMurdo Station.

Locations	Color	Number of Samples	Minimum	Maximum	Mean	Standard Deviation	Standard Error Mean
			g/cc				
Quarry Red (Fortress)	Reddish brown, some with vesicles	25	1.35	2.49	1.96	0.30	0.06
Quarry Gray (Fortress)	Light gray to gray, some with vesicles	21	1.65	2.37	2.01	0.16	0.04
Rock Quarry Gray #1	Gray to darker gray basalt	27	1.66	2.73	2.48	0.25	0.06
Site 5 at 1.5–2.3 m depths	Mostly dark gray basalt	26	2.45	2.82	2.65	0.10	0.02

4.6 Ice characteristics

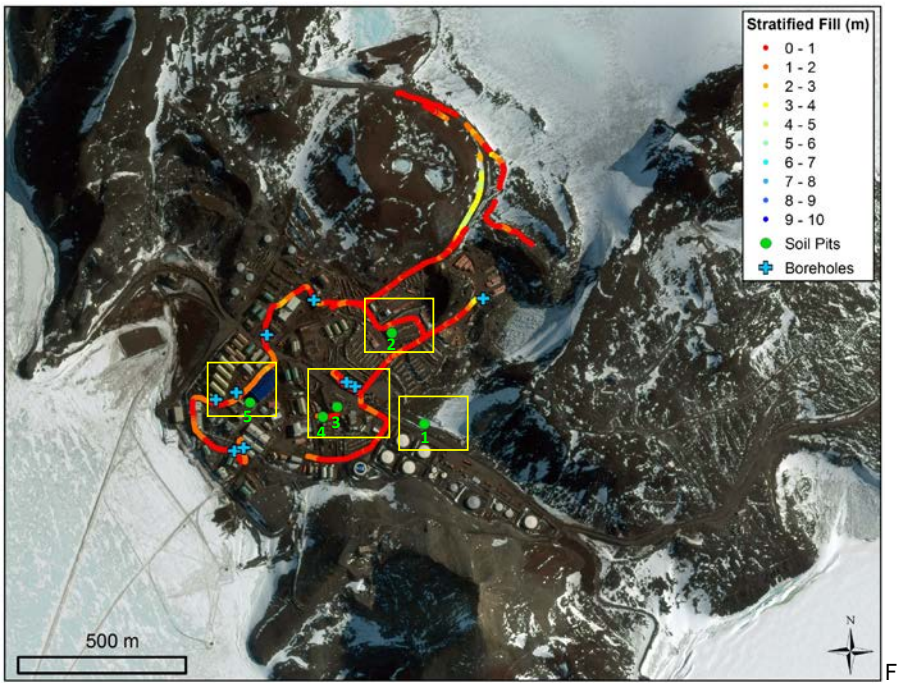
Although the density of the ice layer at Site 2 (Figure 11) and Site 4 (Figures 9 and 5) were somewhat similar (between 0.8 and 0.95 g/cc), the characteristics of the massive-ice layers encountered at both sites were distinct in how they were formed. The consolidated ice at Site 2 was formed from a man-made snow deposit while Site 4 was likely formed through a natural process from an ice melt or snowmelt deposit that froze seasonally.

The ice found at Site 2 was cloudy with debris and flaky when fractured or excavated. On the other hand, the ice found at Site 4 was clear or clean (no debris found) and blocky when fractured. The average sediments content in the ice at Site 2 contained 10% by volume while Site 4 contained only clear ice with 1% by volume of fine sediments. These pockets of massive ice likely extend laterally for several meters because this area is on a slope and adjacent to the toe of a steep embankment where subsurface drainage from snowmelt is potentially trapped. For design, it is important to determine where these pockets of massive ice are and to maintain their existing thermal regime for ground stability or remove the ice entirely.

4.7 GPR interpretation of bedrock and fill

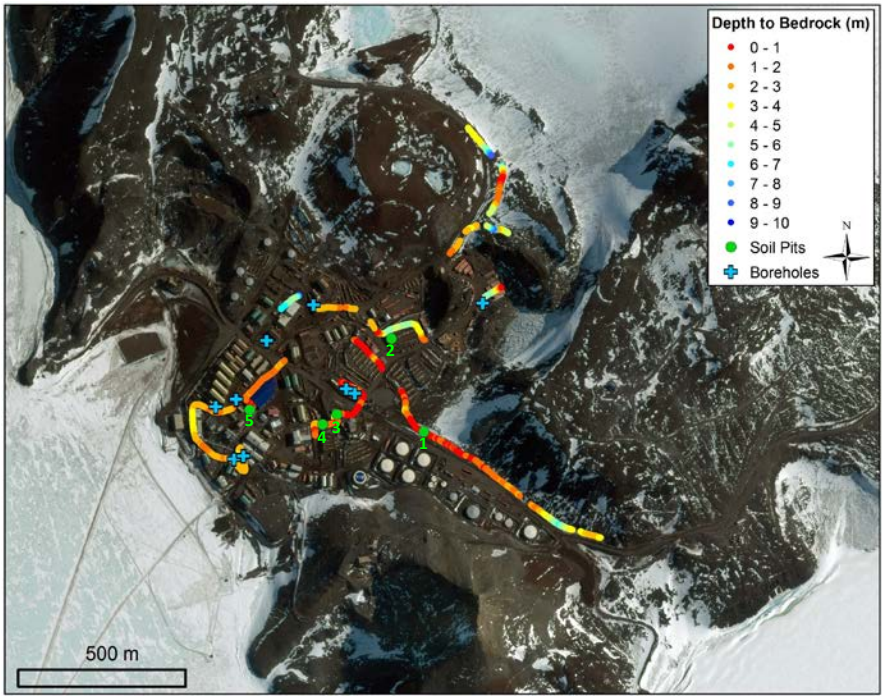
McMurdo Station is located on terrain that slopes to the south-southwest and is constrained by Observation Hill, Twin Crater, and Arrival Heights to the east, north, and west, respectively (Figure 1). In general, the station consists of a series of constructed fill or raised stratified sediment platforms placed over a sloping bedrock base to facilitate the construction of facilities or outside storage space (Figure 16). Roadways typically consist of a similar stratified fill to a 1–3 m depth over naturally unstratified till and heavily fractured bedrock (Figure 10). Depth to bedrock is highly variable, which is consistent with the rough outcrops situated around McMurdo (Figure 17), suggesting a rough, small-scale basin-and-trough structure. The variable thicknesses of anthropogenic fill is dependent on this rough bedrock surface; that is, fill was used to fill depressions between bedrock outcrops. Fill thickness tends to be greater towards the south, suggesting that the region closer to the ocean has been consistently built up or that through natural geomorphological processes fill is washed downhill towards the ocean, therefore creating thicker bedding relative to the upslope region. This interpretation is supported by numerous bedrock outcrops being exposed near T-Sit, and Main Street; but no bedrock outcrops are detected near the shoreline to the east and south of Winter Quarters Bay and McMurdo Station, respectively. The stratified fill layer is most easily identified by semi-parallel surface conformable horizon or horizons with crosscut at the surface due to construction activities following the initial filling effort. Boreholes and pits have revealed substantial ice within fill pore spaces and under fill.

Figure 16. Map of GPR profiles showing interpreted thickness of stratified fill. *Green circles* indicate the five soil pits dug in the area, *blue crosses* show boreholes dug near GPR profiles, and each *yellow box* shows the close-up map with the GPR profiles and pits comparison in Figs. 18, 20–25.



F

Figure 17. Map of GPR profiles showing interpreted depth to bedrock. *Green circles* indicate five soil pits dug in the area, and *blue crosses* show boreholes dug near GPR profiles.



Personnel who are familiar with McMurdo Station construction activities over the past few decades (Zellerhoff 2015) confirmed that many fill platforms have been constructed on solid snow or firn patches, likely resulting in metamorphosed ice under fill. Many dipping stratified horizons also terminate oblique to a rough and semi continuous horizon that is often characterized by a series of diffractions. We interpret this horizon to generally represent the solid bedrock contact below the stratified fill based on the unconformity, numerous diffractions, and generally higher relative attenuation below this horizon, which seems consistent with observations of GPR profiles collected over shallow bedrock on and immediately north of Main Street.

4.8 GPR and pits comparison

Profiles from two boreholes and five pits in Section 4.1 are used to verify the GPR profiles collected over and extending from each site. GPR profiles shown in this report are topography corrected.

4.8.1 Site 1

A 200 MHz GPR profile collected near pit 1 was 930 m long and oriented parallel to Main Street. The profile originated near the top of a fill pad situated north of Main Street and traversed to the valley between Observation Hill and T-Site Hill. The sole ground-truth pit extracted along this entire transect reveals a 0.5 m thick overburden of stratified fill with the top 0.3 m generally being thawed and the bottom 0.2 m being frozen (Figure 5). Below the overburden, a generally poorly sorted and ice-rich fractured rock matrix exists. The corresponding GPR profile (Figure 18) reveals two subparallel and continuous horizons between 0.3 and 0.5 m ($\acute{\varepsilon} = 8$), the lower of which we interpret to be a transition between the overburden to ice-rich fractured rock matrix. The parallel horizons we interpret to be stratified fill that has been worked by heavy equipment during construction operations. Minimal other reflections were visible below this horizon along the length of the GPR profile from its origin to the pit. We suggest that solid bedrock is likely deeper than we could image over the fill pad. However, further to the east, the profile significantly improves, showing very apparent multiple continuous horizons. We interpret these multiple horizons to be snow and ice residing over multiple layers of fill and eventually heavily fractured bedrock between 5 and 7 m depth Figure 19.

Figure 18. 200 MHz unprocessed GPR transect along Site 1 (*middle*) and translated profile (*bottom*) showing interpretation of fill and fractured rock over ice-rich fractured bedrock (*bottom*). Zoomed in map showing Site 1 (*top*) of box 1 from Fig. 16.

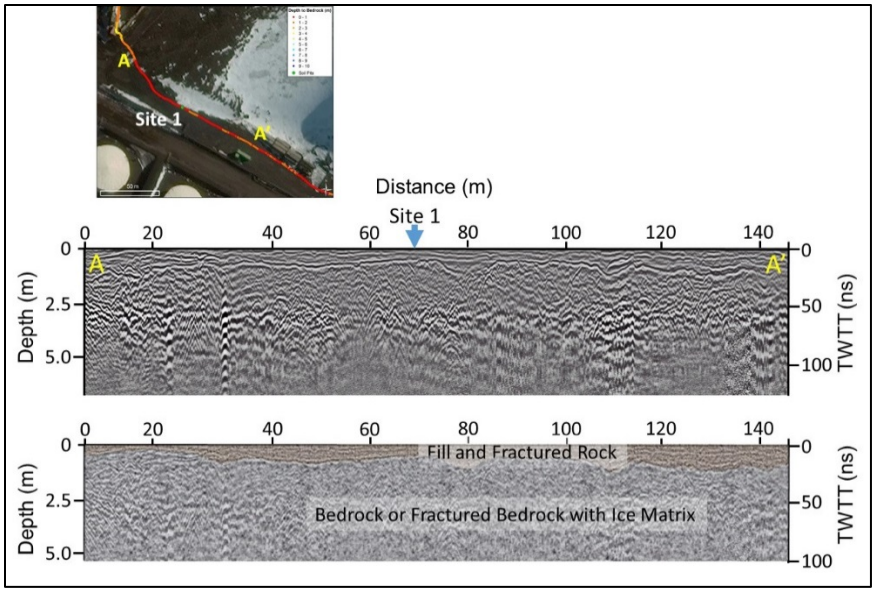
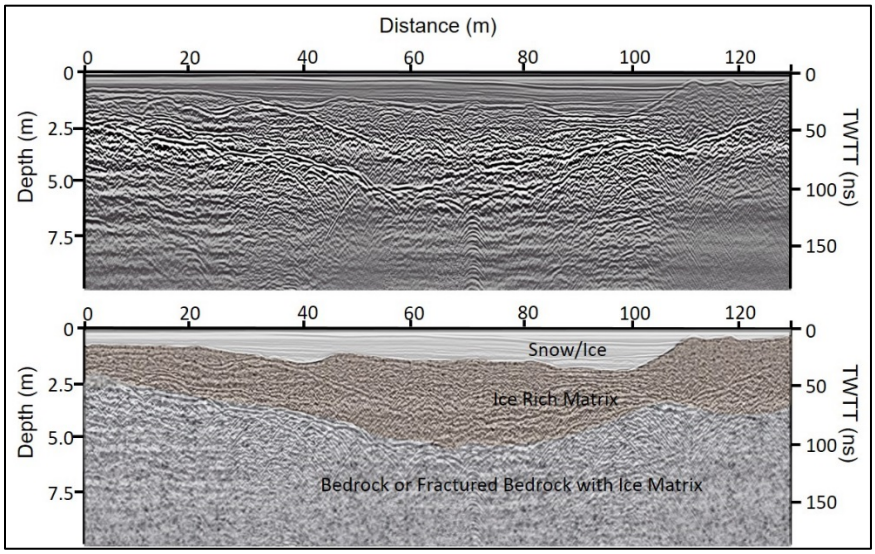


Figure 19. 200 MHz processed GPR profile (*top*) between T-Site and Observation Hill oriented parallel to and north of Main Street. Profile is located east of Site 1 where a ground truth pit was excavated. The interpretation (*bottom*) shows snow and ice over a stratified ice-rich matrix, and bedrock at greater depths.

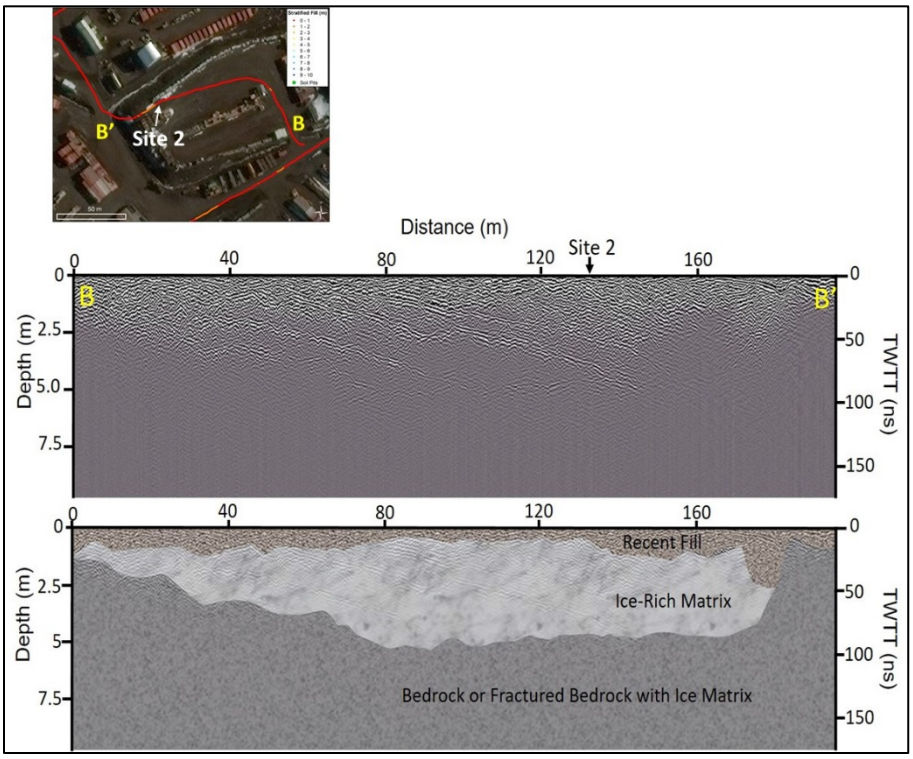


4.8.2 Site 2

At Site 2, a borehole and pit were both excavated for comparison to GPR profiles (Figure 11). This site is located on a raised pad towards the northern region of McMurdo Station. Information from the pit at Site 2 and

borehole by Fenwick and Winkler (2016) revealed dipping and stratified sediment within a predominantly ice-rich matrix to 3.35 m and 2.21 m, respectively. A 200 MHz GPR profile across the pit and borehole reveal two major dipping horizons, suggesting progressive decreases in $\acute{\varepsilon}$ values with depth to a horizon at 100 ns TWTT (Figure 20). At that depth, the dipping horizons are truncated by another parallel horizon; that interface suggests an increase in $\acute{\varepsilon}$ at greater depths. We interpret the two internal horizons as sediment-rich ice lenses within the ice-rich matrix from prior fill events, and the interpreted horizons correspond well with borehole and pit observations. The deepest horizon is interpreted as bedrock, based on the increase in $\acute{\varepsilon}$, truncated stratigraphy above, and known shallow bedrock surrounding this raised platform. However, ground truth does not reach this depth for absolute confirmation of the interpretation or true depth.

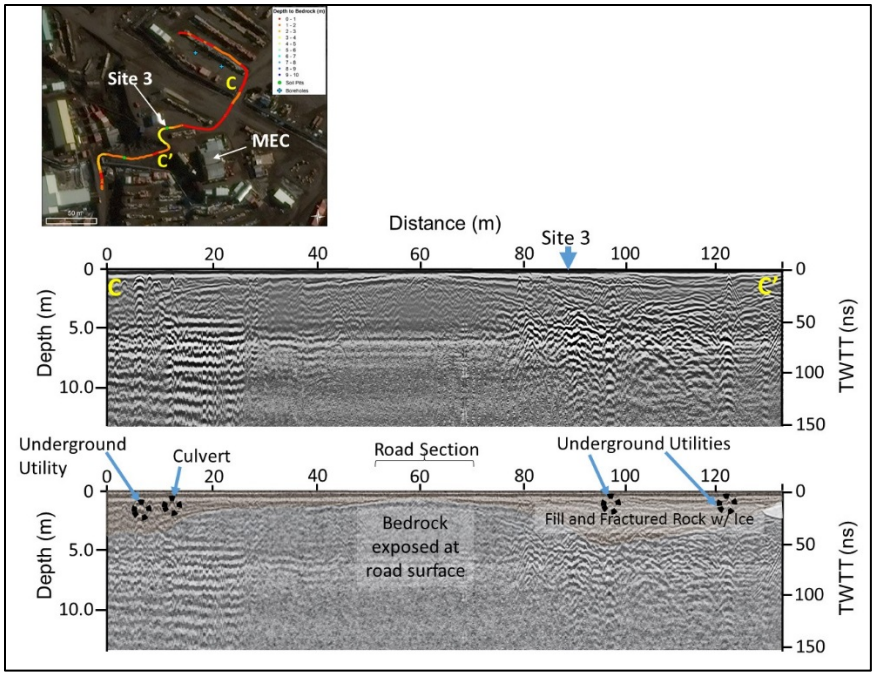
Figure 20. A 200 MHz GPR profile collected across Site 2 (*middle*), which was excavated from a raised fill platform along the transect location in yellow box 2 in Fig. 16 (*top*), with GPR profiles marking from *B* to *B′*. The profile reveals dipping stratified fill, with primarily horizons likely representing ice lenses within fill deposits (*bottom*). Fill is truncated at depth by a higher $\acute{\varepsilon}$ relative to the fill. We interpret this horizon to represent a transition to solid bedrock.



4.8.3 Site 3

A corresponding 200 MHz profile (Figure 21) was collected across Site 3 and traversed approximately northeast to southwest across and perpendicular to Main Street and near a steep slope above the Mechanical Equipment Center (MEC). As noted in Section 4.1.3, the pit revealed man-made fill stratified fill with significant amounts of construction debris and hydrocarbon odors. The 200 MHz profile collected in this region crossed bedrock exposed on Main Street, which acted as an excellent ground-truth point for the rest of the profiles collected in this area due to its easily traceable horizon beneath fill laterally from the surface outcrop. Stratification of fill was visible where the profile crossed the pit location, and bedrock appears to dip to the south from the road surface to 4 m depth or more under the excavated pit.

Figure 21. A 200 MHz profile (*middle*) collected across and perpendicular to Main Street, also crossing a pit extracted from Site 3 (*top*) for ground-truth. Our interpretation (*bottom*) shows bedrock exposed at the surface on Main Street and the bedrock horizon dipping under stratified fill to the north and south. Also note multiple underground utilities and a culvert line to the north and South of Main Street.

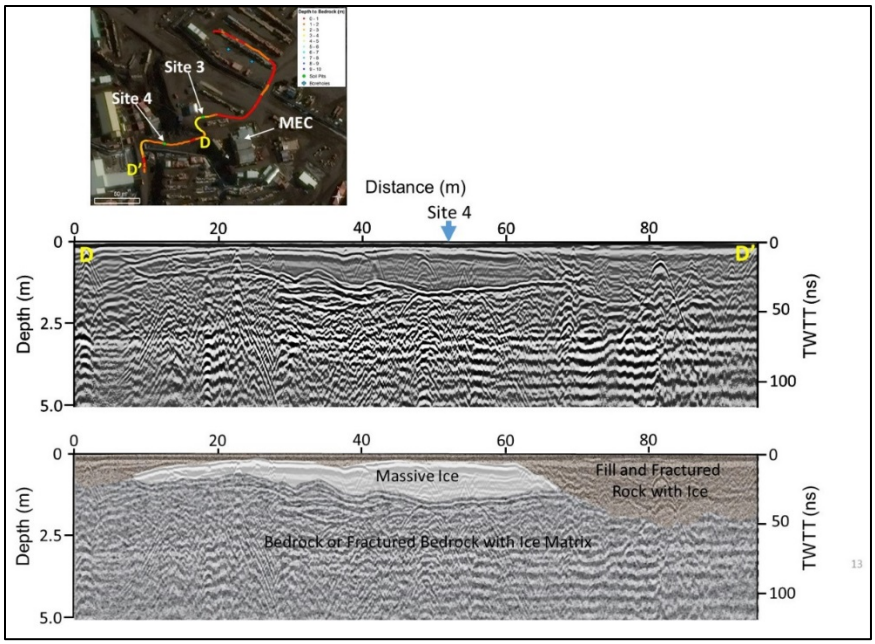


4.8.4 Site 4

The 200 MHz profile collected across Main Street and Site 3 (Figure 22) continues southward downslope where a pit was excavated at Site 4

(Figure 13). The pit was excavated immediately south of a steep (~20°) south-southeast–facing hillside. This hillside, therefore, receives significant solar insolation; however, the pit was excavated on a lower angle (~5°) road cut, likely resulting in lower solar insolation due to shading. For Site 4 we used multiple methods to validate depth because the precise location of the pit relative to the GPR transect was unknown and because the horizon depth to buried massive ice was quite variable within the pit. Several classic hyperbolas existed within the GPR profile, which also had real-time kinematic GPS precision for horizontal geo-referencing within ± 0.1 m. Through migration techniques used for calculating a slope of diffraction tails originating near the surface, we determined the top 0.5–0.8 m of fill to be $\dot{\varepsilon}$ = 11.4–12.4 with respective wave velocities of 0.089 and 0.085 m ns^{-1}. These resulted in a 6 cm uncertainty between the two methods when calculating depth to the top of massive ice (1.55 or 1.49 m, respectively). The massive ice was assumed to have an $\dot{\varepsilon}$ of about 3. We therefore calculated an ice thickness between 2 and 4 m based on a 25–50 ns TWTT. We used our GPR interpretation of massive ice to select this site for pit ground truth. This indicates the utility of GPR for locating and delineating massive ice because it has a very clear boundary and exhibits far less speckle noise and ringing relative to the surrounding near-surface geology.

Figure 22. A 200 MHz GPR profile (*middle*) and interpretation (*bottom*) of the location of Site 4 and the extent of massive ice along the transect location (*top*). Note the clear and speckle-free massive ice relative to the surrounding geology.



4.8.5 Site 5 and hydrocarbons in soil

Site 5 revealed 0.23 m of fine-grained, thawed, stratified, reddish sands that likely originate from heavily weathered local scoria, described in Section 4.1.5 (Figure 10). The same fine-grained and stratified sands existed below this point, only frozen, to 0.36 m depth. Below these sands, an ice-rich, heavily fractured, and unstratified bedrock fill existed to the bottom of the pit. At this location was the strong presence of hydrocarbon odor. Prior studies (Kennicutt et al. 2010; Klein et al. 2012) mapped petroleum hydrocarbons between 500 and 1000 ppm in this region. A 200 MHz profile collected over this area revealed stratified layers that we interpret as the sand fill noted above within the top 15–20 ns TWTT or 0.79–1.0 m depth where $\acute{\varepsilon}$ is assumed to be approximately 8 (Figure 23). Below this fill, some noted low-frequency hyperbolic reflections occur that we assume to be off-axis reflections from local buried debris or building foundations. The most note-worthy feature in this profile appears to be a difference in high-frequency noise and signal attenuation (Figure 24) between a 100 and 180 m distance along the profile, relative to either side of this region. We interpret this region to contain high concentrations of buried hydrocarbons, likely from a spill event.

Figure 23. A 200 MHz GPR profile (*middle*) with interpretation (*bottom*) along the transect on the map (*top*) in area shown in Fig. 16, showing the fill and fractured rock.

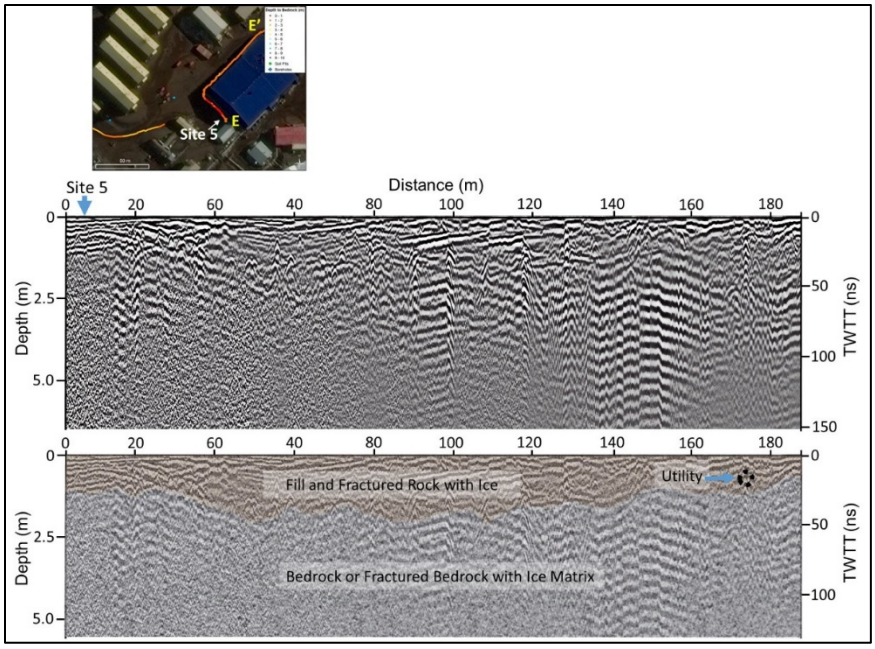
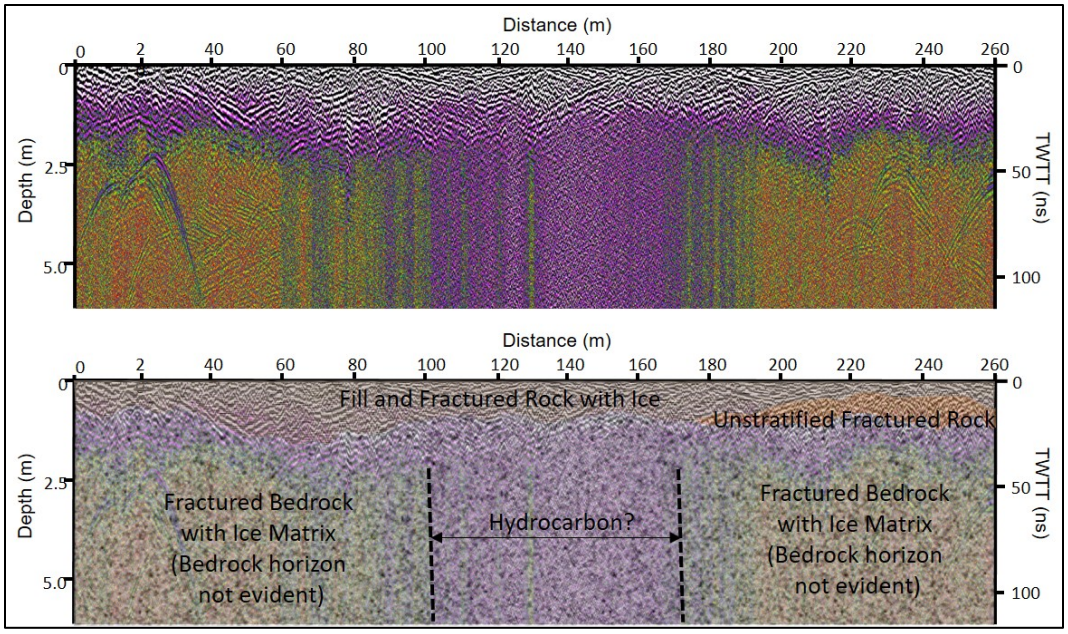


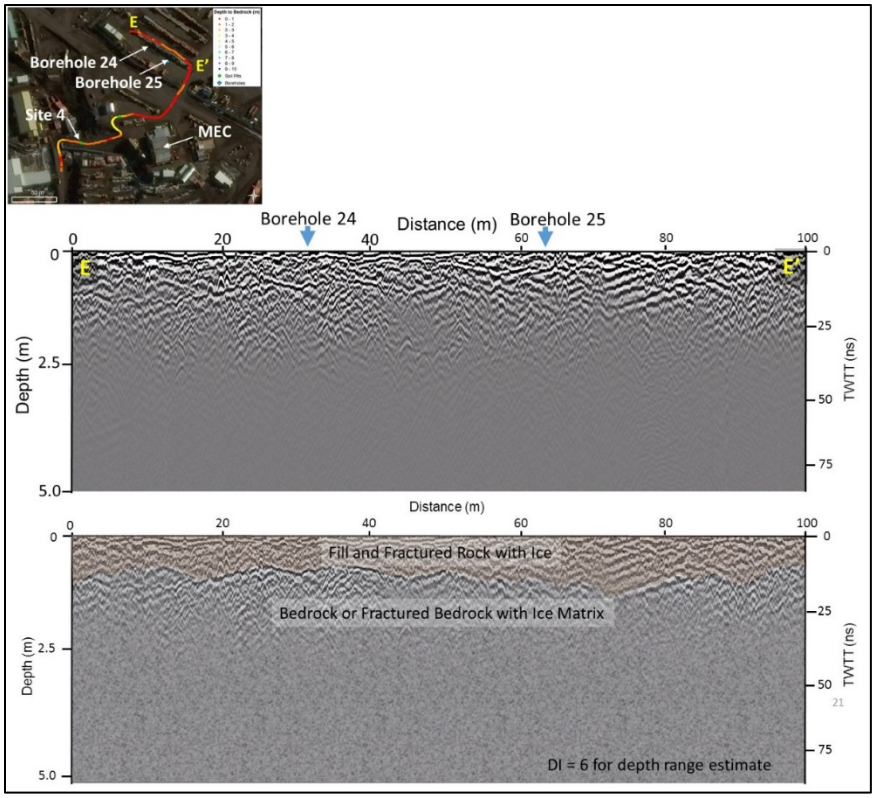
Figure 24. A 200 MHz GPR profile (*top*) with interpretation (*bottom*) showing approximate extent of hydrocarbon pollution within the fill and fractured rock, which significantly increases attenuation and noise in the radar signal along the transect in box 5 in Fig. 16.



4.8.6 Boreholes

Immediately north of Main Street in the McMurdo Open Storage area, Fenwick and Winkler (2016) extracted two boreholes (Borehole 24 and Borehole 25, Figure 25) 30 m apart from each other as part of a drilling effort to study McMurdo near-surface geology. The boreholes revealed stratified and ice-rich sands and gravels in the top 0.7 to 1.2 m with the depth of fill increasing west to east (from Borehole 24 to Borehole 25). Below this well-graded fill, ice-rich and un-stratified fill, fractured scoria, and ultimately solid bedrock existed in the extracted cores. We collected a corresponding 200 MHz profile over the two boreholes at nearly the same time as the drilling of the boreholes. The GPR profile reveals a relatively continuous horizon at 11–20 ns TWTT, which we interpret as the transition from stratified sands and gravel to weathered bedrock. The TWTT of this transition corresponds with a $\acute{\varepsilon}$ of approximately 6, which is reasonable for dry or ice-rich sands and gravels.

Figure 25. A 200 MHz GPR profile (*middle*) with interpretation (*bottom*) showing the GPR transect location (*top*) of stratified fill and fractured ice-rich rock situated over bedrock.



4.9 Soil-temperature profiles

The soil-temperature profiles, particularly near the surface, depicted diurnal behavior as shown in Figures 26 and 27 at both M&T #1 (in a partially shaded location) and on the M&T #2 site (a pad in an open location). Heating at the soil surface commenced early in the morning, continued and peaked between noon and mid-afternoon, and declined as the day went on. However at M&T #1, the midday heating at the soil surface was interrupted because the ground was shaded by the building from about 11 am to 5 pm; and surface heating resumed its increase as the sun moved to the other side of the building. In the nighttime hours, the soil's surface cooled, responding to the dropping air temperature. The large diurnal variation of surface temperature between the two locations influenced the wave of heating into the surface profile. Also, the higher the amplitude of the diurnal wave of surface temperature, the deeper the warm air penetrates into the very permeable thawed soil, providing influences of thermal conductivity and heat capacity at this layer. The peak temperature below

the surface (i.e., 0.076 m) lagged between 4 to 6 hours behind the surface peak, and the amplitude of the diurnal wave decreased with depth. The diurnal wave almost completely damped out at the 0.305 m depth at the M&T #2 site (Figures 26b and 27b) and entirely damped out at the 0.152 m bgl depth at the M&T #1 site; hence, the diurnal thermal regime was relatively shallow at this location (Figures 26a and 27a). The variations between the two sites are likely ascribable to the differing amount of solar input (direct sunlight) at each location with one being in an open, flat area and the other on a partially shaded and gently sloping area.

The 24-hour mean soil-temperature profiles were calculated from the data collected every 15 minutes to illustrate the summertime ground-warming progression. Figure 28 shows the 24-hour mean soil-temperature profiles during the austral summers of 2009–10, 2010–11, and 2015–16 at the M&T #1 site. The 24-hour mean soil-temperature profiles during the austral summers of 2009–10 and 2010–11 at the M&T #2 site are depicted in Figure 29. Although the soil-temperature profiles varied greatly between the two sites, the seasonal ground-warming progression followed the air temperature trend from November to late January. The ground was fully frozen in October with temperatures in the soil profile well below –12°C, as shown at both locations (summer 2010–11). The surface temperatures showed distinct fluctuations from one day to the next following the oscillations of heating and cooling events; particularly the temperature near the surface and above the frozen zone indicated freezing and thawing incidents throughout the season. Thawing at the M&T #1 site occurred early in December, and the active layer deepened as the summer progressed. An important note to highlight is that for all three summers at M&T #1, the temperature at the lower depth (0.61 m bgl) always warmed to –5°C, which seemed very consistent despite the difference in the surface curves. And although the surface temperature was much different at the M&T #2 site, the temperatures at the lower depth (0.61 m bgl) were only slightly higher than –5°C, which were consistent with the M&T #1 site.

Figure 26. Air and soil temperature collected in the ground every 15 minutes at (*a*) the M&T #1 site and (*b*) the M&T #2 site from 17 to 19 December 2009.

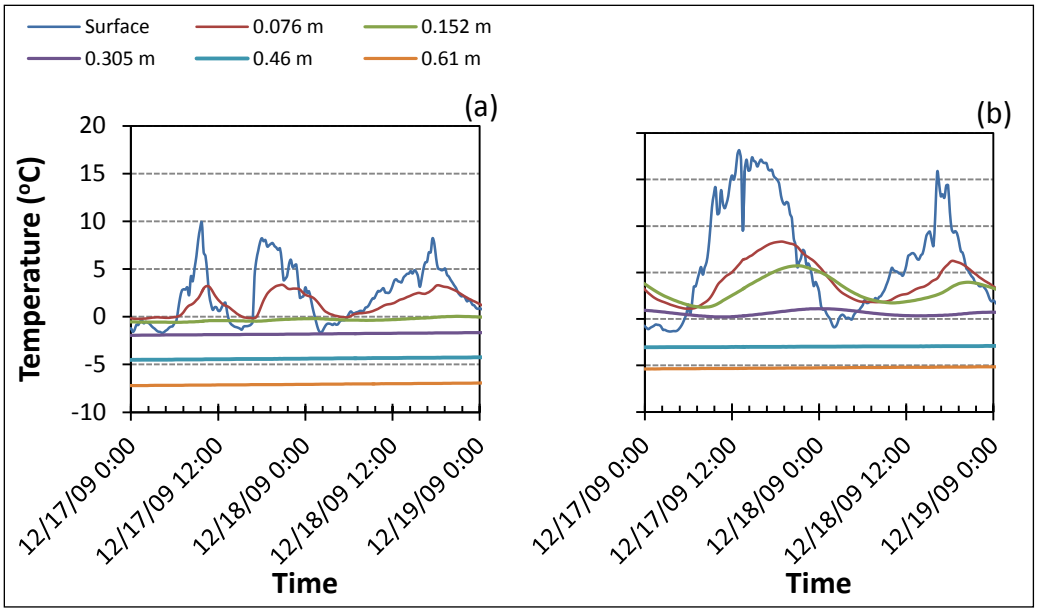


Figure 27. Air and soil temperature collected in the ground every 15 minutes at (*a*) the M&T #1 site and (*b*) the M&T #2 site from 17 to 19 December 2010.

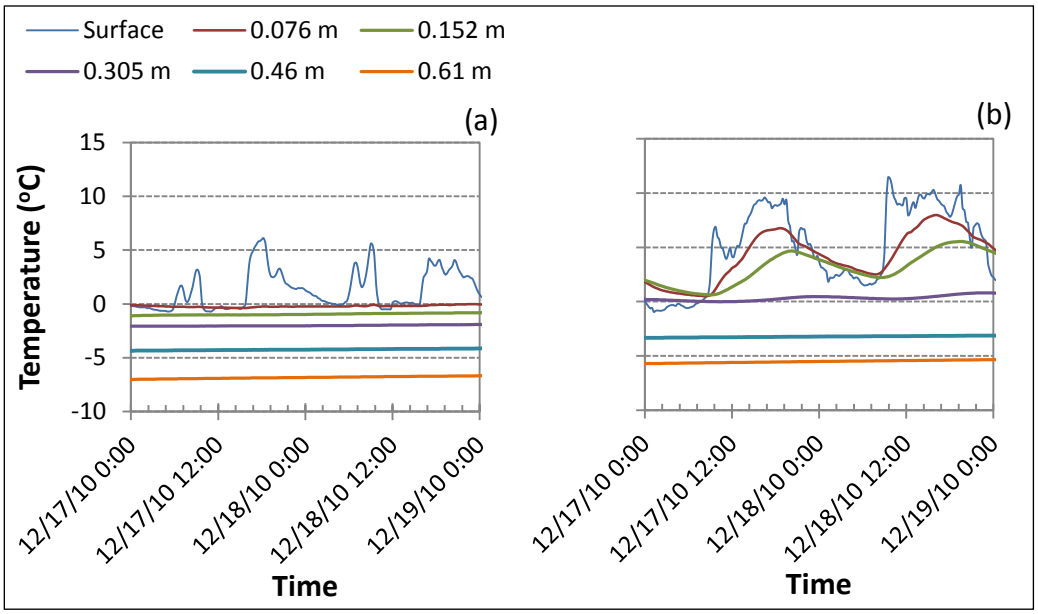


Figure 28. Maximum and minimum daily air and mean daily soil temperatures at the M&T #1 site for austral summers 2009–10, 2010–11, and 2015–16.

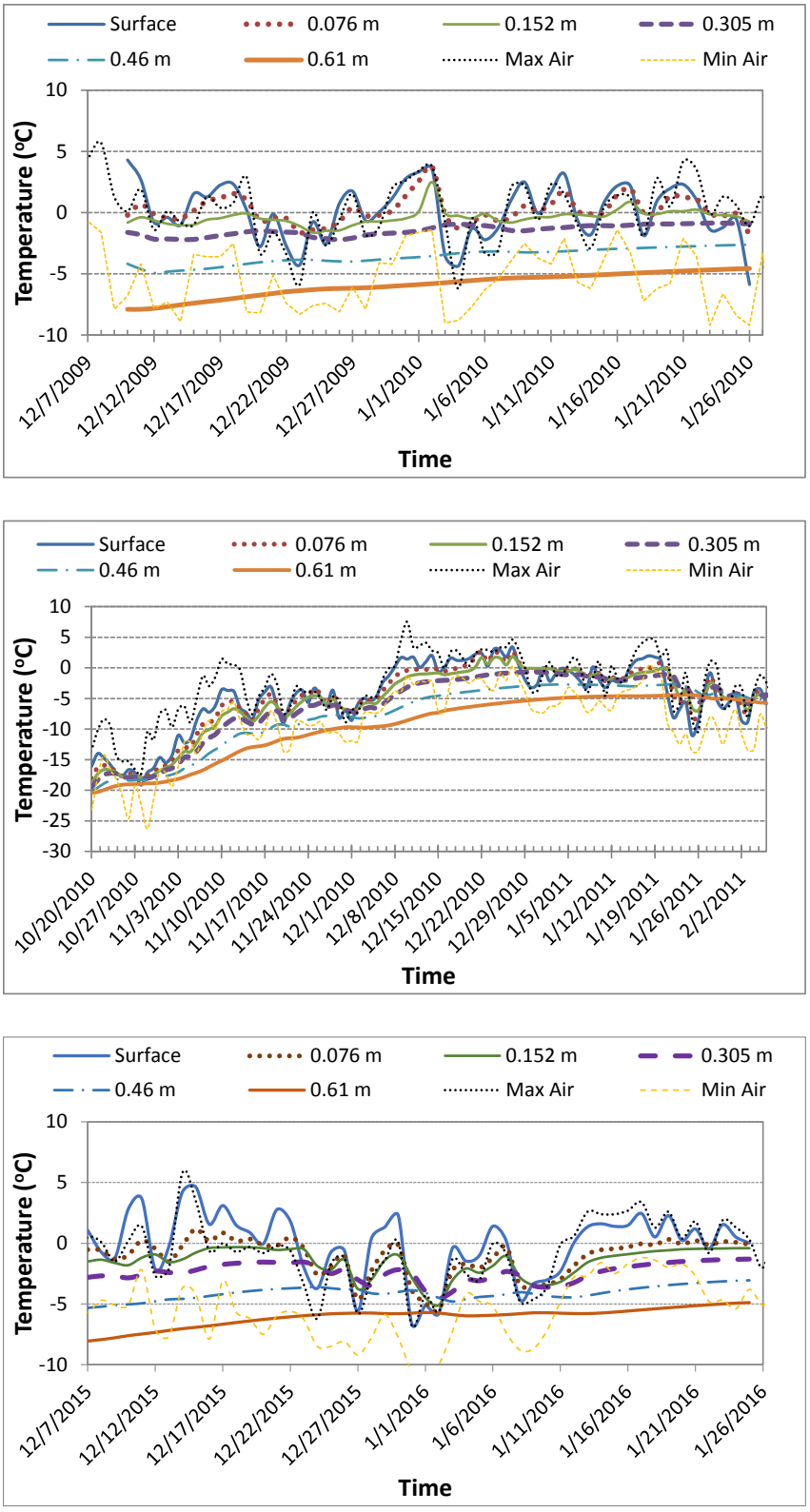
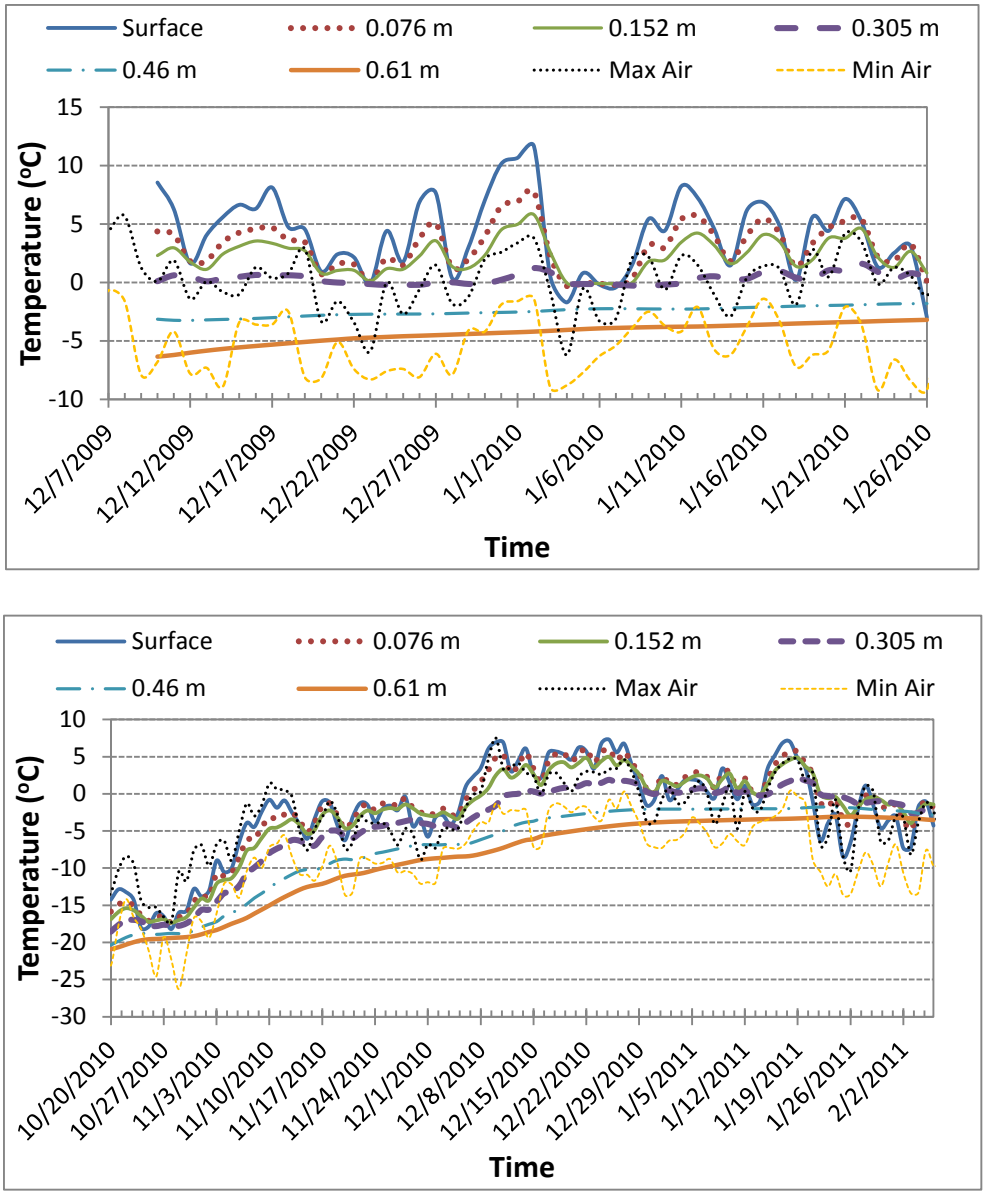


Figure 29. Maximum and minimum daily air and mean daily soil temperatures at the M&T #2 site for austral summers 2009–10 and 2010–11.



Although these diurnal fluctuations were not occurring in the frozen or permafrost layer (i.e., below a 0.305 m depth), the temperatures at these depths gradually increased from early summer until the end of January and early February or until the air temperatures were hovering below freezing. In the partially shaded and gently sloping area, the thaw depth progressed slowly. The temperature profile showed that the soil was definitely frozen at depths between 0.152 and 0.305 m at M&T #1; the temperatures at 0.152 m (Figure 28) hovered near 0°C and at 0.305 m between

−1°C and −2°C during the height of the austral summer (from the beginning of December to late January). In the open, flat area surface when thawing occurred, the soil temperatures (near the surface) at the M&T #2 site were much higher with deeper thaw depth than at M&T #1, as evidenced by the maximum temperature of 27.8°C in austral summer 2009–10 data. Heat is retained in the active layer in the beginning of the summer; then thaw depth increased through the end of December or early January. The soil was frozen below 0.305 m at the M&T #2 in the middle of the summer. At the end of January, the surface sediments began to refreeze as air temperatures decreased and the cooling trend began to return.

Figure 30 shows vertical profiles of mean temperatures during the austral summers of 2009–10, 2010–11, and 2015–16 at the M&T #1 site. At the M&T #1 site, the ground began thawing on approximately 10 December and deepened as the summer progressed, similar to the other location. The maximum thaw depths (corresponding to zero degree isotherm) were at 0.25, 0.26, and 0.1 m on 2 January 2010, 27 December 2010, and 15 December 2015, respectively. As the ground temperature gradually lost heat sometime in mid-January or by the end of January, the temperature profile in the active layer declined in a rebounding fashion; and the temperature profile showed almost vertically symmetrical in both the seasonally active and (near-surface) permafrost layers by 27 January 2011 and 5 February 2011.

Figure 31 shows vertical profiles of mean temperatures during the austral summers of 2009–10 and 2010–11 at the M&T #2 site. Ground thawing at the M&T #2 site commenced a few days earlier and had a deeper active layer than at M&T #1. The maximum thaw depths were between 0.35 and 0.37 m on 2 January 2010 for austral summer 2009–10 and 27 December 2010 for austral summer 2010–11, respectively. A similar cooling trend occurred at this location with soil temperature dropping at the end January then causing the upper part of the soil profile to cool rapidly.

Figure 30. Vertical profiles of mean daily soil temperatures for selected dates at M&T #1 during austral summers 2009–10, 2010–11, and 2015–16.

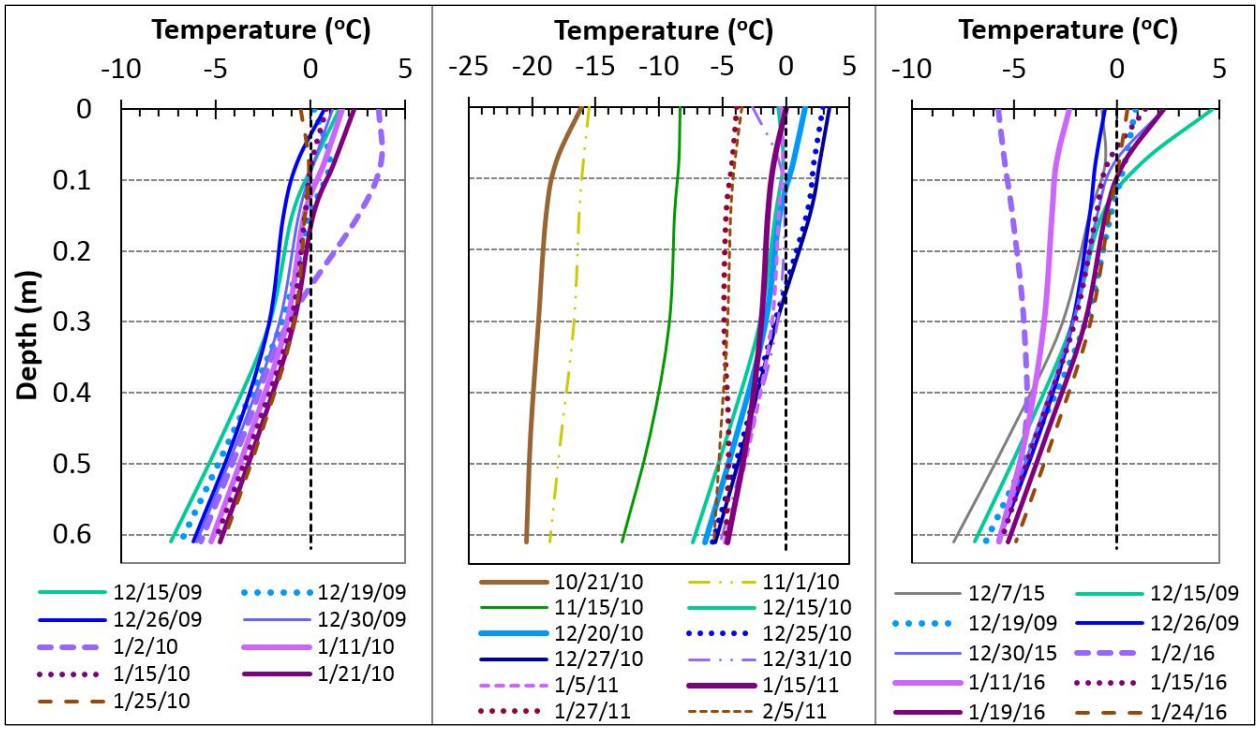
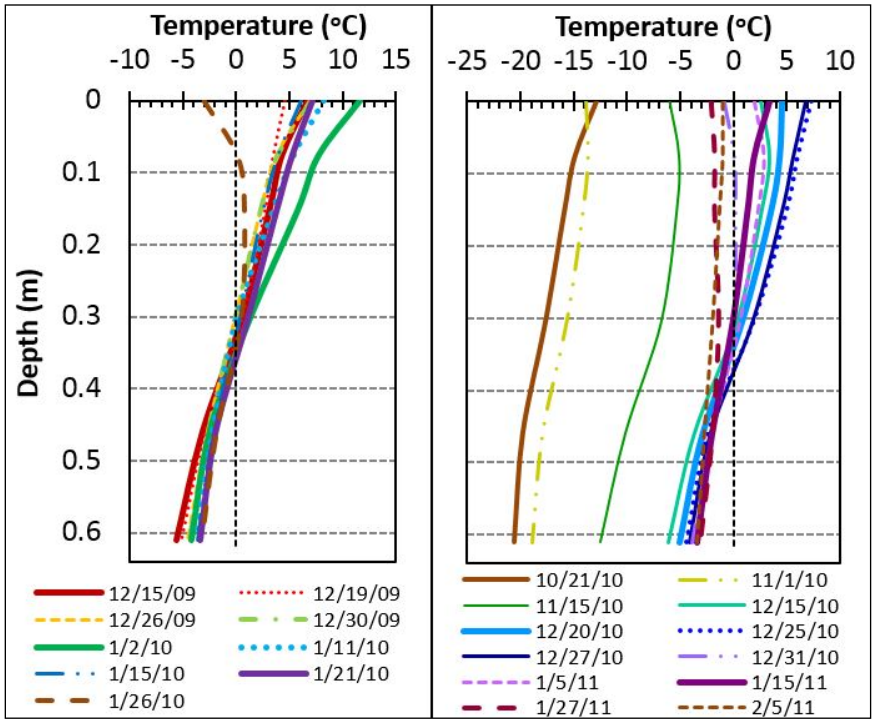


Figure 31. Vertical profiles of mean daily soil temperatures for selected dates at the M&T #2 site during austral summers 2009–10 and 2010–11.



4.10 Temporal soil moisture

The soil moisture collected from the temperature sensors provided for this study the temporal soil-moisture profiles illustrating the relative soil moisture changes within a season. Figure 32 shows the temporal soil-moisture profiles for three summers at the M&T #1 site, and Figure 33 shows two summers at the M&T #2 site. The soil moistures varied with time, mainly near the surface, in the active layer and just below the permafrost table. Below the permafrost table, the soil-moisture contents were consistent during summer seasons with less than 10% moisture content, particularly at the M&T #1 site (a partly shaded and sloping location). The most moisture appeared to be at the interface between the permafrost table and the active layer (just above the frozen layer or right below the permafrost table), confirming that there was some subsurface movement of water at this layer. At this depth, the soil had a maximum moisture by volume of approximately 30% (2 January 2010) and 44% (25 December 2010) during the summers 2009–10 and 2010–1, respectively (Figure 32). During 2015–16, the active layer was shallow; and the soil moisture was high near the surface when snow and ice melting occurred. With a deeper active layer at the M&T #2 site, soil moisture propagated deeper below the permafrost table with maximum soil moisture ranging from 13% to 29% and 10% to 33% for summer 2009–10 and 2010–11, respectively (Figure 33). In permeable soil, these high moisture contents in the active layer at both locations corresponded to the moisture from melted surface snow or ice when ground temperature was high or above freezing (Figures 30 and 31). In addition, lateral flows from melted ice accumulated in the subsurface (i.e., the active layer) above and along the impermeable frozen soil layer (Affleck et al. 2012). Likewise, the ice or snowmelt migration and surface water flow through the area in the summer months are influenced by ground slope.

Figure 32. Vertical profiles of mean daily soil moisture from PR2 sensors at the M&T #1 site for selected dates during austral summers 2009–10, 2010–11, and 2015–16.

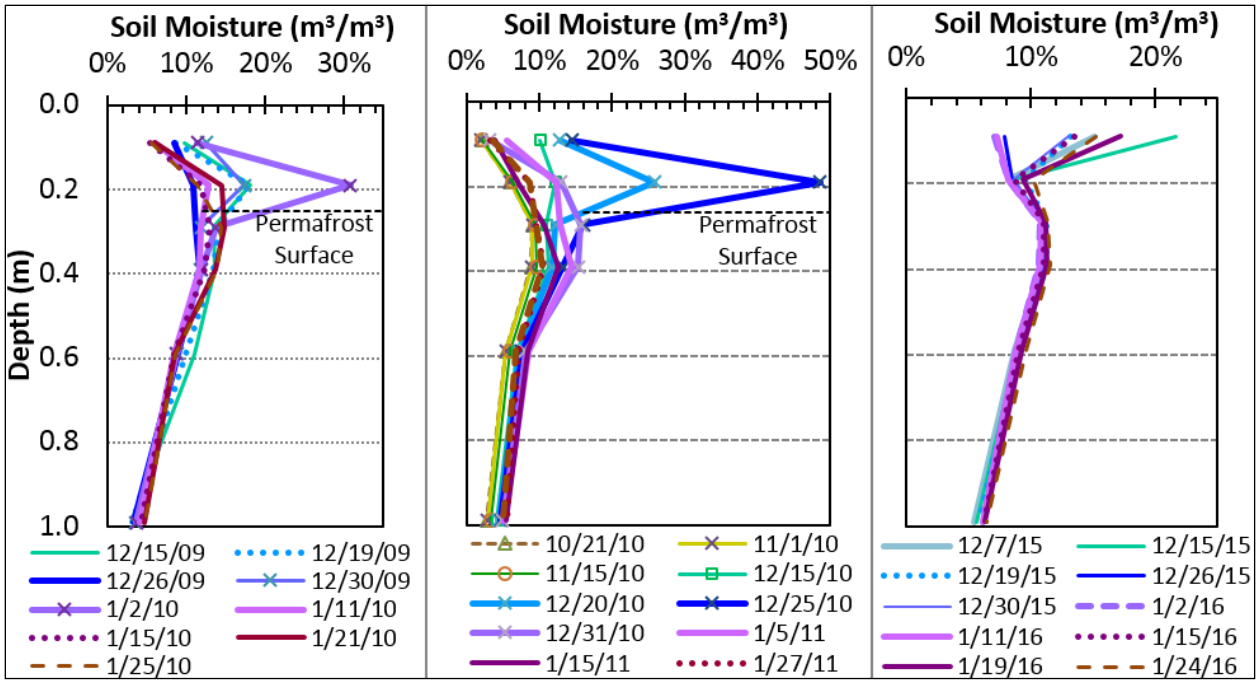
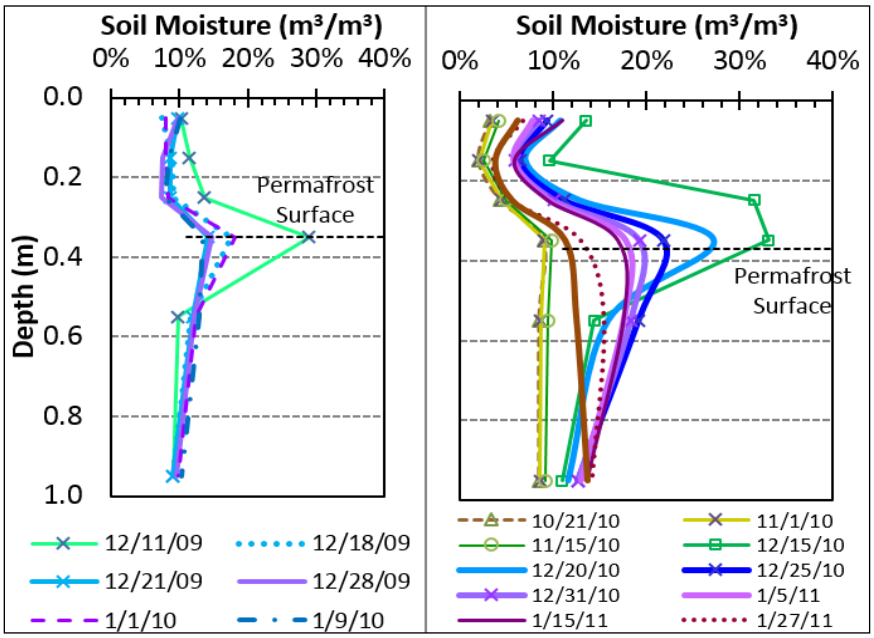


Figure 33. Vertical profiles of mean daily soil moisture at the M&T #2 site for selected dates during austral summers 2009–10 and 2010–11.



5 Discussion

5.1 Active layer, permafrost and ice

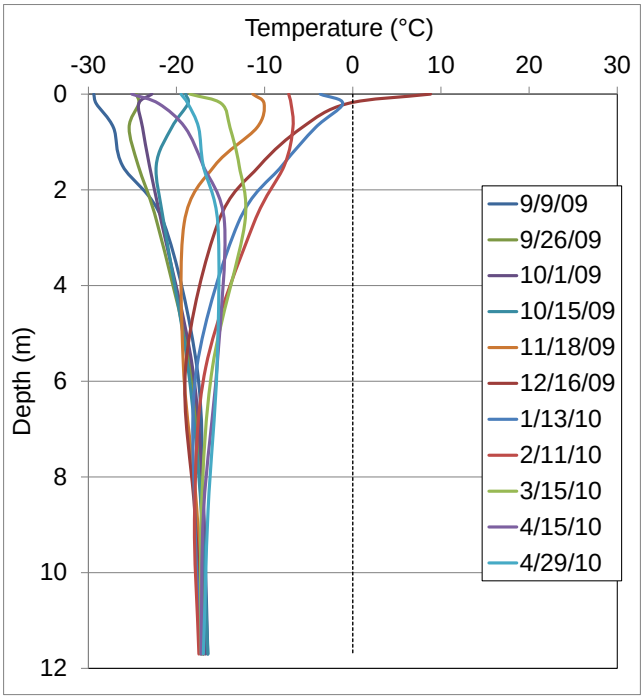
Results from pits revealed that the stratified (man-made) fill, unstratified (undisturbed) fill, and heavily fractured bedrock across almost all of McMurdo is ice rich. The GPR profiles collected in early November when the ground was frozen produced a strong radar signal compared to the profiles collected when the ground was thawing in December. As another example, radar collected in early November below a south-facing hillslope near the center of McMurdo revealed a nearly 2 m thick massive-ice feature in the subsurface (Figure 22). This massive ice likely formed from melt off the hillslope percolating into the subsurface as water flowed through the coarse-grained permeable active layer (Affleck et al. 2012) and refreezing on an annual basis. Our interpretation of the GPR results indicate that permafrost below the active layer is based on the radar triplet response (Arcone et al. 2003) of the interface, which suggests a higher $\acute{\varepsilon}$ above a lower $\acute{\varepsilon}$, consistent with thawed fill over frozen fill. Saturated sands and gravels have an $\acute{\varepsilon}$ between 10 and 30 (Arcone et al. 2014) whereas frozen ground typically exhibits $\acute{\varepsilon}$ values around 5–8 (Briggs et al. 2016); these values and the moist surface conditions during data collection in January, support our permafrost interpretation. A ground-truth pit that was based on our GPR survey conducted in November confirmed our massive-ice interpretation (Figure 22).

5.2 Ground-temperature comparison

Antarctic ground surface temperatures rise above 0°C for short periods in summer and dip to −29°C in September each year. From 15 December 2009 to 25 January 2010, the ranges for minimum and maximum daily mean temperatures at the surface were measured from −4.5°C to 3.6°C at M&T #1 and from −1.7°C to 11.6°C at M&T #2. The ranges for minimum and maximum daily mean temperatures at 0.61 m bgl from 15 December 2009, to 25 January 2010 were approximately from −7.4°C to −4.6°C at M&T #1 and −5.6°C to −3.2°C at M&T #2. For comparison, ranges for the minimum and maximum temperatures collected at the T-site (Figure 1) from 16 December 2009 to 11 February 2010 were approximately between −7.3°C and 8.8°C, −6.8°C and −4.2°C, −14°C and −9°C, −19°C and −17°C, and −18°C and −16°C at the surface, 0.6, 2, 6, and 10 m, respectively

(Oswell et al. 2010) (Figure 34). At 0.6 m, the temperature at the T-site was slightly (i.e., 1°C) higher than at M&T #2 during the same timeframe. The small difference in ground temperature between M&T #2 and the T-site could likely be due to different type of sensors used, topography, and elevation. The T-site is on a scraped hilltop approximately 1 km away from and 100 m higher than M&T #2 (Figure 4). At low altitudes, such as at McMurdo Station, ground temperatures varied slightly near the surface; but the temperatures below the permafrost table were comparable.

Figure 34. Ground-temperature data collected at the T-site for design and construction of a foundation for a wind turbine (after Oswell et al. 2010).



5.3 Surface snowmelt and frost susceptibility

The gravelly sand with silts found in this study is characterized as permeable and homogeneous coarse-grained material (Tables 3 and 3). There are various methods to determine the frost susceptibility of soils; these include particle size characteristics, pore size distribution, soil–water–ice interaction, and frost heave (Chamberlain 1981). Under natural conditions, soils with less than 3% finer than 2 μ (or o.02 mm) are considered “non-frost susceptible” materials. We did not perform the hydrometer test to analyze fines distribution; however, with a few exception, most of the samples contained less than 10% passing 0.074 mm, and previous gradation analyses

of the samples collected on-site indicated that the materials ranged between 2 and 7% finer than 2 μ (Affleck et al. 2012). Based on the fines content, these gravelly sand with silt materials found at McMurdo Station are classified as "possibly frost susceptible" and "non-frost susceptible" according to void ratio results. (Gravelly soils such as GW, GP, GW-GM, and GP-GM with void ratios of less than 0.25 are characterized as "possibly or moderately frost susceptible" soil; sandy soils such as SW, SP, SW-SM, and SP-SM with void ratios of less than 0.3 would be "possibly or moderately frost susceptible" soil.) However, the interaction of soil with water and ice, especially the presence of significant amounts of ice for frost-susceptible soils can be problematic in foundations if not designed appropriately.

Snowmelt flows through the coarse-grained permeable soil in the base of the active layer and along the top of the frozen soil layer. Segregated ice is potentially formed from snowmelt that refreezes to the permafrost table. Excess snowmelt creates soil erosion, forming ephemeral rills or gullies due to soil-particle displacement on slope pads (Affleck et al. 2012); and in low laying areas, thick aufeis formation, ice that is formed from the freezing of successive flows of water over the top of previously formed ice, have been observed on-site (Figure 35). Likewise, excess snowmelt will potentially degrade the permafrost through thermo-erosion or thaw sink, especially with extended and warm summers.

Figure 35. Examples of surface snowmelt eroding the thawed permeable soil and its effects on freezing. The *left* photo shows gullies that formed in the summer of 2008–09 on a gentle sloping pad. The *right* photo shows aufeis formation underneath a building in the summer of 2009–10.



5.4 Buried hydrocarbons and contaminant implications

Assessment of environmental contamination was not in the scope of this study. However, in digging the pits for this study, environmental contamination was evident through smell and visual observation. Hydrocarbon odor was detected at two sites (Sites 3 and Sites 5), and trace amounts of building debris were found at Site 3. Before future development at any site, the extent of the environmental contamination and impacts on human health should be examined. Hydrocarbon-contaminated soils need to be examined in foundation design because of possible chemical incompatibility with build materials and potential leaching or migration during construction or excavation of soil. Although a soil cooker is used at McMurdo Station to treat hydrocarbon-contaminated soils captured during spill incidents, this treatment is costly and could not handle large volumes of soil. Remediation methods exist; however, techniques to treat hydrocarbon-contaminated soils need to be assessed for the site because of low ambient temperature that limits microbial activities and degradation of the organic contaminants in such locations.

GPR has proven useful under certain conditions for mapping subsurface hydrocarbon pollution or other chemical spills (e.g., Atekwana et al. 2000; Cameron and Goodman 1989; Daniels et al. 1995; Lopes de Castro and Branco 2003), particularly when prior profiles were collected at a site for comparison to the region after a spill. Buried hydrocarbons or other light, nonaqueous phase liquids (such as gasoline, diesels, and other petroleum products) result in higher local attenuation rates and speckle noise in GPR profiles relative to the surrounding region. Similar effects can occur from pore spaces filled with water; however, both hydrocarbons and water signatures are distinct from buried debris or general attenuation from the matrix material because buried debris is often point specific, resulting in diffractions, and general attenuation should be relatively consistent spatially when surveying over the same geological material. Near the center of McMurdo Station, we show a case example of likely hydrocarbon contamination (Figure 24) based on the speckle noise and attenuation of the location relative to the surrounding region. A pit excavated at this site also revealed significant hydrocarbon levels within the sediments. Other studies have also noted high hydrocarbon concentrations in this region (Kennicutt et al. 2010; Klein et al. 2012). Both findings support our interpretation;

however, our interpretation should be combined with more detailed chemical and physical analysis of borehole data to definitively confirm this finding and to estimate the total spatial extent of the spill if it does in fact exist.

5.5 Buried utilities

Utilities are readily visible within most radar datasets. At McMurdo, the 200 and 400 MHz antennas were able to image buried utilities at 0.3–8 m in depth (e.g., Figures 21 and 23). Utilities are typically imaged by GPR as finite hyperbolic reflectors with the apex of each reflection providing an estimate of where the GPR antenna crossed the center of a utility line. The slope of the hyperbolic diffraction tail is a function of the angle of approach relative to the orientation of the utility line and the radio wave velocity as it travels within the geological medium above and surrounding the utility. A classic response from electrical utilities is ringing of hyperbola to greater depths under the most-shallow hyperbola (e.g., Figures 21 and 23). Other objects can cause similar reflections, such as buried debris, within the surrounding geological matrix (e.g., stones or old construction debris). Interpretation of the triplet response typically resolves any ambiguity in the cause of these hyperbolas due to metallic objects having an $\acute{\varepsilon}$ assumed to approach infinity (∞).

5.6 General impacts on engineered structures

Soil and permafrost properties are strongly influenced by the climate, such as surface radiation, moisture, thermal conditions, and excess ice. These factors have engineering design implications. Although this study explored only five locations (and did not sample across McMurdo Station), the ground is considered as thaw unstable in places where the subsurface conditions contained excess ice in soils and buried massive ice. (Thaw-unstable frozen soils is when on thawing the soils show significant loss of bearing strength, or below its' normal strength, or significant ground settlement as a direct result of the melting of the excess ice in the soil.) The design of engineered structure at this site should consider various methods such as modifying the soil prior to construction or preventing thawing of the frozen ground by using passive or active cooling. Soil or massive-ice thawing would result in differential settlement. Pre-thawing or removing ice-rich soil and massive ice is recommended for additional engineering measures, including excavation and site grading. Depending on the depth of excavation of thaw-unstable materials, the benefit may outweigh the

costs. Foundation options common in these types of conditions are shallow foundations, such as individual at-grade column footings, which are currently used at the site. The aircraft hangar in Thule, and most huge facilities, uses excavated and placed piles and deep-driven piles founded on bedrock (Bjella 2010). Our recommendations are that all foundations be constructed with seismic susceptibility considerations and that the design of shallow foundations should incorporate releveling mechanisms in the footing to adjust the structures in the event of differential settlement. Because the topography at the site has a significant gradient, heavy buildings, such as garages and large storage hangers, may require a combination of column footing and piles supporting elevated foundations with insulated structural floors. As such, the use of passive cooling (a method to control the heat dissipation and gain in the soil) and insulation of both the ground and the structures is highly practical to maintain the temperature of the ice-rich ground.

In addition to assessing for creep settlement, bearing capacity of frozen soil for shallow foundations is a function of time, soil temperature, and shear strength of the soil. The highest temperature of the ground will control the resistance to ice creep and shear failure of the soil as long as foundations are constructed in permanently frozen soil and all steps are taken to keep the ground in a frozen state (Johnston 1981).

Depending on the design chosen, building engineered structures potentially requires excavation of ice-rich soil, and soil will be replaced with non-frost-susceptible and ice-free fill materials. Fill material with high ice content is not advisable to use in practice because proper compaction of ice-rich soil is difficult to achieve (Andersland and Ladanyi 1994). However, if ice-rich soil were excavated and thawed, soils with the proper soil distribution could be satisfactorily compacted at near-freezing temperatures. The required frozen density may be equal to the maximum unfrozen density with low moisture content. Compaction of fill materials for constructing wind turbine foundations at the T-site commenced under freezing temperatures of −18°C and −20°C (Oswell et al. 2010). Given that the summer season is short, compacting soils in freezing conditions must be balanced with other design requirements.

For foundations and supporting infrastructure, erosion is a critical issue. Loosely compacted soils and aggregates are more susceptible to erosion

(Rollings and Rollings 1996) when soil fines are eroded by water flow, creating voids and undermining the soil structure (e.g., eroded soil in Figure 35). Drainage control is critical as snowmelt can potentially alter the thermal regime and impact engineered structures. Appropriate design of the overall surface snowmelt management is recommended to ensure proper drainage. Design should incorporate positive surface gradients by draining snowmelt away from any engineered structures (i.e., foundations and structural walls).

5.7 Study limitations

5.7.1 GPR limitations

GPR is an excellent tool for rapid near-surface and nondestructive assessment of local geology and for geotechnical purposes such as those outlined here. Some challenges exist that limit its efficacy or that must be considered when interpreting results. Radar signals are significantly attenuated by certain materials, such as metals and salt water (both highly conductive) and magnetic rocks. High free (pore) water content within a geological medium also significantly attenuates signals. In contrast, resistive materials, such as permafrost, cold ice, snow, firn, dry sands, and gravels, provide a good medium to propagate electromagnetic waves. Sources of noise include poor ground coupling or interference from radios or local transmitters nearby that transmit on similar frequencies. Poor ground coupling causes loss of energy at the surface and usually occurs when the terrain is rough or irregular. Rough terrain includes boulder-strewn surfaces and pothole or washboard-covered gravel roads, whereas snow cover (common in the early season) provides good ground coupling and less associated energy loss at the surface. Radio interference is usually of greatest concern in urban areas; however, any location that relies heavily on radio transmissions can negatively impact GPR data if center frequencies overlap because bandpass filtering is no longer an option.

A comparison of data collected in McMurdo during the early (October–November) and late (January–February) seasons revealed significantly higher noise and attenuation during the spring. We attribute the poor quality of data collected during the spring to a lack in snow cover (which caused bouncing of the antenna off exposed rocks and poor ground coupling) and meltwater within the subsurface. We therefore suggest that future McMurdo surveys be conducted during the early season to minimize

attenuation and to improve ground coupling. However, if the primary goal is to image the active layer and to locate massive ice within the near surface, mid-season studies are appropriate because a strong contrast exists between the thawed active layer and frozen material below. Certain materials, such as some basalts and silt, also have inherent high attenuation rates; this issue cannot be mitigated within this case study. Radio transmission interference and highly conductive metal reflectors (e.g., culverts, buildings and foundations, and buried utilities) limit GPR applications in many locations. For example, the transmissions of radio signals by McMurdo operations can cause noise between certain frequencies. Also, syncing the GPR system with an RTK GPS system to improve spatial accuracy worked for the 200 MHz dataset; however, the RTK system transmitted at 418 MHz. This resulted in significant noise within the 400 MHz dataset. Because of the similarity in frequencies, we were unable to filter the RTK noise from the 400 MHz GPR data. Hence, we opted to not use the RTK system with that antenna, which resulted in about a 1–3 m spatial accuracy as opposed to the roughly 0.25 m accuracy of the 200 MHz data that was collected with RTK GPS.

5.7.2 Additional GPR and ground-truthing

Vast quantities of GPR data can be collected over this terrain; however, without adequate ground truthing, numerous assumptions are required to quantify geophysical results into water–ice content; attenuation rate of materials; and depth to various horizons, such as bedrock. Therefore, to better constrain geophysical results, we recommend that future studies in such complex locations focus on providing significant ground truth at specific locations of interest that correspond with known continuous strong horizons or diffractions within GPR profiles. It is likely that with this design, quantitative data analysis of GPR profiles could include quantification of radar signal attenuation that could be used to determine subsurface water flow pathways and transitions between near-surface geological structures (till or bedrock) with greater certainty.

Approximately 40% of collected GPR transects were post-processed for this study. We recommend that the remaining GPR data collected by CRREL be processed and interpreted prior to any additional drilling efforts; this will extend the spatial coverage to others areas. In addition,

where GPR data are currently sparse or of poor quality, gridded GPR surveys from 5 m to 10 m spacing is recommended where each proposed structure will be built and intersecting previously drilled boreholes as closely as possible and leveraging existing borehole data.

5.7.3 Shallow pits

Soil pits provide the ability to examine the extent of the lateral stratigraphy. However, digging a pit requires space. The pits excavated for this study were shallow due to the limited open area that would not interfere with operations. Also, the boreholes by Fenwick and Winker (2016) and used to ground truth the GPR were also shallow (mostly 3 m bgl). For the modernization of the facilities at McMurdo Station, a deeper quantitative assessment 10 to 20 m bgl (via coring) is recommended to determine the ultimate range of possibilities for foundation types and alternatives to design. A surface-based foundation could transfer heat energy down to depths of 20 m over the life of the structure (Bjella 2016). These extended borings should determine (1) if the massive ice discovered in many of the boreholes in this study and from Fenwick and Winker (2016) are simply surface snow or ice subsequently buried or mechanically placed; (2) if the massive ice discovered in this study represents multiple ice strata existing between episodic volcanic flows (syngenetic formation) and is persistent through an effective depth of 15 to 20 m; and (3) if bulk ice content decreases with increasing depth in the native permafrost soils below the mechanically filled layer, and if so, how significantly does the bulk gravimetric moisture (ice) content change within these depths.

Although we believe that results from this study provide baseline geotechnical information, extending the geotechnical assessment to examine the deeper horizons will provide more in-depth information to definitively narrow the foundation alternatives and to provide extensive ground-ice knowledge to inform the structures-design team for the proposed engineered structures. Moreover, this in-depth information should be focused on reducing design, logistics, construction, and long-term energy and maintenance costs and should look ahead to bearing capacity changes due to changing climate.

6 Summary and Conclusion

Our study provides near-surface geotechnical information at McMurdo Station. We were able to distinguish between stratified anthropogenic fill, unstratified or heavily fractured fill, and bedrock by using a variety of assumptions in conjunction with ground truth via boreholes and excavated pits. Variability of $\acute{\varepsilon}$ from 8 to 12 across McMurdo Station results in depth uncertainties of 1 m or more, particularly in areas where ground truth is nonexistent. This is particularly true for deeply buried bedrock. More fill exists in the southwest region of McMurdo Station near the shoreline whereas bedrock outcrops in northeast McMurdo are numerous, providing good ground truth for extrapolation of GPR profiles. Much of the stratified and unstratified fill or heavily fractured bedrock is ice rich throughout McMurdo, according to boreholes and pits; this is generally confirmed with GPR profiles. Fill materials varied from well-graded sand or gravel to poorly graded sand or gravel.

This study established several recommendations that may improve the efficacy and benefits of GPR at McMurdo Station or at other similar sites situated in cold regions. First, to improve ground coupling, minimize attenuation, and maximize depth of penetration, data collection should occur during the early season when snow covers much of the ground and minimal meltwater exists within the fill. However, if assessment of the active-layer thickness variability is of interest, then a late season data collection should occur. Also, if salt is applied to the road at any time, attenuation rates increase significantly. Subsurface conditions vary significantly temporally and spatially depending on slope, aspect, summer and winter temperatures, and snow cover.

Soil contaminations were observed from off gassing of hydrocarbon and debris from construction materials, as human activities around the Station introduced a wide variety of foreign materials and wastes into the soils. Proposed construction for the new development on-site will likely expose large amounts of contaminated soil that require environmental attention. It is advisable to apply suitable decontamination methods for soil remediation to mitigate environmental impact and health hazards.

The natural ground explored in this study was ice-rich glacial till composed of interconnected boulders, rock, gravelly sand, and ice materials. The characteristics of ice in the permafrost layer, either as visible ice or inferred from ice-bonded material, greatly differed in fill and in the natural ground. The ice-cemented materials in fill were poorly bonded, friable, and easily disaggregated when scraped with the point of a ripper. The ice-cemented layer of the natural glacial till, on the other hand, was well bonded with segregated and stratified ice formations that were irregularly distributed throughout the profile and required an excavator hammer attachment to break the layer of ice-rich boulder, rock, and gravel materials. The gravelly sand earth fractions of the soils were characterized as homogeneous coarse-grained materials of gravel with sand and minimal silt fractions. These coarse-grained materials were typified as angular and subangular grains.

During the austral summer, the temporal changes in soil moisture varied with time mainly within the active layer and at the permafrost table; this seasonal variation confirmed that there was some subsurface movement of water at this layer. Below the permafrost table, soil-moisture contents in the permafrost stayed consistent throughout the summer season. The soil-moisture contents from the samples collected were high at the permafrost table and in the permafrost layer. The variability in soil densities indicated that both the fill and the natural ground could be considered loose where voids were fully filled with large ice inclusions in the soil. Within the permafrost, the corresponding degree of saturation with ice showed near or greater than 100% in some cases, indicating that the pores were fully filled with large ice inclusions or ice deposits in the soil. It is important to note that the soil moisture from the soil samples provided the snapshot of the moisture content taken in the pit while the soil moisture collected from these sensors provided the temporal soil moisture illustrating the relative soil-moisture changes within a season.

In general, the ground condition was fully frozen in October with temperatures well below –12°C within the 0.6 m soil profile. The seasonal ground-warming progression followed the air temperature trend from November to late January. The large diurnal variation of surface temperature was influenced by the oscillations of heating and cooling events. Also, the higher the amplitude of the diurnal wave of surface temperature, the deeper the

warm air penetrates into the very permeable thawed soil, providing influences of thermal conductivity and heat capacity at this layer. During the study period, the maximum active layer in a partially shaded area was 0.26 m and was 0.37 m in an open area. The ground temperature gradually lost heat sometime at the end January as lower air temperatures advanced, causing the ground to refreeze.

Buried massive ice found at the site was formed either through man-made or natural processes. This buried ice extends a couple of meters vertically in the profile. These pockets of massive ice likely extend laterally for several meters and exist in various locations on-site. For design, it is important to determine the geospatial extent and distribution of the massive ice and to maintain its existing thermal regime for ground stability or to remove the ice entirely that impacts the proposed engineered structures.

Permafrost properties in the area have been strongly influenced by the landscape and climate and are necessary to include in the decision making for the design of proposed engineered structures. This is particularly important at McMurdo Station because of its environmental uniqueness and remoteness. Attention to these factors can minimize operational challenges and reduce logistical costs for construction and material acquisition.

References

Adlam, L. S., M. R. Balks, C. A. Seybold, and D. I. Campbell. 2010. Temporal and Spatial Variation in Active Layer Depth in the McMurdo Sound Region, Antarctica. *Antarctic Science* 22:45–52.

Affleck, R., and M. Carr. 2015. Predicting When Peak Discharge Occurs for Ephemeral Flow at McMurdo Station Watershed. In *Proceedings of the 2015 International Conference on Cold Regions Engineering: Developing and Maintaining Resilient Infrastructure, 19–22 July 2015, Salt Lake City, Utah*.

Affleck, R., C. Vuyovich, M. A. Knuth, and S. Daly. 2012. *Drainage Assessment and Flow Monitoring at McMurdo Station During Austral Summer*. ERDC/CRREL TR-12-3. Hanover, NH: U.S. Army Engineer Research and Development Center.

Affleck, R., M. Carr, B. West. 2014a. *Flow Control and Design Assessment for Drainage System at McMurdo Station, Antarctica*. ERDC/CRREL TR-14-26. Hanover, NH: U.S. Army Engineer Research and Development Center.

Affleck, R. T., M. Carr, M. Knuth, L. Elliot, C. Chan, and M. Diamond. 2014b. *Runoff Characterization and Variations at McMurdo Station, Antarctica*. ERDC/CRREL TR-14-6. Hanover, NH: U.S. Army Engineer Research and Development Center.

Affleck, R. T., M. Carr, L. Elliot, C. Chan, and M. Knuth. 2014c. *Pollutant Concentration in Runoff at McMurdo Station, Antarctica*. ERDC/CRREL TR-14-15. Hanover, NH: U.S. Army Engineer Research and Development Center.

Ames, B. 2015. Personal communication with Rosa Affleck. 24 December. Antarctic Support Logistics.

Andersland, O. B., and B. Ladanyi. 1994. A*n Introduction to Frozen Ground Engineering*. New York: Chapman and Hall.

Arcone, S. A., S. Campbell, and W. T. Pfeffer. 2014. GPR Profiles of Glacial Till and Its Transition to Bedrock: Interpretation of Water Content, Depth and Signal Loss from Diffractions. *Journal of Engineering and Environmental Geophysics* 19 (4): 207–228. http://doi.org/10.2113/JEEG19.4.207.

Arcone, S. A., P. R. Peapples, and L. Liu. 2003. Propagation of a Ground-Penetrating Radar (GPR) Pulse in a Thin-Surface Waveguide. *Geophysics* 68 (6): 1922–1933.

ASTM International. 2009a. *Standard Test Methods for Laboratory Determination of Density (Unit Weight) of Soil Specimens*. ASTM D7263-09. West Conshohocken, PA: ASTM International. www.astm.org.

———. 2009b. *Standard Test Methods for Particle-Size Distribution (Gradation) of Soils Using Sieve Analysis*. ASTM D6913-04. West Conshohocken, PA: ASTM International. www.astm.org.

———. 2010. *Standard Test Methods for Laboratory Determination of Water (Moisture) Content of Soil and Rock by Mass*. ASTM D D2216-10. West Conshohocken, PA: ASTM International. www.astm.org.

———. 2016. *Standard Practice for Description of Frozen Soils (Visual-Manual Procedure)*. ASTM D4083-89. West Conshohocken, PA: ASTM International. www.astm.org.

Atekwana, E. A., W. A. Sauck, and D. D. Werkema. 2000. Investigations of Geoelectrical Signatures at a Hydrocarbon Contaminated Site. *Journal of Applied Geophysics* 44 (2–3): 167–180. http://doi.org/10.1016/S0926-9851(98)00033-0.

Balks, M. R., J. López-Martínez, S. V. Goryachkin, N. S. Mergelov, C. E. G. R. Schaefer, F. N. B. Simas, P. C. Almond, G. G. C. Claridge, M. McLeod, and J. Scarrow. 2013. Windows on Antarctic Soil-Landscape Relationships: Comparison Across Selected Regions on Antarctica. In *Antarctic Palaeoenvironments and Earth-Surface Processes*, ed. M. J. Hambrey, P. F. Barker, P. J. Barrett, V. Bowman, B. Davies, J. L. Smellie, and M. Tranter, 381:397–410. Special Publication. London: Geological Society. http://dx.doi.org/10.1144/SP381.9.

Bjella, K. 2016. Personal communication. 10 December. Fairbanks, AK: U.S. Army Engineer Research and Development Center.

Bjella, K. L. 2010. Air-Ducted Hangar Foundations at Thule, Greenland. In *Proceedings of the 63rd Canadian Geotechnical Conference and the 6th Canadian Permafrost Conference, 12–16 September, Alberta, Canada*.

Bockheim, J. G. 1997. Properties and Classification of Cold Desert Soils from Antarctica. *Soil Science Society of America Journal* 61:224–231.

Briggs, M. A., S. Campbell, J. Nolan, M. A. Walvoord, D. Ntarlagiannis, F. D. Day-Lewis, and J. W. Lane. 2016. Surface Geophysical Methods for Characterising Frozen Ground in Transitional Permafrost Landscapes. *Permafrost and Periglacial Processes* (April 2015). http://doi.org/10.1002/ppp.1893.

Cameron, R. M., and K. S. Goodman, K. S. 1989. Detection and Mapping of Subsurface Hydrocarbons with Airborne Ground-Penetrating Radar. In *Proceedings of the 3rd National Outdoor Action Conference on Aquifer Restoration, Ground Water Monitoring, and Geophysical Methods, 22–25 May, Orlando, FL*.

Campbell, I. B., and G. G. C. Claridge. 2004. Soil Properties and Relationships in Cryosols of the Region of the Transantarctic Mountains in Antarctica. In *Cryosols Permafrost-Affected Soils*, ed. J. M. Kimble, 713–726. Berlin: Springer.

———. 2009. Antarctic Permafrost Soils. In *Soil Biology Permafrost Soils*, ed. R. Margesin, 17–32. New York: Springer.

Campbell, I. B., G. G. C. Claridge, and M. R. Balks. 1994. The Effect of Human Activities on Moisture Content of Soils and Underlying Permafrost from McMurdo Sound region, Antarctica. *Antarctic Science* 6 (3): 307–314.

Chamberlain, E. J. 1981. *Frost Susceptibility of Soil, Review of Index Tests*. CRREL Monograph 81-2. Hanover, NH: Cold Regions Research and Engineering Laboratory. https://www.nsf.gov/geo/plr/antarct/ajus/nsf9828/9828html/m4.htm.

Cole, J. W., P. R. Kyle, and V. E. Neall. 1971. Contributions to Quaternary Geology of Cape Crozier, White Island and Hut Point Peninsula, McMurdo Sound Region, Antarctica, New Zealand. *Journal of Geology and Geophysics* 14 (3): 528–546. doi: 10.1080/00288306.1971.10421946.

Crockett, A. B. 1998. Background Levels of Metals in Soils, McMurdo Station, Antarctica. *Environmental Monitoring and Assessment* 50:289–296.

Daniels, J. J., R. Roberts, and M. Vendl. 1995. Ground Penetrating Radar for the Detection of Liquid Contaminants. *Journal of Applied Geophysics* 33 (1–3): 195–207. http://doi.org/10.1016/0926-9851(95)90041-1.

Elshafie, A., and E. Heggy. 2012. Dielectric Properties of Volcanic Material and Their Role for Assessing Rock. In *Proceedings of the 43rd Lunar and Planetary Sciences Conference*, 43:43–44.

———. 2013. Dielectric and Hardness Measurements of Planetary Analog Rocks in Support of In-Situ Subsurface Sampling. *Planetary and Space Science* 86:150–154. http://doi.org/10.1016/j.pss.2013.02.003.

Fenwick, J., and D. Winkler. 2016. *Geotechnical Assessment Report: McMurdo Station, Ross Island, Antarctica*. Report number 1535646_7407-002-R. Golder Associates.

Goodman, R. E. 1980. *Introduction to Rock Mechanics*. New York: John Wiley and Sons.

Holtz, R. D., and W.D. Kovacs. 1981. *An Introduction to Geotechnical Engineering*. Englewood, New Jersey: Prentice-Hall.

International Union of Soil Sciences. 2006. *World Reference Base for Soil Resources 2006*. World Soil Resources Report No. 103. Rome: Food and Agriculture.

Johnston, G. H., ed. 1981. *Permafrost Engineering Design and Construction*. New York: John Wiley & Sons.

Kanevskiy, M., Y. Shur, T. Krzewinski, and M. Dillon. 2013. Structure and Properties of Ice-Rich Permafrost near Anchorage, Alaska. *Cold Regions Science and Technology* 93:1–11.

Kennicutt, M. C., II, A. Klein, P. Montagna, S. Sweet, T. Wade, T. Palmer, J. Sericano, and G. Denoux. 2010. Temporal and Spatial Patterns of Anthropogenic Disturbance at McMurdo Station, Antarctica. *Environmental Research Letters* 5 (3): 034010.

Klein, A., M. Kennicutt, G. Wolff, S. Sweet, T. Bloxom, D. Gielstra, and M. Cleckley. 2008. The Historical Development of McMurdo Station, Antarctica, an Environmental Perspective. *Polar Geography* 31:119–144.

Klein, A. G., M. C. Kennicutt, G. A. Wolff, S. T. Sweet, D. A. Gielstra, and T. Bloxom. 2004. Disruption of Sand-Wedge Polygons at McMurdo Station, Antarctica: An Indication of Physical Disturbance. In P*roceeding of the 61st Eastern Snow Conference, 9–11 June, Portland, ME*, 159–172.

Klein, A. G., S. T. Sweet, T. L. Wade, J. L. Sericano, and M. C. Kennicutt. 2012. Spatial Patterns of Total Petroleum Hydrocarbons in the Terrestrial Environment at McMurdo Station, Antarctica. *Antarctic Science* 24 (5): 450–466.

Knuth, M. A., and T. Melendy. 2012. *Rock Material Management at McMurdo Station, Antarctica*. ERDC/CRREL TR-12-13. Hanover, NH: U.S. Army Engineer Research and Development Center.

Lopes de Castro, D., and R. M. G. C. Branco. 2003. 4-D Ground Penetrating Radar Monitoring of a Hydrocarbon Leakage Site in Fortaleza (Brazil) During its Remediation Process: A Case History. *Journal of Applied Geophysics* 54 (1–2): 127–144. http://doi.org/10.1016/j.jappgeo.2003.08.021.

Oswell, J. M., M. Mitchell, G. Chalmers, and H. Mackinven. 2010. Design, Construction and Initial Performance of Wind Turbine Foundations in Antarctica. In *Proceeding GEO2010—63rd Canadian Geotechnical Conference, 12–16 September*, 997–1003.

Péwé, T. L. 1959. Sand-Wedge Polygons (Tesselations) in the McMurdo Sound Region, Antarctica: A Progress Report. *American Journal of Science* 257:545–552.

———. 1991. Permafrost. In *The Heritage of Engineering Geology: The First Hundred Years*, ed. G.A. Kiersch, 277–298. Geological Society of America, Centennial Special Vol. 3. Boulder, CO: Geological Society of America.

Rollings, M., and R. Rollings. 1996. *Geotechnical Materials in Construction*. McGraw-Hill, New York.

Rust, A. C., J. K. Russell, and R. J. Knight. 1999. Dielectric Constant as a Predictor of Porosity in Dry Volcanic Rocks. *Journal of Volcanology and Geothermal Research* 91 (1–2): 79–96. http://doi.org/10.1016/S0377-0273(99)00055-4.

Seman, P. M., and R. Affleck. 2012. *Recommendations for Vehicle Dust Control at McMurdo Station, Antarctica*. ERDC/CRREL SR-12-1. Hanover, NH: U.S. Army Engineer Research and Development Center.

Seybold, C. A., M. R. Balks, and D. S. Harms. 2010. Characterization of Active Layer Water Contents in the McMurdo Sound Region, Antarctica. *Antarctic Science* 22:633–645. doi:10.1017/S0954102010000696.

Soil Survey Staff. 2010. *Keys to Soil Taxonomy*. 11th ed. Washington, DC: United States Department of Agriculture (USDA)–Natural Resources Conservation Service.

Sullivan, W. 1957. *Quest for a Continent*. New York: McGraw-Hill.

Tedrow, J. C. F. 1977. *Soils of the Polar Landscapes*. New Brunswick, NJ: Rutgers University Press.

Tedrow, J. C. F., and F. C. Ugolini. 1966. Antarctic Soils. In *Antarctic Soils and Soil Forming Processes*, ed. J. C. F. Tedrow, 161–177. Washington, DC: American Geophysical Union.

Tumeo, M. A., and M. A. Cummings. 1996. Subsurface Soil Temperature Measurements at McMurdo Station, Antarctica. *Antarctic Journal Review*, 268–272.

Ugolini, F. C., and J C. Bockheim. 2007. Antarctic Soils and Soil Formation in a Changing Environment: A Review. *Geoderma* 144:1–8.

Zellerhoff, S. 2015. Personal communication with Rosa Affleck. 16 November. Antarctic Support Logistics.

Appendix A: Ground-Penetrating-Radar Raw Data

CRREL collected several transects using both 200 and 400 MHz ground-penetrating radar (GPR) in McMurdo during January, October, and November of 2015. The GPR raw profile are shown below. Interpreted GPR results show that McMurdo Station represents a complex permafrost character, with ice-rich fill, scoria, fractured volcanic bedrock, massive ice, and buried anthropogenically generated debris. Some of the GPR collected by CRREL remains to be processed and interpreted.

Figure A-1. 400 MHz unprocessed GPR profile showing the transect location in the map.

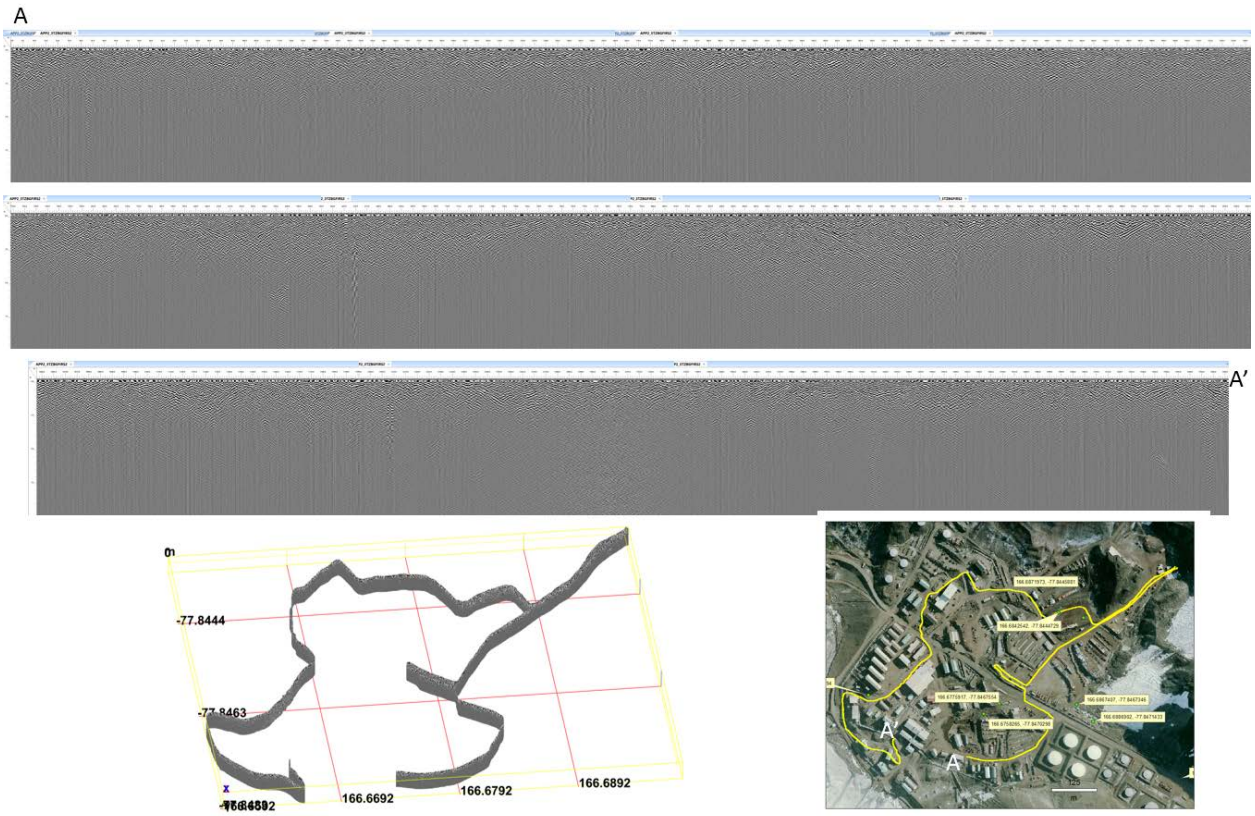


Figure A-2. Another 400 MHz unprocessed GPR profile for transect west and north of Crary and ending north of Building 166.

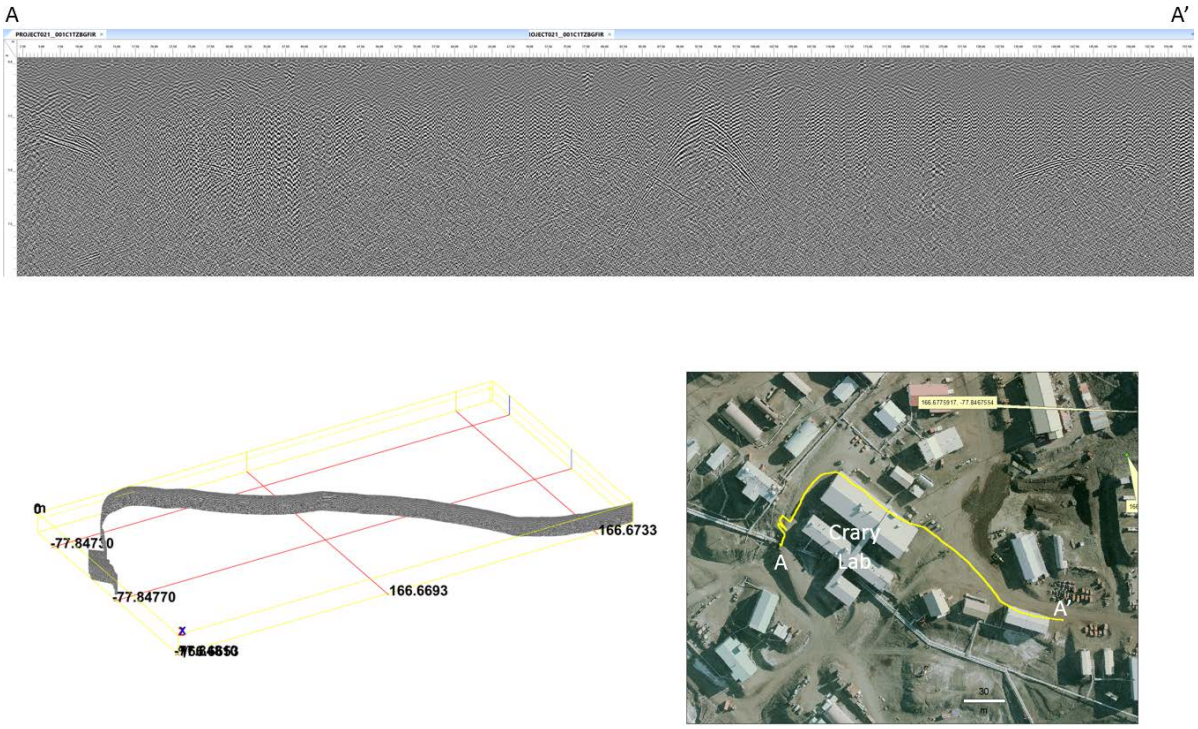


Figure A-3. 200 MHz unprocessed GPR profile for transect on the road north of Building 4 towards Main Street and looping around Dorm 210.

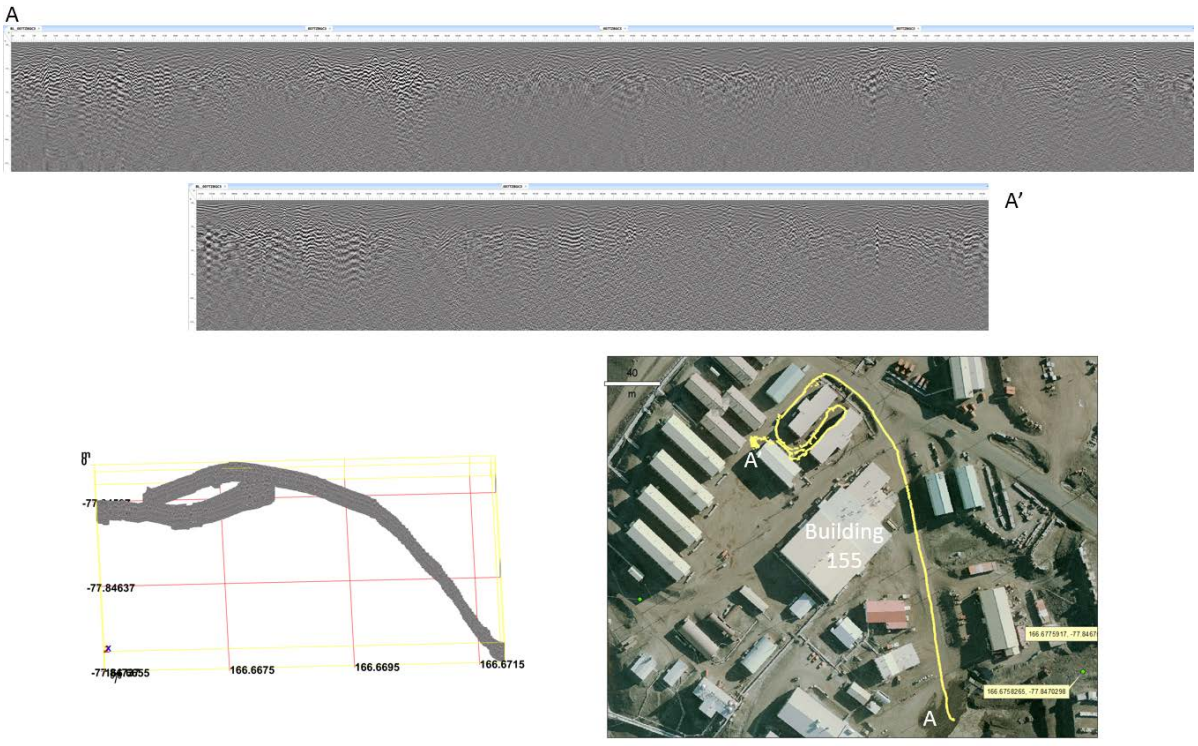


Figure A-4. 200 MHz unprocessed GPR profile showing the transect location in the map.

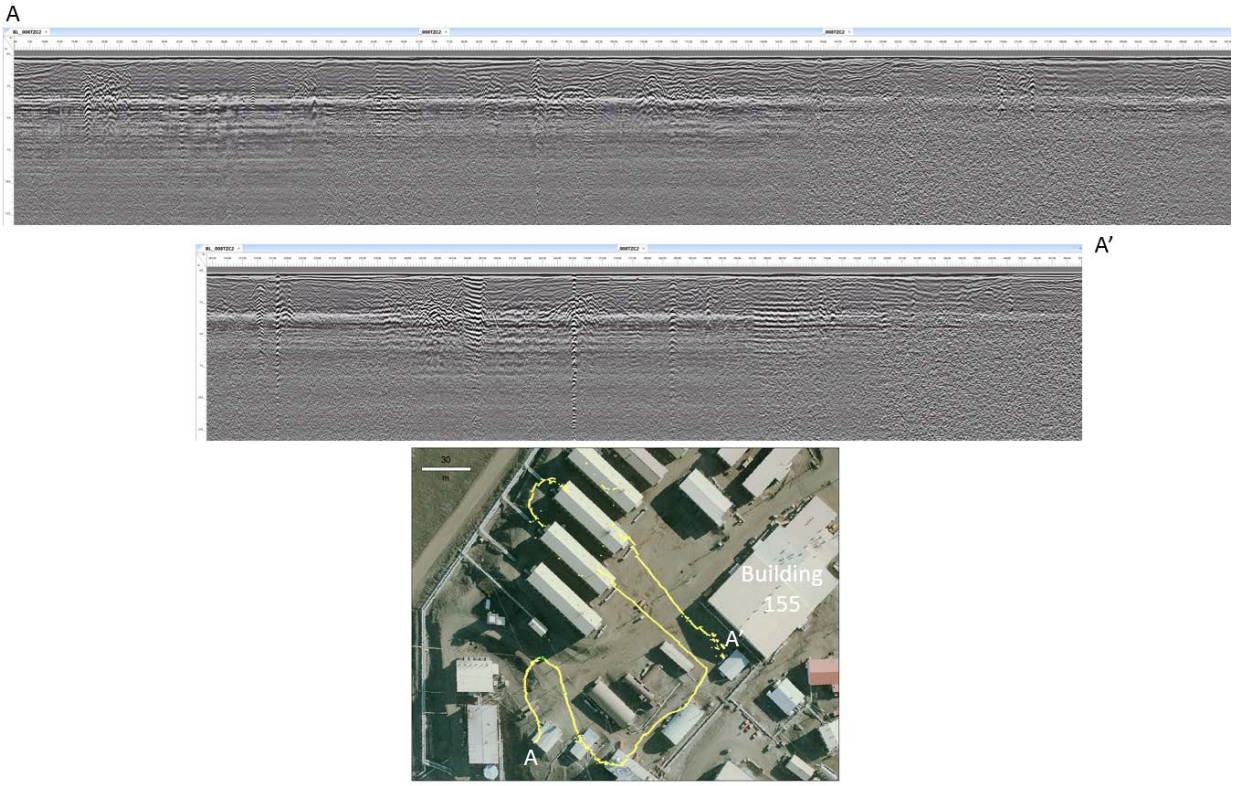


Figure A-5. 200 MHz unprocessed GPR profile for transect southwest and north of building 155.

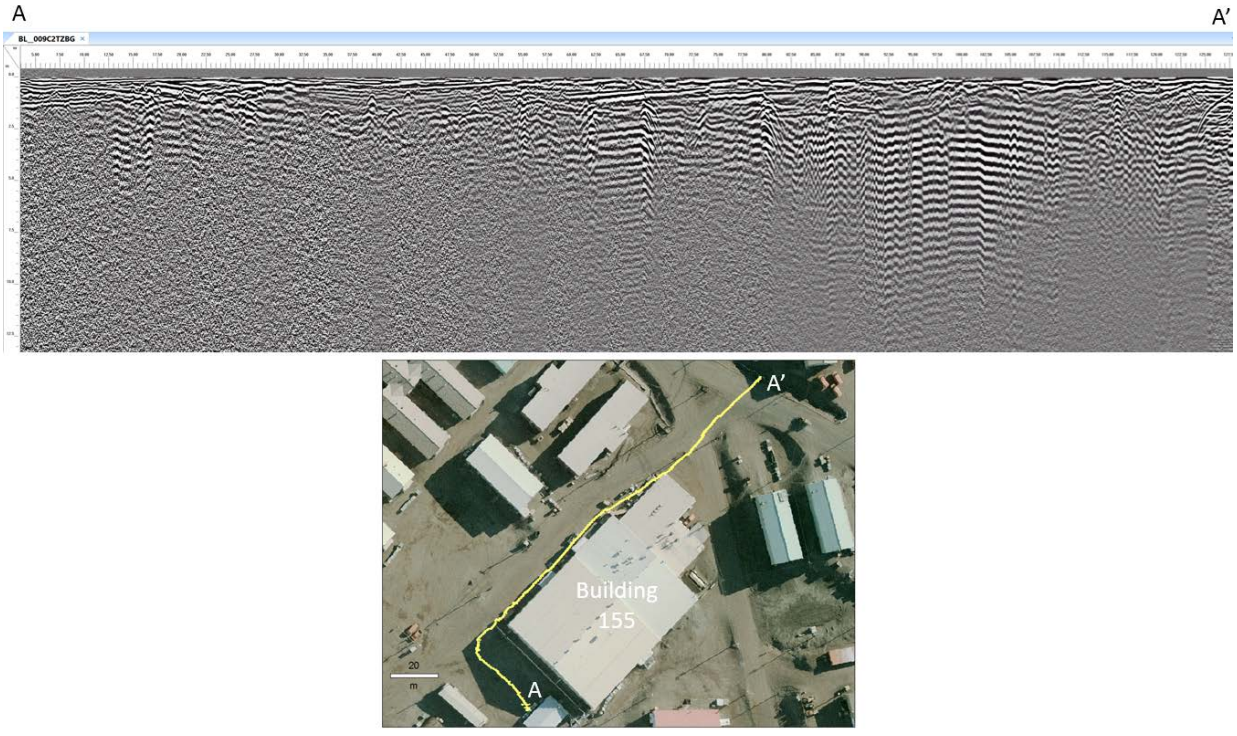


Figure A-6. 200 MHz unprocessed GPR profile showing the transect location in the map.

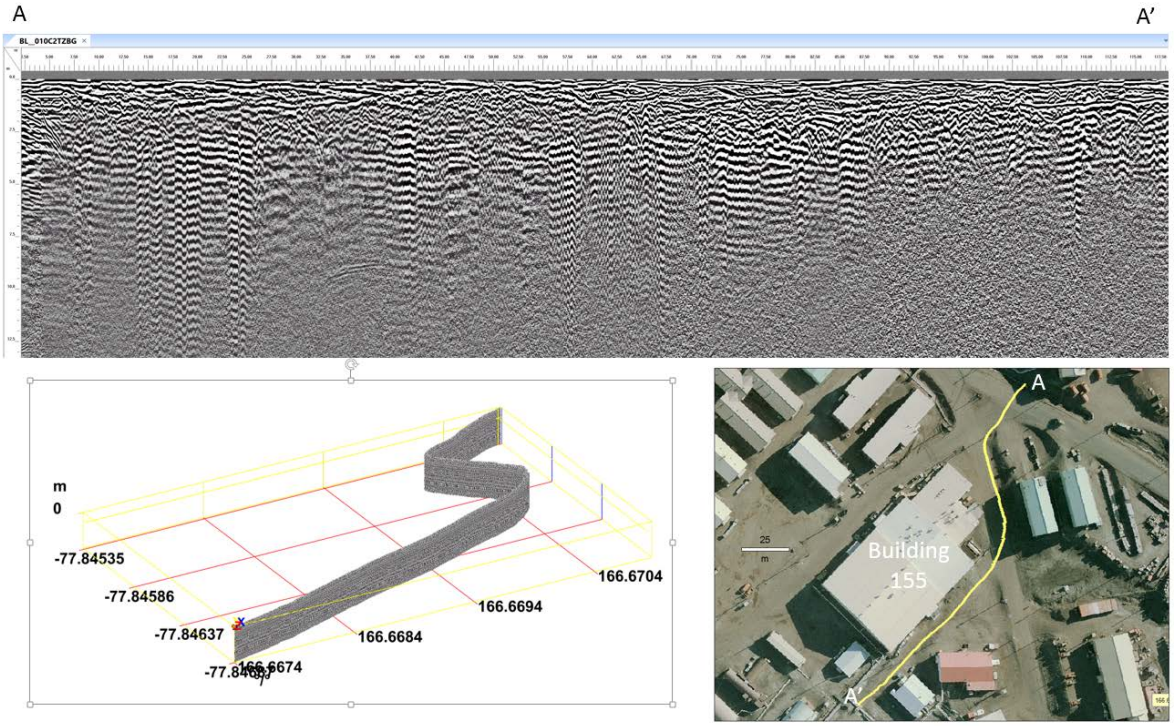


Figure A-7. 200 MHz unprocessed GPR profile for transect between Buildings 155 and 147 towards building 136.

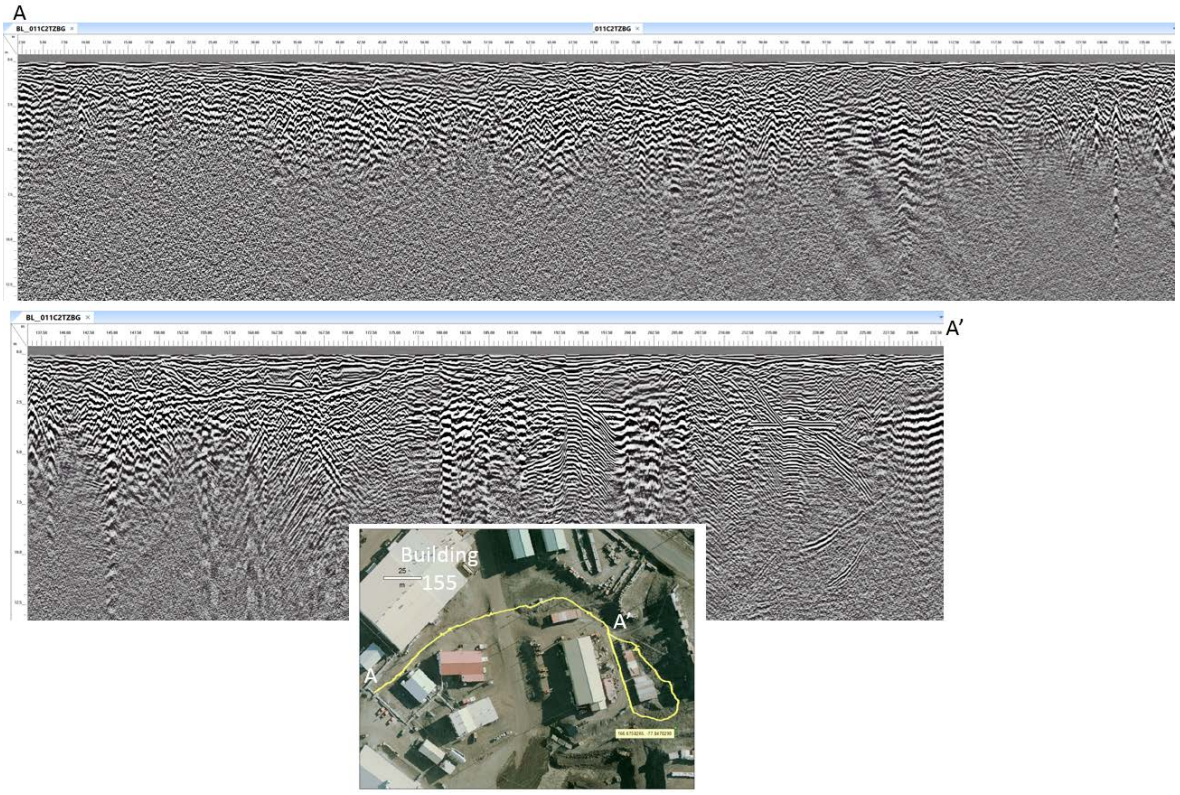


Figure A-8. 200 MHz unprocessed GPR profile for a transect starting from building 136 and going across the road toward the pads.

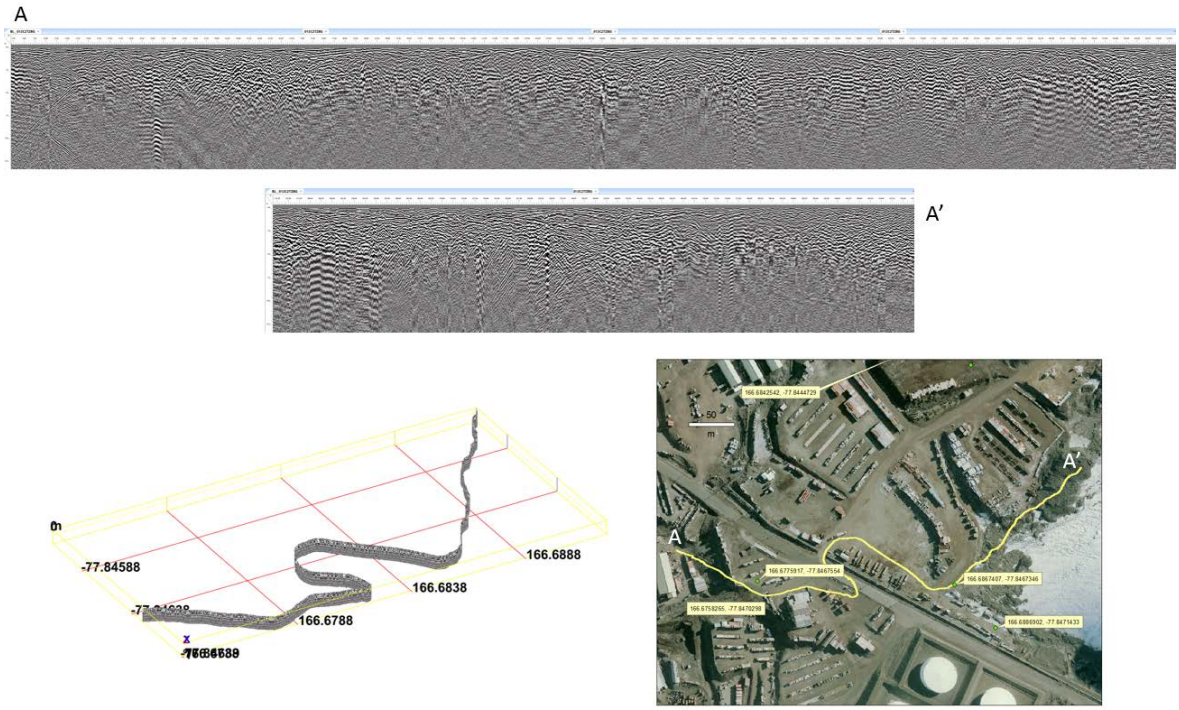


Figure A-9. 200 MHz unprocessed GPR profile for a transect on the pads north of Main Street.

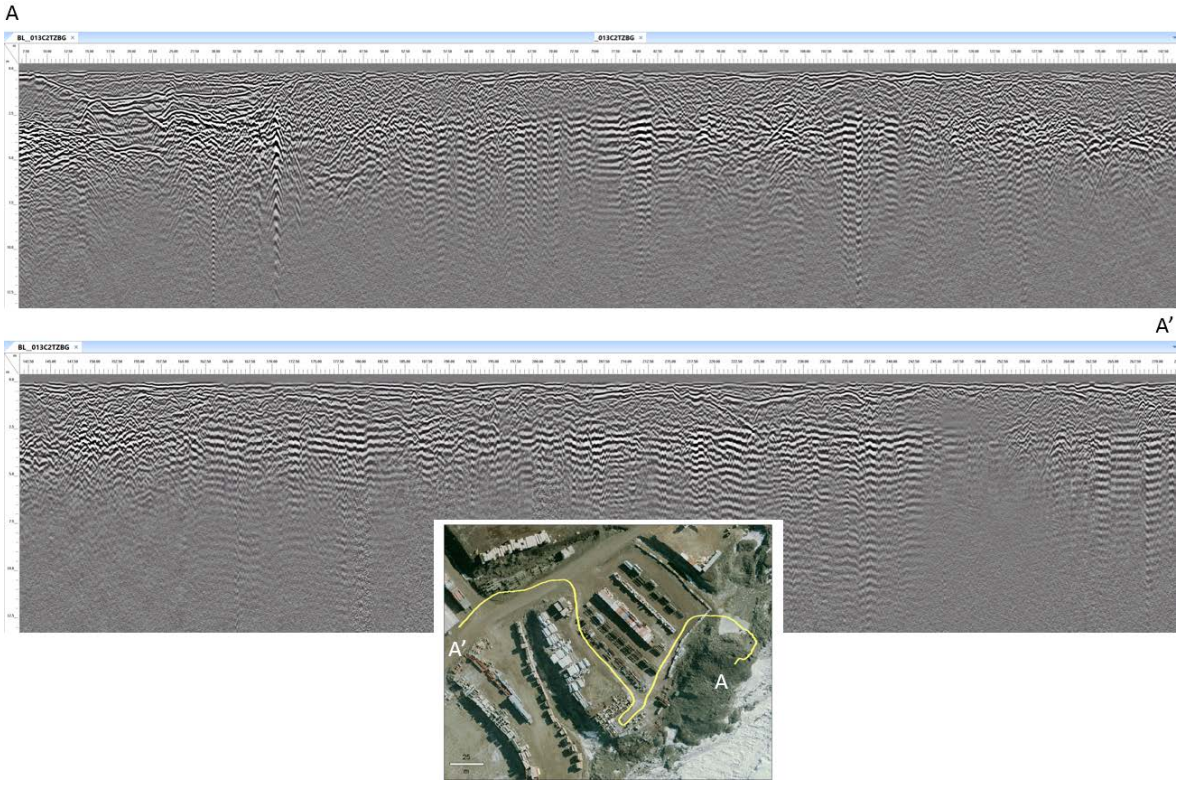


Figure A-10. 200 MHz unprocessed GPR profile for transect north of tank farms toward Scott Base.



Figure A-11. 200 MHz unprocessed GPR profile for a transect north of tank farms towards Crary.

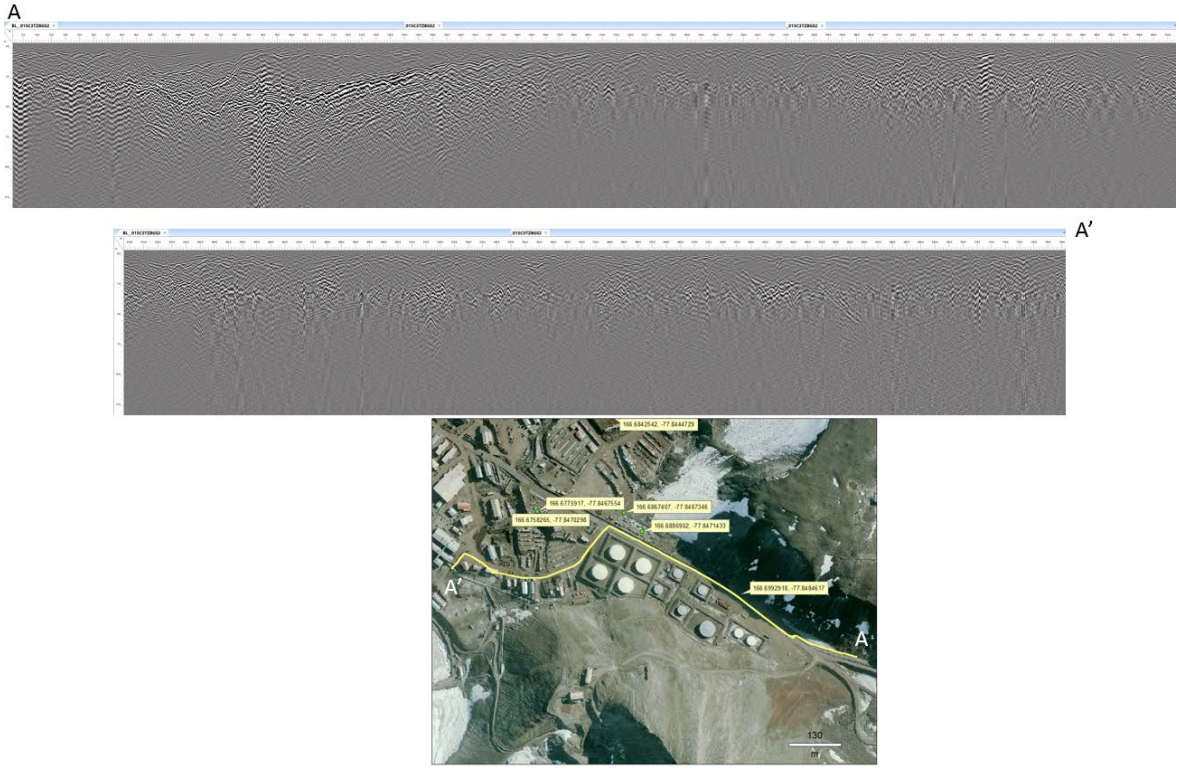


Figure A-12. 200 MHz unprocessed GPR profile for a transect along open space east of Crary.



Figure A-13. 200 MHz unprocessed GPR profile showing the transect behind Building 136 and across Building 182.

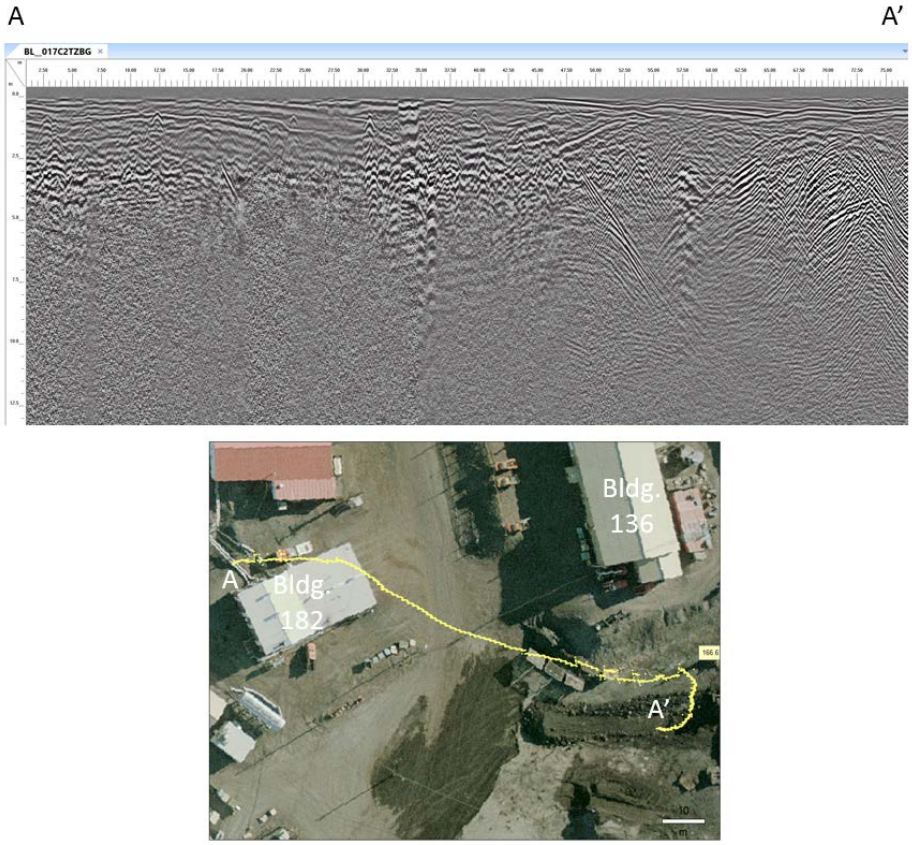


Figure A-14. 200 MHz unprocessed GPR profile showing the transect location around Crary Lab.

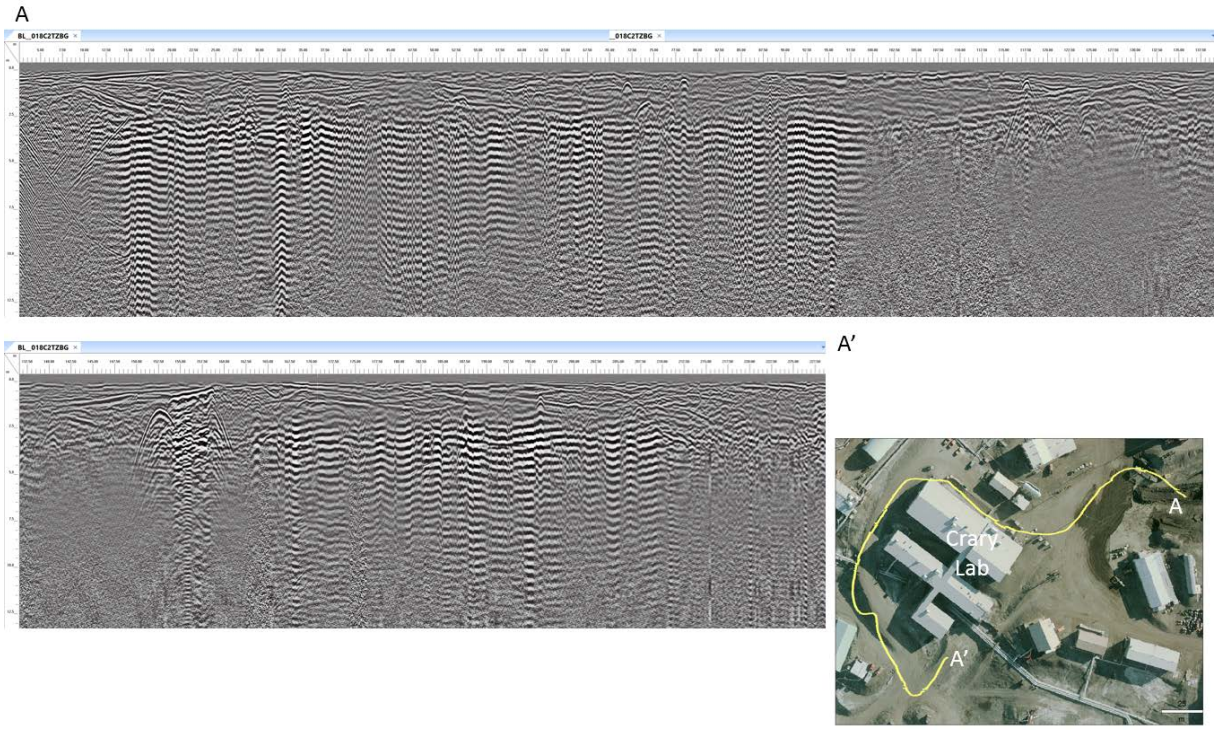


Figure A-15. 200 MHz unprocessed GPR profile showing the transect along the road toward the sea ice transition.

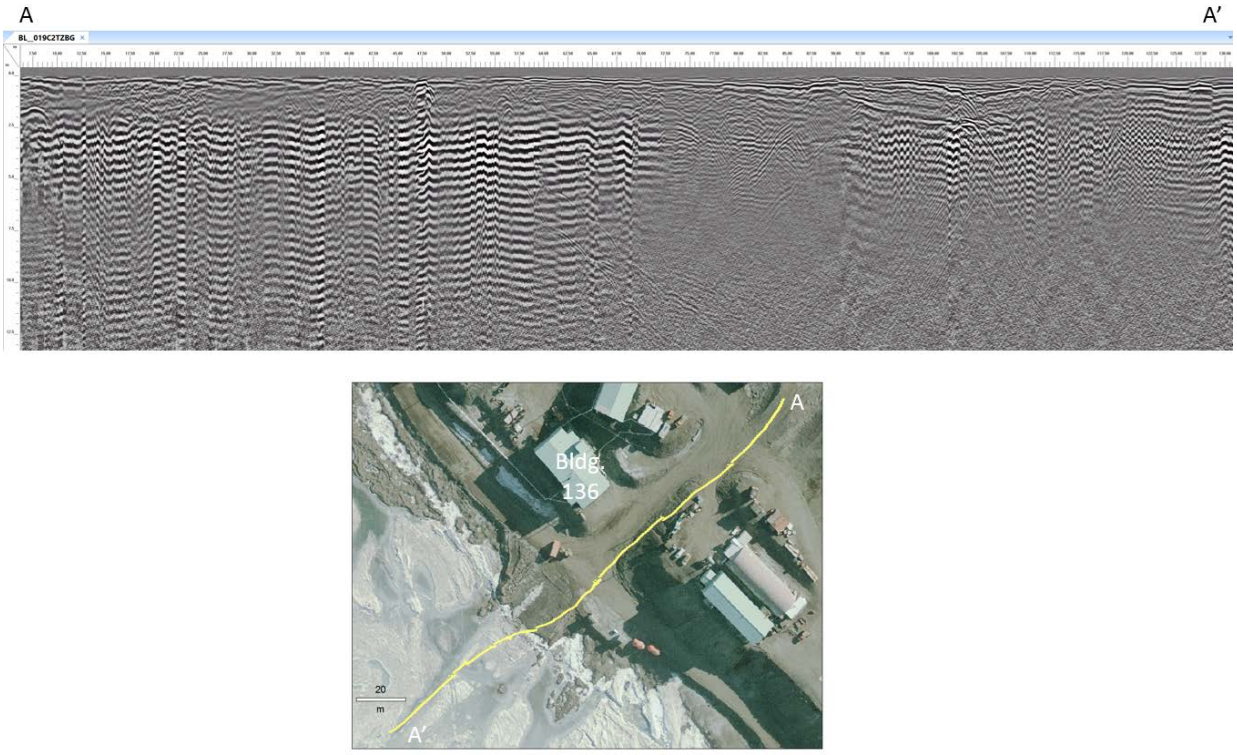


Figure A-16. 200 MHz unprocessed GPR profile showing the transect location on the sea ice transition.

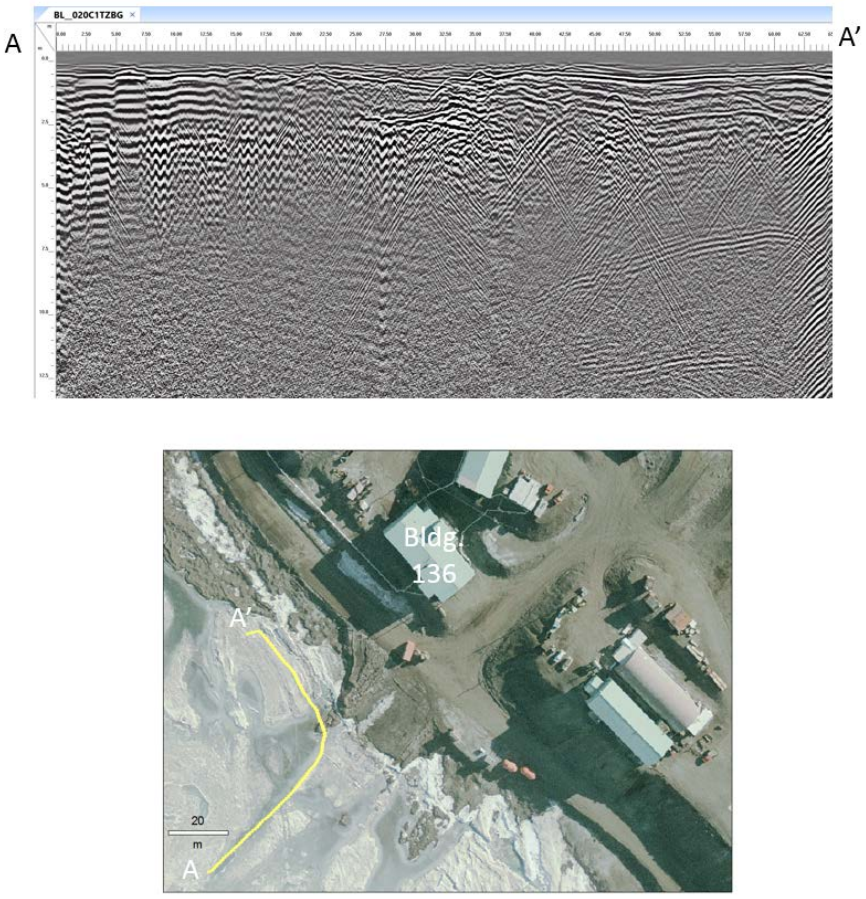


Figure A-17. 200 MHz unprocessed GPR profile showing the transect between Buildings 136 and 191, across the Main Street to the pad.

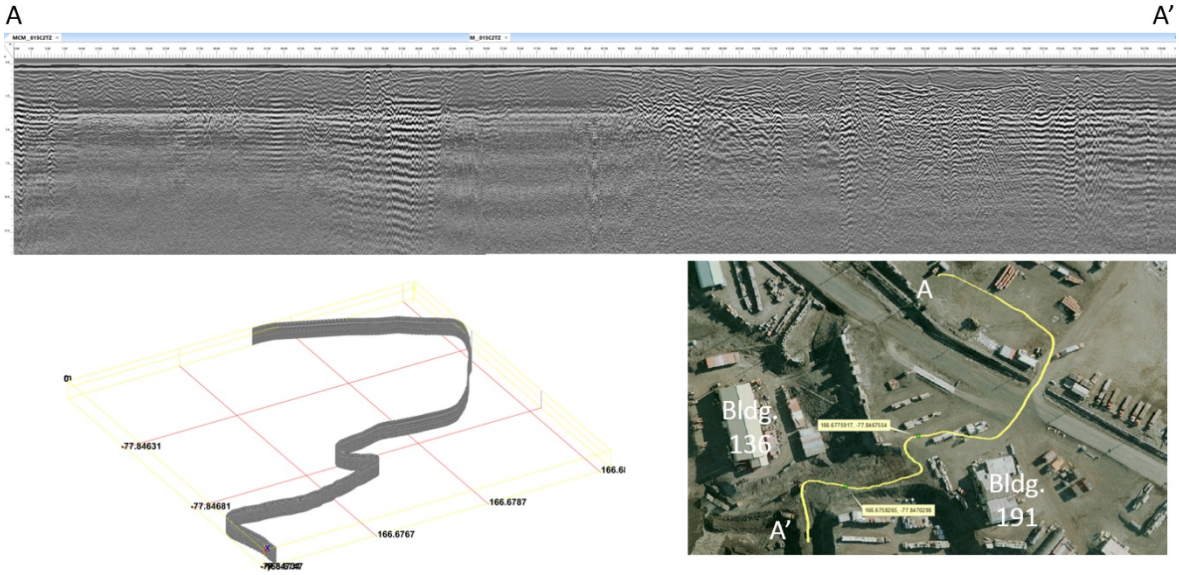


Figure A-18. 200 MHz unprocessed GPR profile showing the transect location in the pad area.

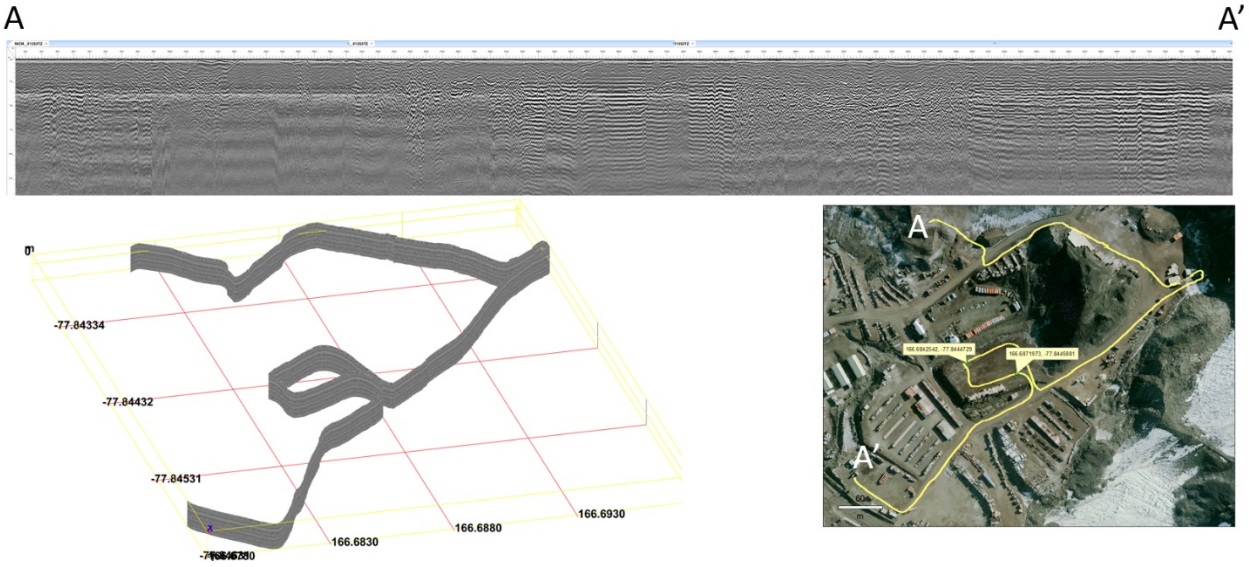


Figure A-19. 200 MHz unprocessed GPR profile for transect towards Arrival Heights.

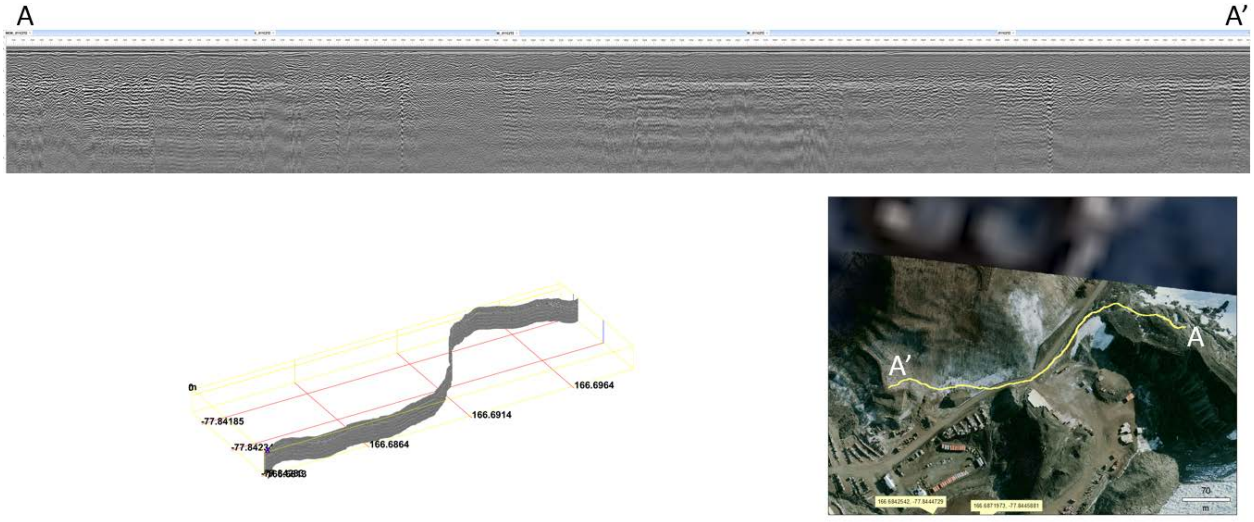


Figure A-20. 200 MHz unprocessed GPR profile for transect along Main Street all the way down to Hut Point.

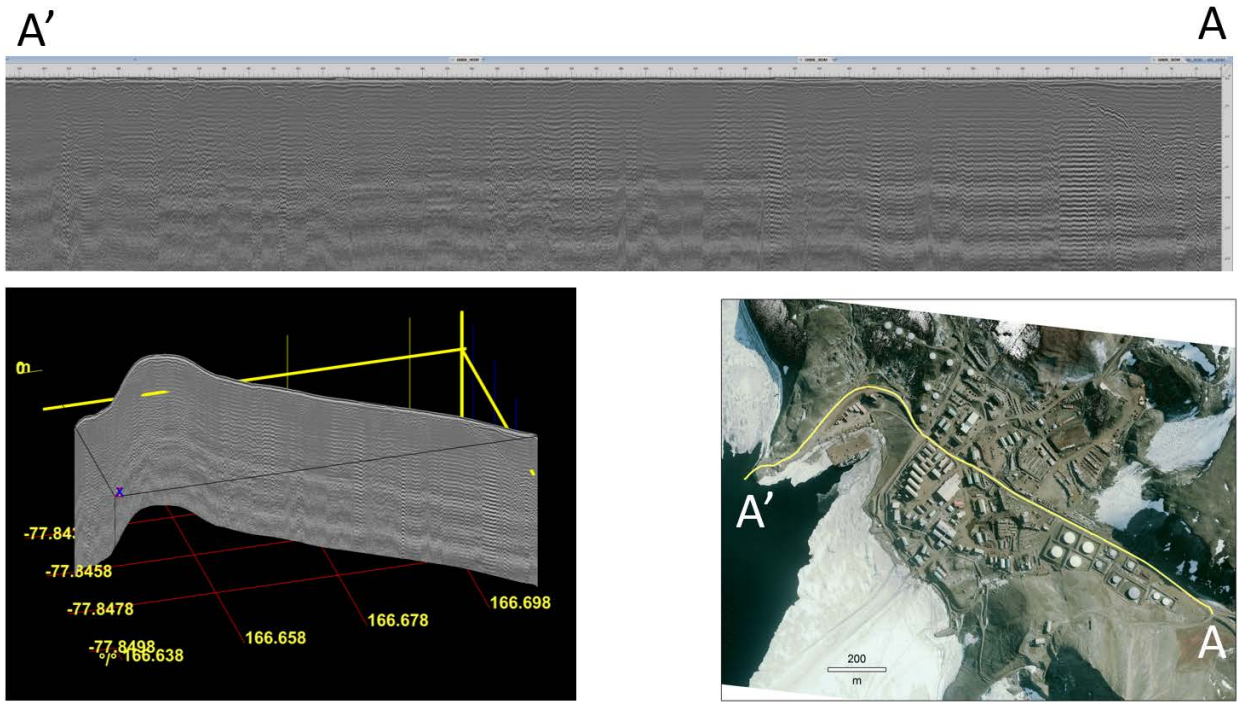
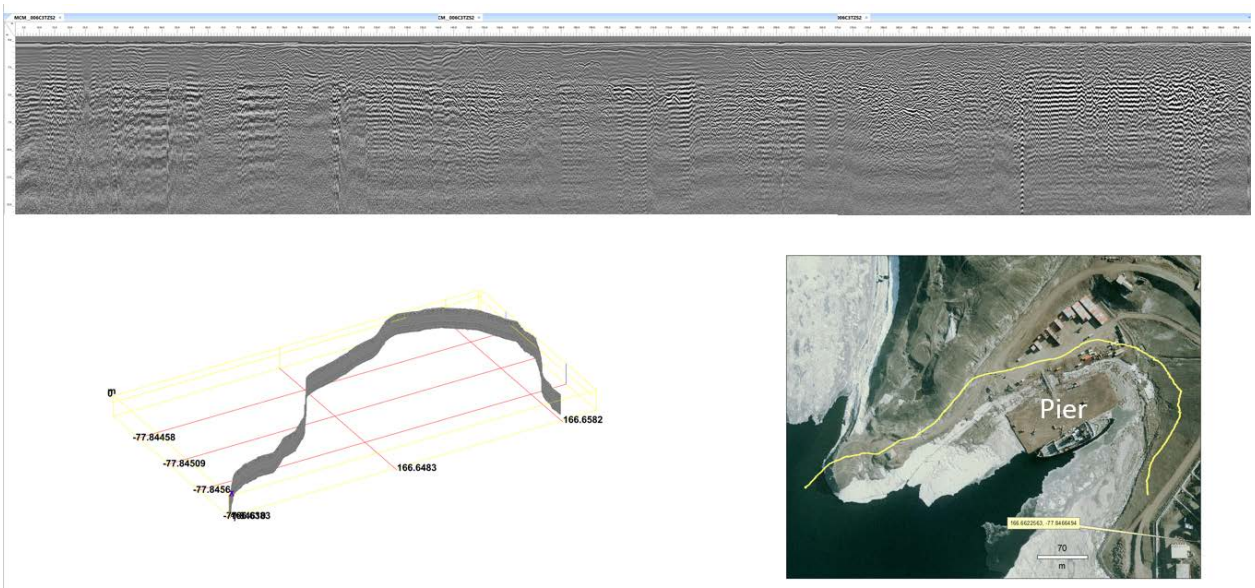


Figure A-21. 200 MHz unprocessed GPR profile for transect along the slope above the pier.



Appendix B: Picture and Notes for Individual Pits

B.1 Site 1

Site 1 is located on a road. This pit was dug down to 5 ft on 23 December 2015. The thawed layer is approximately 1 ft bgl. The excavator was able to scoop down to 1.5 ft. Ice lenses are found at 1 ft. Then, the hammer was used to loosen the materials from 1.5 down to 5 ft.

A mechanically constructed layer is found from the surface down to between 12 and 16 in. Below the mechanically constructed layer is the natural material, which is composed of a conglomeration of fractured basaltic rock and ice. This ice-cemented rock and sediments material is frozen solid and hard to break. The profiles of the pit are depicted in Figures B-1–B-6. The chunks of samples that we collected from this layer are very hard to break with pickax (Figure B-6).

Figure B-1. The active or thawed layer.



Figure B-2. The bottom of the active showing ice lenses at 1.5 ft.



Figure B-3. Hammering and breaking the ice-cemented hard rock.



Figure B-4. Close-up profile of the ice-cemented rock and sands in the pit at Site 1.

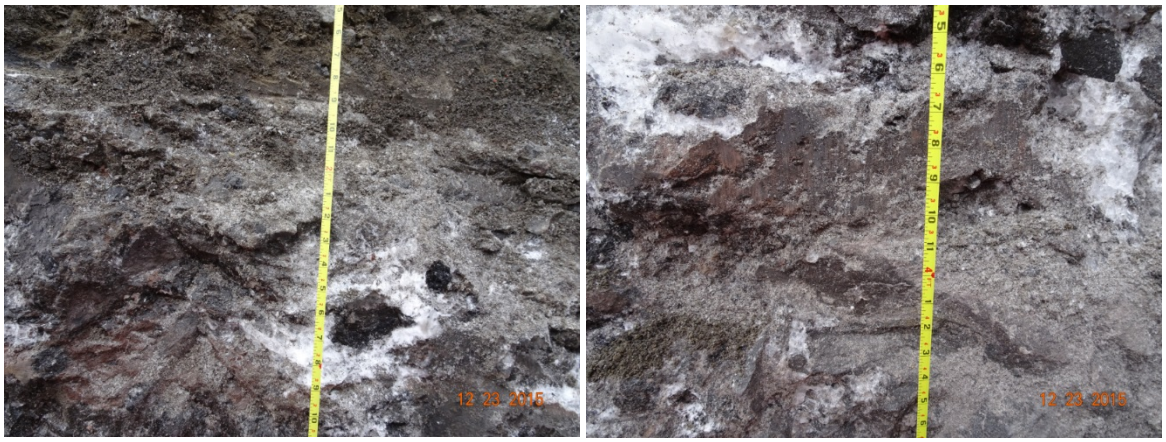


Figure B-5. Overall profile at Site 1.



Figure B-6. Excavated fractured boulder, rocks, and sands for Site 1.



B.2 Site 2

Site 2 is located on a pad above the Hazmat storage area. The surface is littered with wood chips, and the material is mostly reddish fine sand (Figure B-7). The top 24 in. is fine sand and the ice layer was encountered at 24 in. (Figure B-8). The area was used as a snow dump to pile snow every year until 1995. While the snow was piled every year, the ground was bladed to expose snow in the summer months as part of the process to melt the snow (Ames 2015). The area became stable, and fill materials were placed. The area is now used as a pad.

Within 2 hours, Site 2 was excavated to approximately 11 ft. The ice layer was found from 2 to 11 ft deep, indicating that the snow deposits had consolidated (Figure B-9). The ice layer is mixed with rocks, sediments, and debris (i.e., wood chips and plastic materials, Figures B-10 to B-12). The ice is flakey with some platy-like chunks when excavated (Figure B-11).

Figure B-7. Materials near the surface.



Figure B-8. The profile at the fill and ice interface.



Figure B-9. Digging into the consolidated snow and ice by using the ripper tooth to break the layer.



Figure B-10. Site 2 profile and close-up photos at various depths showing compacted sediments and foreign debris in ice.

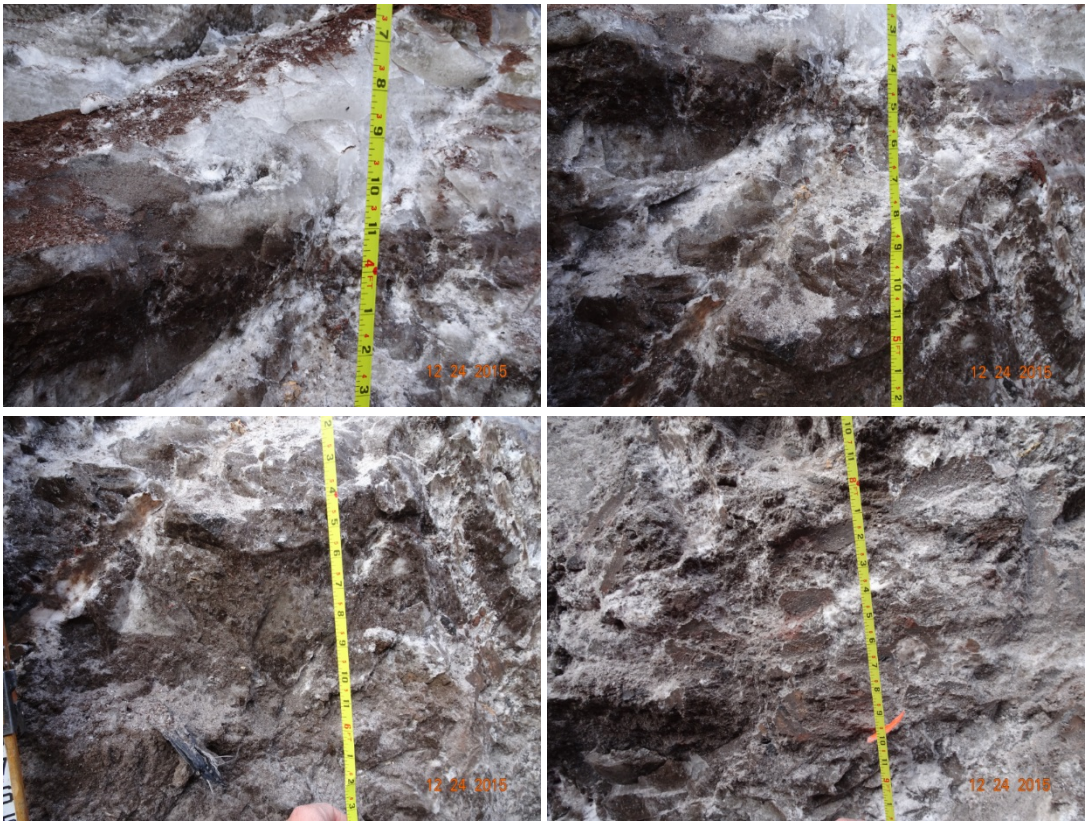


Figure B-11. Excavated ice from the pit at Site 2.



Figure B-12. Overall profile for Site 2.



B.3 Site 3

Site 3 is located on a pad near the carpenter shop (Building 191). This pit was dug down to 5.5 ft on 23 December 2015 (Figures B-13 to B-17).

Based on the visual survey, the top 6 in. is a light brown fine sand with small rocks. From 6 in. and down to 24 in., the material is somewhat moist, very friable with pickax or hand shovel, and very easy to crumble with hand pressure. Approximately the top 24 in. seemed thawed or unfrozen. At 24 in., the hammer was used to loosen up the hard materials. Chunks and blocks of frozen material were produced while using the hammer. The fill material continued down to 5.5 ft where we stopped digging because we were not equipped to handle contaminated soils. A smell of petroleum was encountered down at 5 ft deep. Wood debris were found while digging and at depth of 5.5 ft. It is unclear how deep the fill is on this pad, but we believe that it varies from 20 to 30 ft. A few feet away south of Site 3 is a steep slope leading to another pad for Building 136.

Figure B-13. Relatively easy digging for the first few scoops.



Figure B-14. The active or thawed layer.



Figure B-15. Using the hammer attachment to break the frozen materials.



Figure B-16. The soil profile from the surface down to 4 ft bgl (*left*) and debris found below 5 ft depth (*right*).



Figure B-17. The overall soil pit profile at Site 3.



B.4 Site 4

Site 4 is located on an inclined road between Buildings 191 and 04. We found massive ice below the soil material (Figures B-18 to B-20. The depth of the surface soil material ranged between 1.25 and 2.5 ft from the surface. The massive ice below is likely from the glacial ice with what seemed be several layers of seasonal melt. The ice layers were clear with ice bubbles and no foreign debris in the ice. In each layer, the ice was sandwiched with fine sediments. During the excavation, the ice broke in irregular-big chunks (not small and crumbly). A hard rock (gray basaltic material) layer was found at approximately 10 ft from the surface and below the massive ice.

Figure B-18. The fill layer on top.



Figure B-19. Ice layers at Site 4. *Bottom right* shows hard rock (gray basaltic material) layer at the bottom of pit.

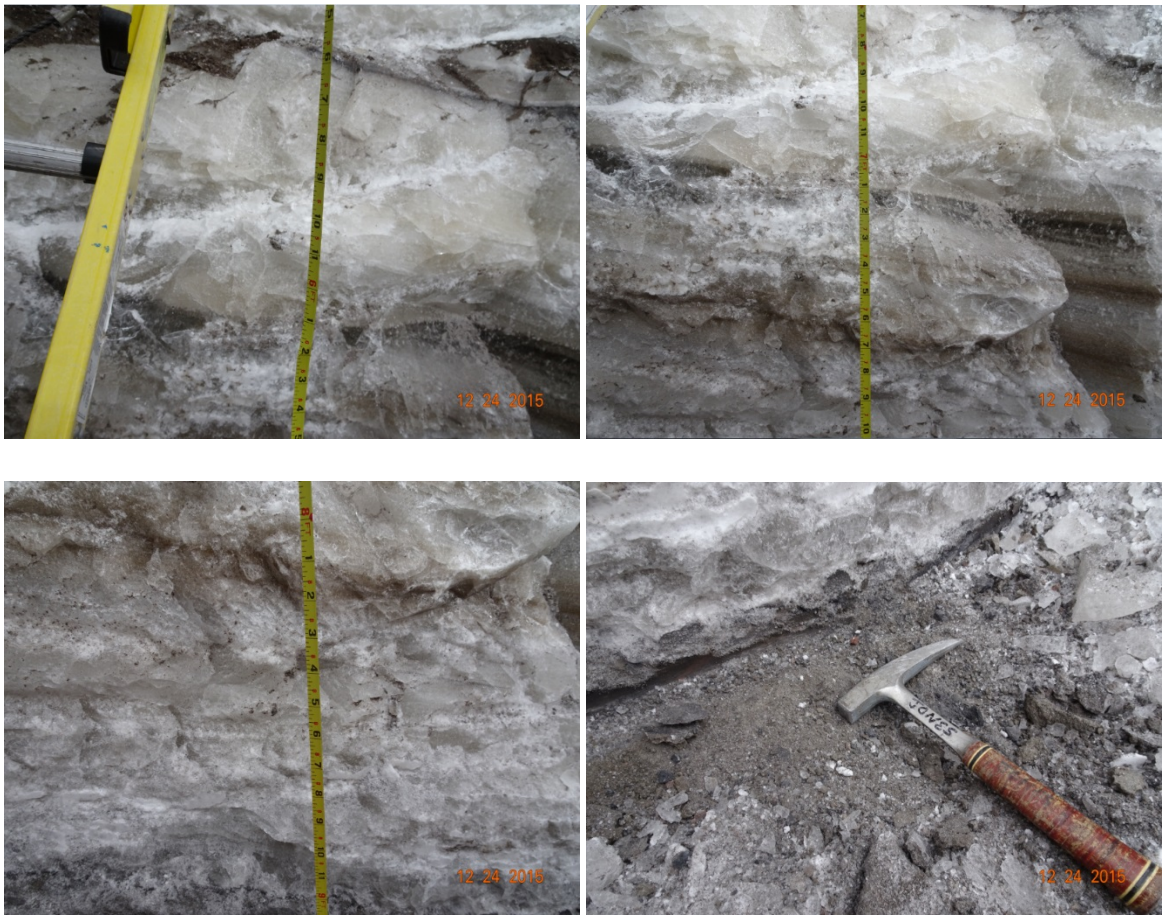


Figure B-20. Site 4 profile and excavation down to 10 ft.



B.5 Site 5

Site 5 is located south of Building 155, and Figures B-21 to B-24 show the evacuation and profiles. The top 8 or 9 in. is primarily reddish fine fill materials. A mix of red and gray fill materials was encountered between 9 and 14 in. The ground was frozen at 14 in. or so below the surface, and we smelled fuel vapor at this depth. At approximately 1.5 ft, ice lenses were visible; and the ground was hard to scoop. A ripper was used to loosen the materials. At approximately 4.5 ft, the layer changed from red or reddish-brown materials above it to gray materials. Below 4.5 ft bgl, the stratigraphy was interconnected with fractured boulders, rock and ice layer; and the layer was much harder than the layer above it. Then a hammer attachment was used to break the rocks.

Figure B-21. Site 5 thawed layer.



Figure B-22. Digging and using a ripper attachment (*left*) and hammer below five ft (*right*) to loosen the frozen layer at Site 5.



Figure B-23. Profiles at various depths at Site 5 showing ice lenses.

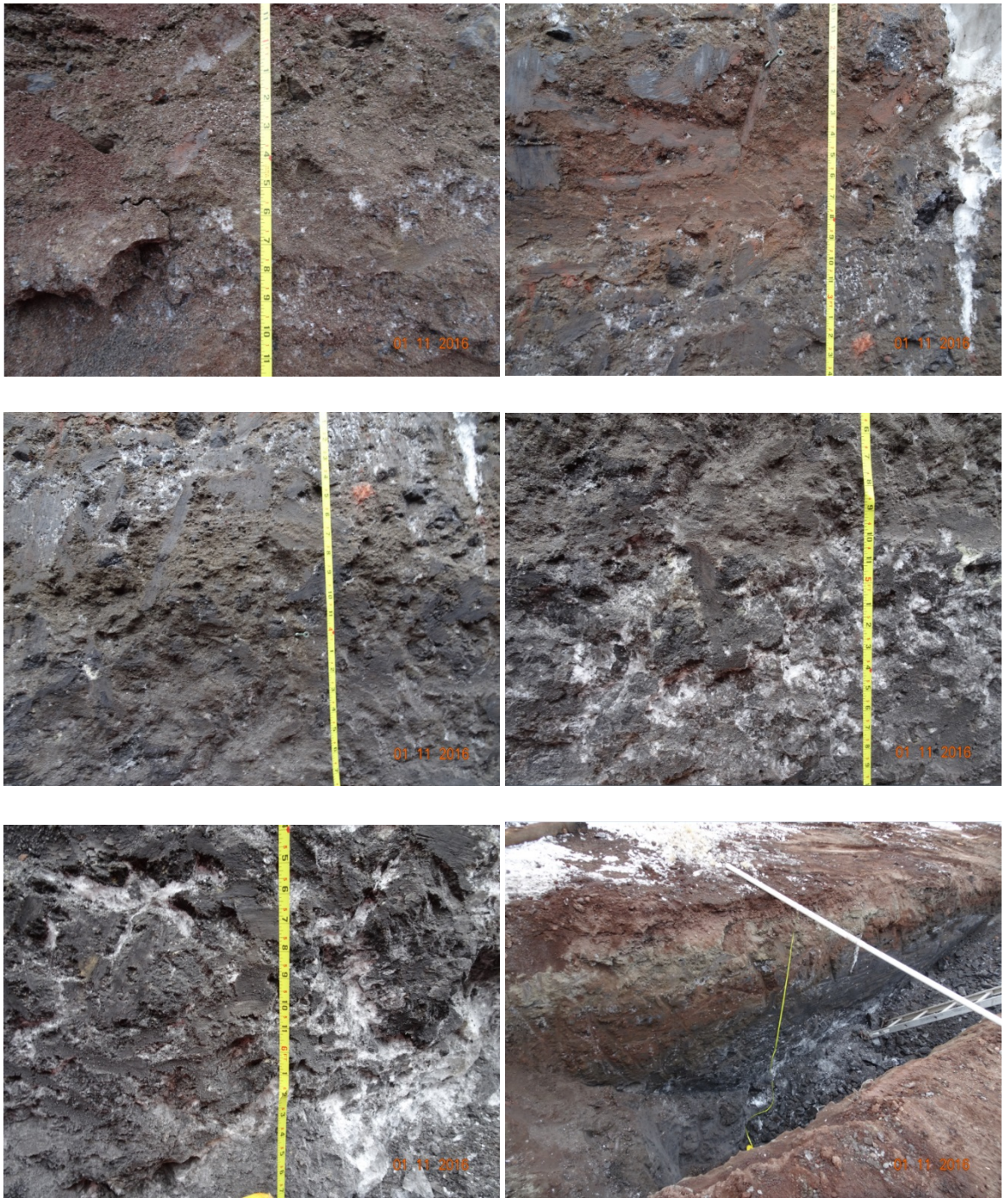


Figure B-24. Entire profile of the pit at Site 5 showing red fill materials, gray fractured rocks, and ice lenses.



Appendix C: Grain Size

The gradation analysis was conducted on the representative samples collected in the pits from five sites of gravelly sand earth fractions (i.e., small rocks or gravel sizes less than 300 mm). Figures C-1 to C-6 depict the gradation from these five sites. Soil moisture and density tests were conducted first before the grain-size analysis was performed.

Figure C-1. Grain-size distribution for samples collected in Site 1.

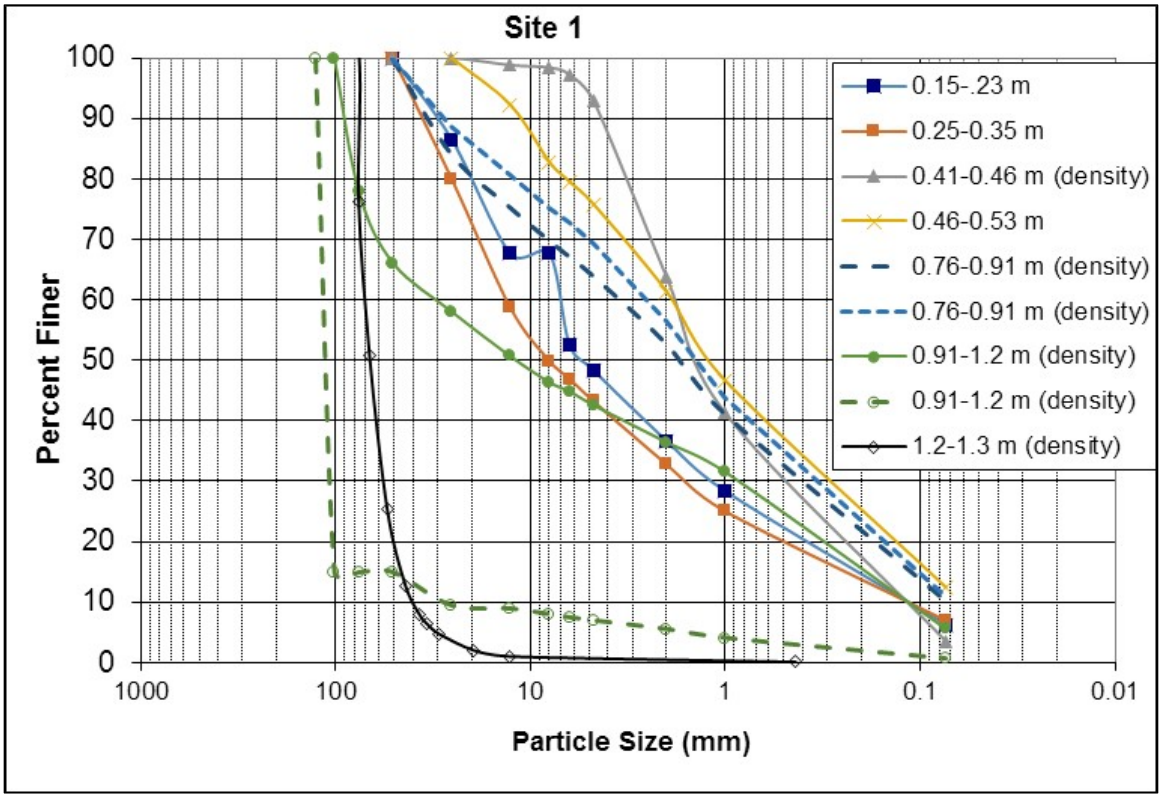


Figure C-2. Grain-size distribution for samples collected in Site 2.

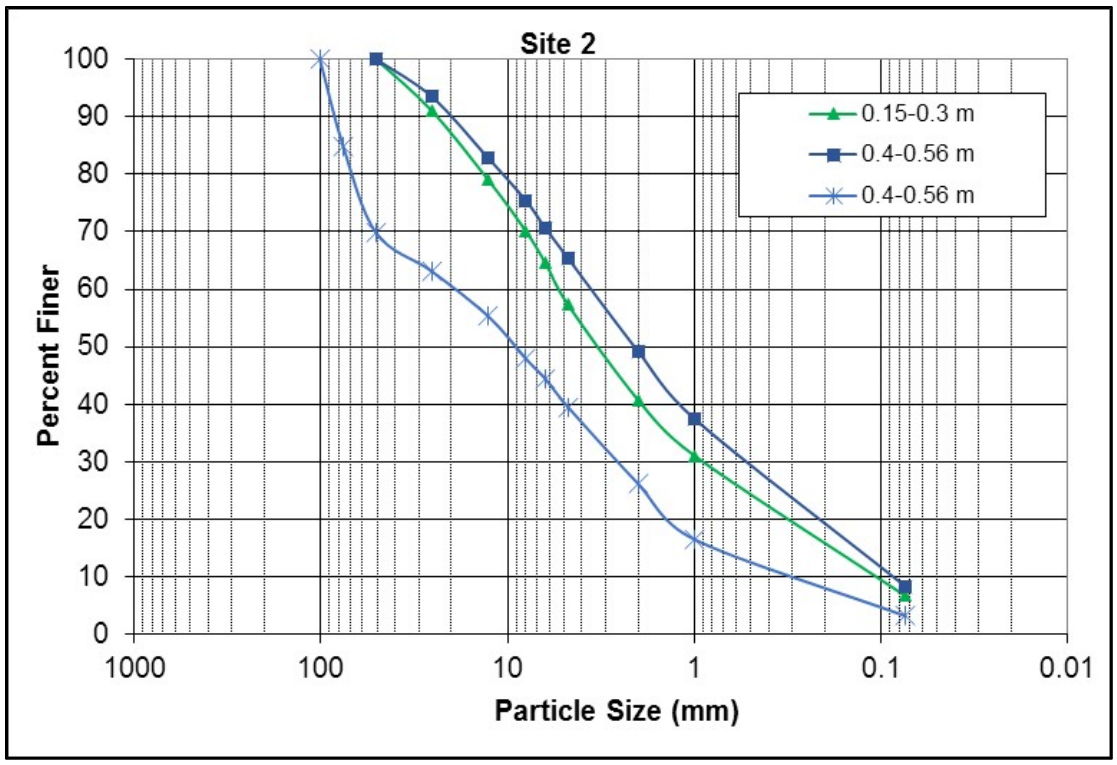


Figure C-3. Grain-size distribution for samples collected in Site 3.

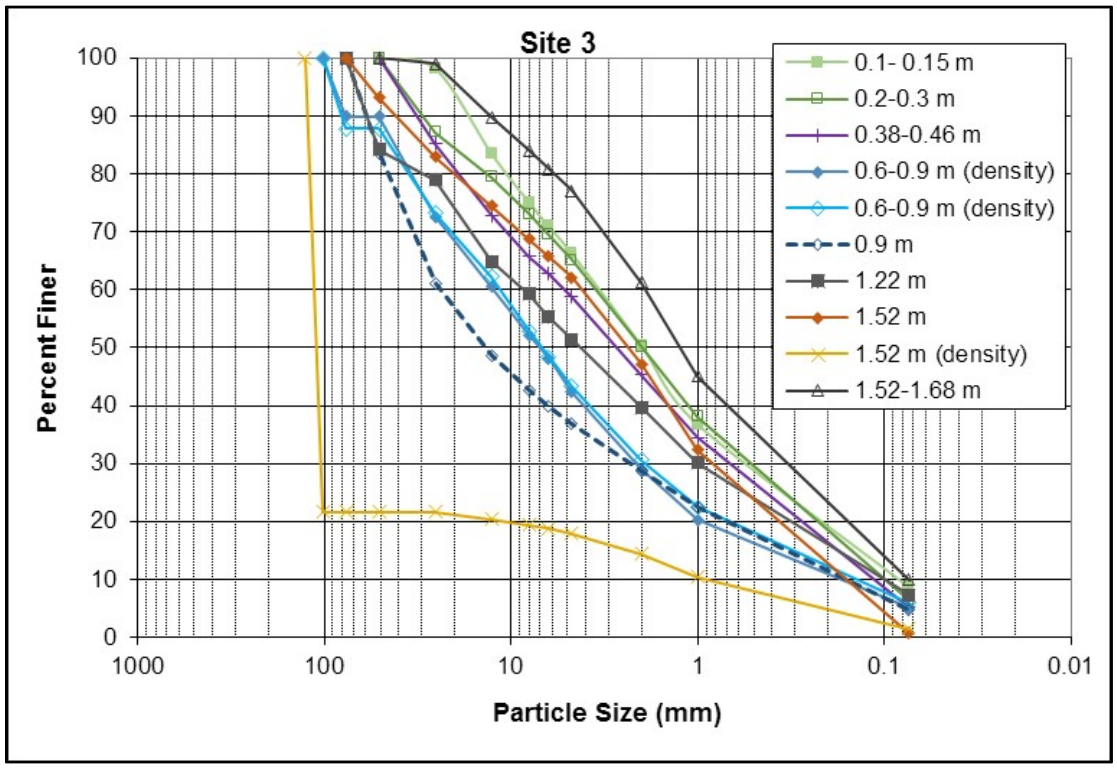


Figure C-4. Grain-size distribution for samples collected in Site 4.

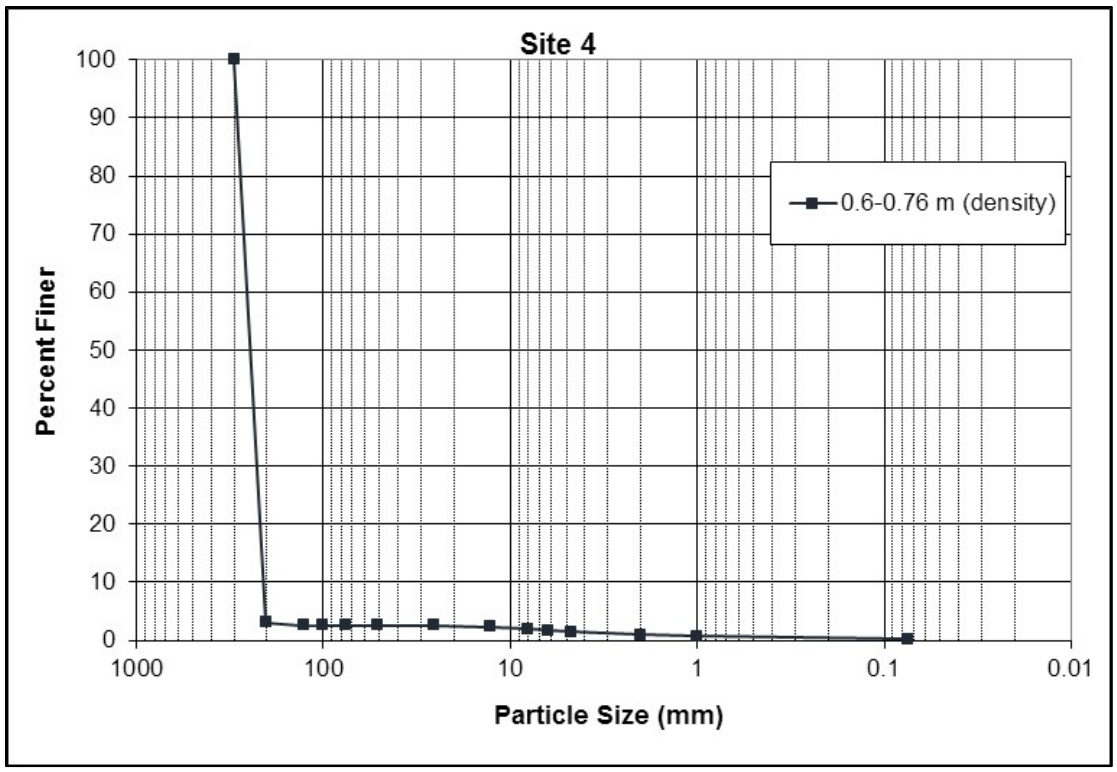


Figure C-5. Grain-size distribution for samples collected in Site 5 down to 1.83 m.

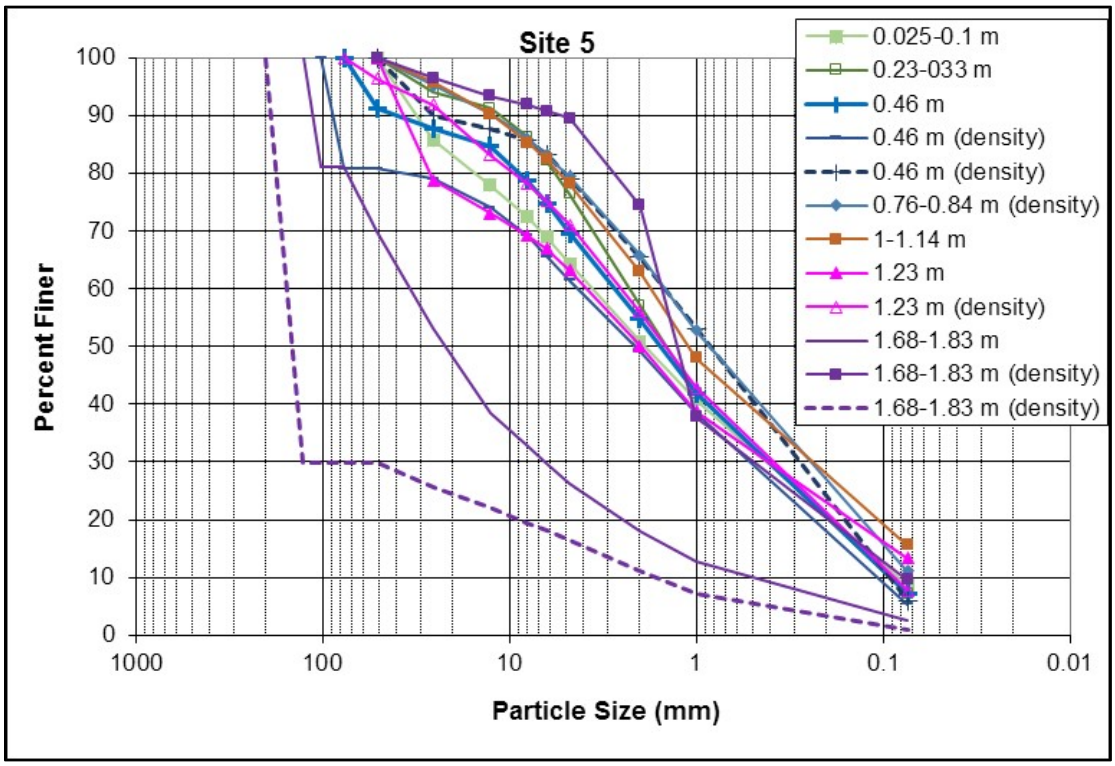
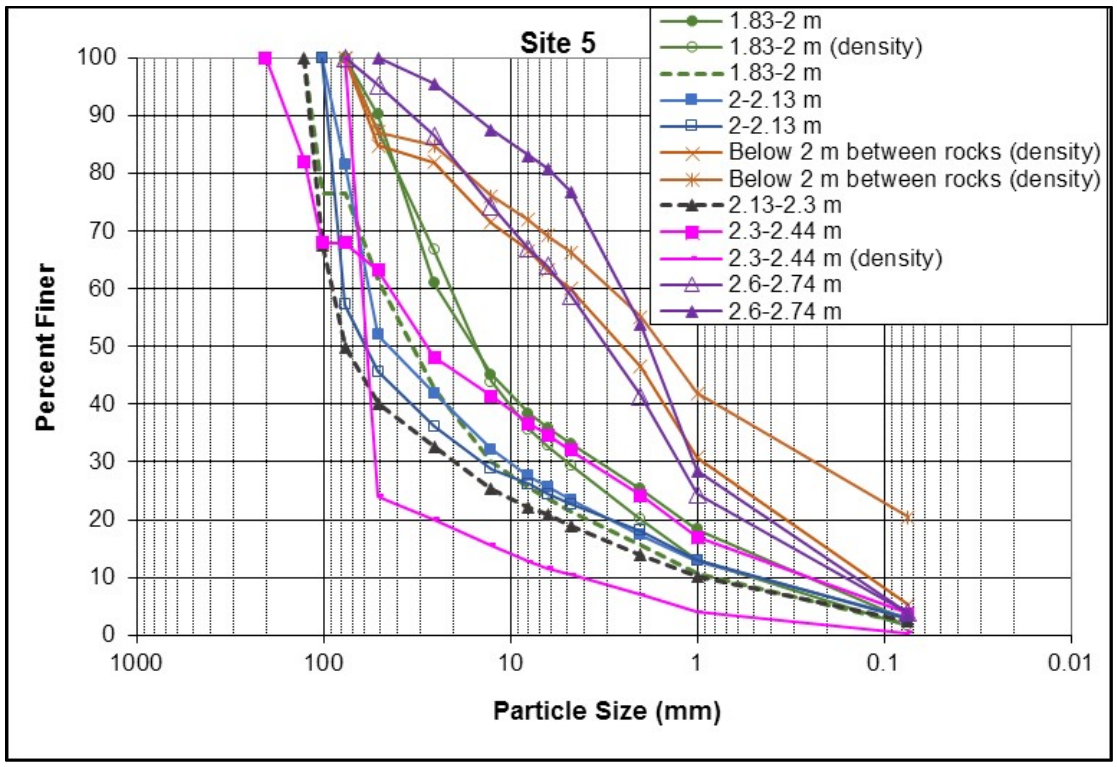


Figure C-6. Grain-size distribution for samples collected in Site 5 down to 2.74 m.



REPORT DOCUMENTATION PAGE

Form Approved
OMB No. 0704-0188

Public reporting burden for this collection of information is estimated to average 1 hour per response, including the time for reviewing instructions, searching existing data sources, gathering and maintaining the data needed, and completing and reviewing this collection of information. Send comments regarding this burden estimate or any other aspect of this collection of information, including suggestions for reducing this burden to Department of Defense, Washington Headquarters Services, Directorate for Information Operations and Reports (0704-0188), 1215 Jefferson Davis Highway, Suite 1204, Arlington, VA 22202-4302. Respondents should be aware that notwithstanding any other provision of law, no person shall be subject to any penalty for failing to comply with a collection of information if it does not display a currently valid OMB control number. PLEASE DO NOT RETURN YOUR FORM TO THE ABOVE ADDRESS.

1. REPORT DATE (DD-MM-YYYY)
February 2017

2. REPORT TYPE
Technical Report/Final

3. DATES COVERED (From - To)

4. TITLE AND SUBTITLE
Subsurface Assessment at McMurdo Station, Antarctica

5a. CONTRACT NUMBER

5b. GRANT NUMBER

5c. PROGRAM ELEMENT

6. AUTHOR(S)
Rosa T. Affleck, Seth Campbell, Samantha Sinclair, and Bruce Tischbein

5d. PROJECT NUMBER

5e. TASK NUMBER
EP-ANT-15-19

5f. WORK UNIT NUMBER

7. PERFORMING ORGANIZATION NAME(S) AND ADDRESS(ES)
U.S. Army Engineer Research and Development Center (ERDC)
Cold Regions Research and Engineering Laboratory (CRREL)
72 Lyme Road,
Hanover, NH 03755-1290

8. PERFORMING ORGANIZATION REPORT NUMBER
ERDC/CRREL TR-17-4

9. SPONSORING / MONITORING AGENCY NAME(S) AND ADDRESS(ES)
National Science Foundation, Office of Polar Programs
Antarctic Infrastructure and Logistics
Arlington, VA 22230

10. SPONSOR/MONITOR'S ACRONYM(S)
NSF

11. SPONSOR/MONITOR'S REPORT NUMBER(S)

12. DISTRIBUTION / AVAILABILITY STATEMENT
Approved for public release; distribution is unlimited.

13. SUPPLEMENTARY NOTES
Engineering for Polar Operations, Logistics, and Research (EPOLAR)

14. ABSTRACT

Installations built on massive ice, permafrost, or seasonal frozen ground require careful design to avoid melting issues. Therefore, efforts to rebuild McMurdo Station, Antarctica, to improve operational efficiency and to consolidate energy resources require knowledge of geology and geotechnical information, particularly soil indices within the near-surface layer subjected to temporal fluctuations and the ice-cemented layer.

Therefore, this study collected both 200 and 400 MHz ground-penetrating radar (GPR) data in McMurdo during January, October, and November of 2015 to detect the active layer, permafrost or massive ice, fill thickness, solid bedrock depth, and buried utilities or construction and waste debris. Five soil pits were excavated to collect soil, ice, and rock samples for gradation, density, and moisture content tests. Information extracted from the soil pits also aided in ground-truthing the GPR profiles. Subsurface investigations revealed distinct features, including ice-bonded fractured basaltic boulders, rocks, and gravelly sand; massive ice; and constructed (friable) fill layer. This paper describes the soil temperature and moisture during austral summers. The presented results are important for designs of new engineered structures at McMurdo Station.

15. SUBJECT TERMS
Active layer, Gradation, Ground penetrating radar, Ice content, McMurdo Station (Antarctica), Permafrost, Soil density, Soil moisture, Soil surveys, Soil temperature

16. SECURITY CLASSIFICATION OF:			17. LIMITATION OF ABSTRACT	18. NUMBER OF PAGES	19a. NAME OF RESPONSIBLE PERSON
a. REPORT	b. ABSTRACT	c. THIS PAGE			19b. TELEPHONE NUMBER (include area code)
Unclassified	Unclassified	Unclassified	SAR	117	